Elucidation of the Molecular and Cellular Perturbations that Underpin the Human Disease Lethal Congenital Contracture Syndrome 1

By

Andrew William Folkmann

Dissertation

Submitted to the Faculty of the

Graduate School of Vanderbilt University

in partial fulfillment of the requirements

for the degree of

DOCTOR OF PHILOSOPHY

in

Cell and Developmental Biology

August, 2014

Nashville, Tennessee

Approved:

Susan Wente, Ph.D.

James Goldenring, Ph.D.

Ronald Emeson, Ph.D.

Ryoma Ohi, Ph.D.

Irina Kaverina, Ph.D.

To my loving parents and wife.

\

ACKNOWLEDGMENTS

This work would not have been possible without the support of my mentor, Dr. Susan R. Wente. Her guidance and rigorous training has shaped me into the scientist that I am today. Moving forward she will remain a role model for both my scientific and personal life.

I would like to graciously thank the past and present members of the Wente laboratory for their support and advice throughout the years. I would also like to thank the members of my Dissertation Committee who have guided and shaped my work.

My thesis work was made possible in part by the hard work of several very talented individuals. Specifically, I would like to thank- Dr. Melanie D. Ohi, Scott Collier, Dr. Yoshimasa Takizawa, Aditi, Dr. Xiaoyan Zhan, and Dr. Toni R. Dawson.

I would like to thank my wonderful wife for her love and support.

TABLE OF CONTENTS

LIST OF TABLES

LIST OF FIGURES

Figure Page

LIST OF ABBREVIATIONS

Δ	Null strain or domain deletion
AMP	Adenine mono-phosphate
ADP	Adenine di-phosphate
ATP	Adenine tri-phosphate
CBC	Cap-binding complex
CTD	C-terminal domain
DNA	Deoxyribonucleic acid
DBP	Dead-box protein
EJC	Exon-exon junction complex
EM	Electron microscopy
FG	Phenylalanine –glycine
FISH	Fluorescence *in situ* hybridization
FRET	Fluorescence resonance energy transfer
GDP	Guanine di-phosphate
GST	Glutathione S-transferase
GTP	Guanine tri-phosphate
IP6	Inositol hexakisphosphate
mRNA	Messenger ribonucleic acid
mRNP	Messenger ribonucleoprotein particle
NegEM	Negative stain electron microscopy
NES	Nuclear export signal
NLS	Nuclear localization signal
NPC	Nuclear pore complex
NTD	N-terminal domain
Nups	Nucleoporins
Pi	Inorganic phosphate
Pol II	RNA polymerase II
RNA	Ribonucleic acid
TREX	Transcription export complex
SVAU	Sedimentation velocity analytical ultracentrifugation

Chapter I

Introduction

Nuclear pores and nucleocytoplasmic transport

The hallmark of the eukaryotic cell is compartmentalization of gene expression events between the nucleus and cytoplasm. In turn, this allows for diverse signaling and regulatory networks that are required for proper embryo development and the maintenance of cellular homeostasis. This fundamental paradigm relies on the regulated transport of material between the nuclear and cytoplasmic compartments. To accommodate this task, eukaryotic cells have evolved to assemble large macromolecular structures called nuclear pore complexes (NPCs) to regulate this nucleocytoplasmic exchange. NPCs are large aqueous channels that function both as a physical barrier and selective filter for nucleocytoplasmic transport events (Nenninger et al., 2010; Roy et al., 2008).

NPCs are embedded in the nuclear envelope. These macromolecular assemblies are estimated to have high molecular masses of 90 to 120MDa (Papadopoulos et al., 2000; Rout et al., 2000). Although NPCs vary in size between different organisms, the basic molecular architecture of the NPC is highly conserved. NPCs are composed of ~30 different proteins termed Nups.

The basic architecture of the NPC is characterized by three structural elements: (1) a symmetric central core that forms a channel, (2) cytoplasmic fibrils, and (3) a nuclear basket (Figure 1.1). These basic structural elements are made up of modular

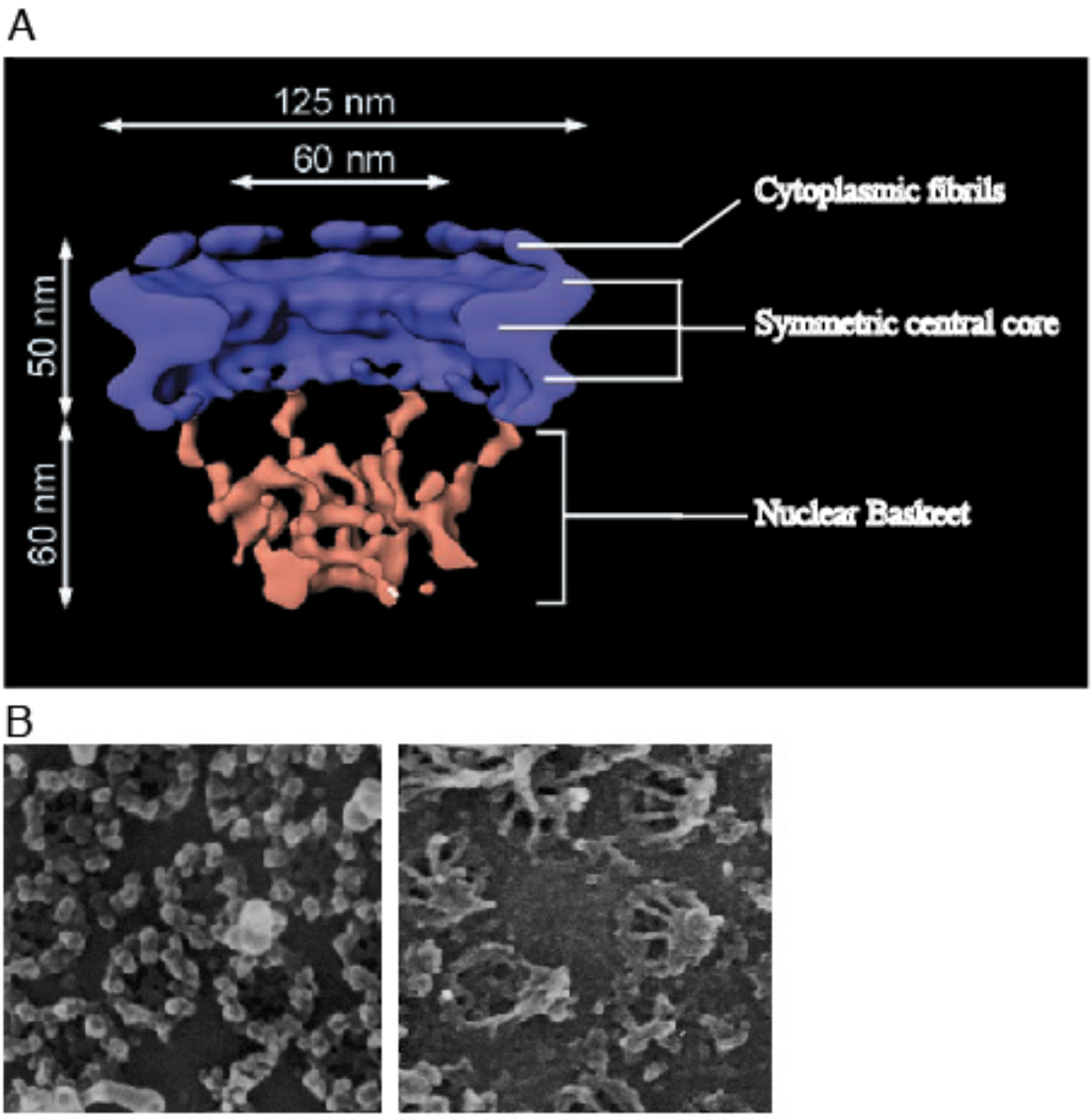

Figure 1.1 Architecture of the NPC (Adapted from Beck et al., 2004, and Goldberg et al., 1995) (A-B) The basic architecture of the NPC is characterized by three structural elements: (1) a symmetric central core that forms a channel, (2) cytoplasmic fibrils, and (3) a nuclear basket. (A) Cyro-electron tomography of NPCs in *Dictyostelium* highlights the basic structural organization of NPC. (B) The cytoplasmic fibrils (Left) and nuclear basket (Right) structural elements have been also documented using scanning field emission electron microscopy.

substructures that are composed of discrete Nup sub-complexes (Hoelz et al., 2011; Rout et al., 2000). A group of Nups (termed FG-Nups) harbors domains with multiple phenylalanine-glycine (FG) amino acid repeats. The FG-Nups line the innermost layer of the NPC channel and constitute the permeability barrier (Terry and Wente, 2009). The semipermeable barrier formed by these overlapping FG repeats allows for small molecules (<40 kDa) to freely diffuse between the nucleus and the cytoplasm (Pante and Kann, 2002). Larger proteins or protein complexes require binding to transport adapter proteins. These transport adapter proteins harbor low affinity FG-repeat binding domains. These binding domains allow the transport factors to interact with specific FG-Nups and translocation of the cargo through the NPC (Terry et al., 2007).

Nucleocytoplasmic transport of large cargo complexes occurs via a step-wise process. First, shuttling transport factors called Kaps recognize specific cargo proteins (Weis, 2003). To recognize potential cargos, each Kap binds to a specific peptide nuclear export sequence (NES) or nuclear localization sequence (NLS) that are located on the cargo protein (Fried and Kutay, 2003). The Kap/cargo complex then docks with the NPC and translocates through the pore. Cargo release from the Kap in the correct destination compartment is achieved by the nucleotide-bound state of the small GTPase Ran (Terry et al., 2007).

High levels of RanGTP are maintained in the nucleus by a chromatin-associated Ran-specific guanine exchange factor (RanGEF), whereas in the cytoplasm, a Ran-specfic GTPase activating protein (RanGAP) promotes RanGTP hydrolysis, keeping cytoplasmic levels of RanGDP high. The contrasting environments are key for dictating the directionality of Kap cargo transport. Specifically, structural rearrangements that

occur within the protein between its nucleotide bound states, GTP-bound (RanGTP) versus GDP-bound (RanGDP), allow for release of the cargo at the appropriate location (Fried and Kutay, 2003; Pemberton and Paschal, 2005) (Figure 1.2).

For cargo import into the nucleus, RanGTP triggers the release of the cargo from the Kap in the nucleoplasm. For protein export from the nucleus, RanGTP stabilizes the Kap-cargo interaction. Following translocation through the NPC, disassembly of the RanGTP-Kap-cargo complex in the cytoplasm is mediated by stimulating GTPase activity of Ran by a RanGTPase activating protein. The conversion of Ran GTP-bound to Ran GDP-bound acts as a molecular switch to promote cargo disassembly from the Kap in the cytoplasm (Fried and Kutay, 2003; Pemberton and Paschal, 2005).

Most of the nucleocytoplasmic trafficking that occurs within the cell involves the Kap/Ran pathway. The vast majority of messenger RNA (mRNA) however is exported from the nucleus in a Ran-Kap independent manner. Instead, mRNA utilizes different evolutionarily conserved transport factors to facilitate export from the nucleus to the cytoplasm. This paradigm along with an overview of mRNA metabolism will be presented.

mRNA processing in the nucleus

The central dogma of DNA to RNA to protein is one of the most fundamental concepts of modern biology. This paradigm places RNA as the cellular intermediate between DNA and proteins. Thus, eukaryotic gene expression has evolved regulatory mechanisms to ensure the proper fate of the transcribed mRNA. At the core of this regulation are multifunctional RNA binding proteins (RBPs) that associate with mRNA

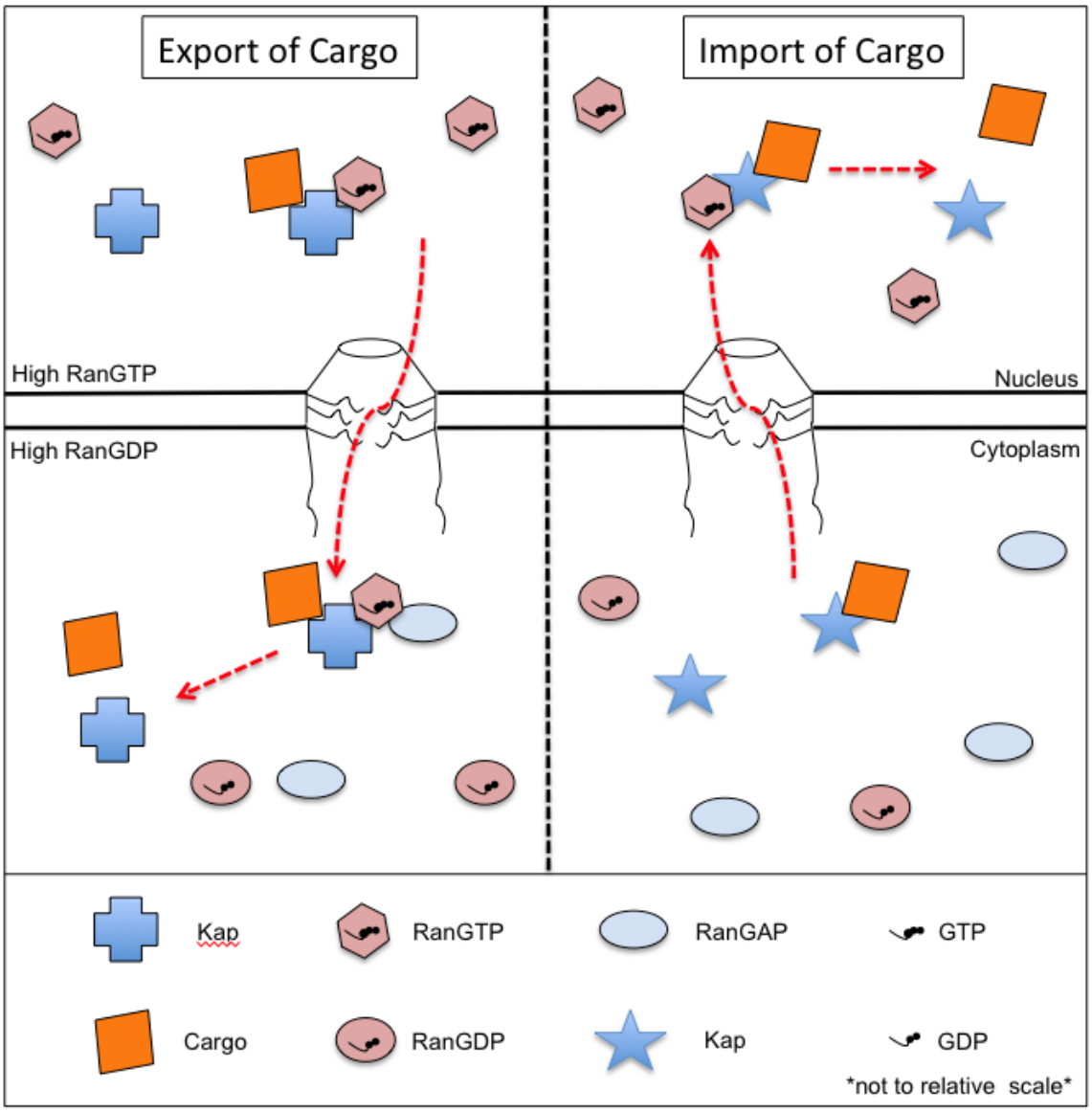

Figure 1.2 Nucleocytoplasmic protein transport is directed by the differential localization of RanGTP and RanGDP. In the nucleus, high levels of RanGTP are maintained in the nucleus by a RanGEF), whereas in the cytoplasm, a RanGAP promotes Ran GTP hydrolysis, keeping cytoplasmic levels of RanGDP high. (Left Panel) In the nucleus RanGTP stabilizes the interaction between the Kap and it's cognate NES-containing cargo. The trimeric complex is transported through the NPC by interaction with FG-binding domains. In the cytoplasm, RanGAP stimulates GTP hydrolysis and results in disassembly of the trimeric complex. (Right Panel) For the import of cargo into the nucleus the Kap interacts with it's cognate cargo in the cytoplasm. Interaction of the Kap-Cargo complex with the FG-domain facilitates transport through the NPC. Upon arrival in the nucleus, binding of the Kap-Cargo complex by RanGTP results in cargo release.

transcripts to form messenger ribonucleoprotein (mRNP) complexes. In the nucleus, a single mRNA molecule undergoes dynamic RBP association to mediate functions such as splicing and nuclear export. Further, following export to the cytoplasm, RBPs help specify multiple mRNP fates, including storage, translation, and degradation (Dreyfuss et al., 2002; Muller-McNicoll and Neugebauer, 2013). A brief overview of these regulatory paradigms is presented below.

In the nucleus, mRNAs are transcribed by the enzyme Polymerase II (Pol II). As soon as Pol II begins synthesizing the precursor-mRNA (pre-mRNA), the C-terminal domain (CTD) of Pol II recruits factors that bind to the pre-mRNA to form an mRNP (Bentley, 2005; Lee and Tarn, 2013). The first processing reaction that occurs is the addition of a modified guanine nucleotide to the 5' of the new pre-mRNA. As soon as 25 nucleotides of pre-mRNA have been produced, the phosphate is removed from the 5' end of the RNA by the phosphatase, and a guanyl transferase links a GMP nucleotide by reverse linkage (5' to 5') to the 5' nucleotide. A methyl transferase then adds a methyl group to the guanosine to complete the generation of the m^7G cap (Shatkin, 1976). The m^7G cap recruits the cap-binding complex (CBC), which plays important roles in promoting mRNA stability, 3' end formation, and translation in the cytoplasm (Lewis and Izaurralde, 1997). Importantly, the m^7G cap marks the 5' end of the mRNA and acts as a landmark that helps the cell distinguish mRNA from other RNA molecules in the cell.

Most pre-mRNA sequences are interrupted by noncoding sequences called introns. Shortly after the 5' capping reaction occurs, the pre-mRNA undergo a processing event called splicing which removes the intervening intron sequences and joins the exon sequences together (Licatalosi and Darnell, 2010). The CTD of RNA Pol

II helps coordinate mRNA capping and splicing by co-transcriptionally loading capping and splicing components as the pre-mRNA emerges form the enzyme (Lee and Tarn, 2013). Splicing sites are marked by specific sequences in both the exons and introns. The splicing protein machinery recognizes these sequences and facilitates the splicing reaction and removal of the intron. The splicing machinery also deposits the exon-exon junction complex (EJC) near the vicinity of the exon-exon junctions. The EJCs function to mark the sites of intron excision and help avoid degradation by factors that target unspliced mRNAs (Lee and Tarn, 2013; Schoenberg and Maquat, 2012).

The signal sequence for 3' end cleavage is specified in the DNA. The CTD co-transcriptionally loads factors that are critical for 3' end formation onto these nucleotide sequences as it emerges from the enzyme. These factors in turn recruit poly-A-polymerase that adds adenosine nucleotides to the 3' end of the mRNA to generate the poly(A) tail (Proudfoot, 2011). Once generated, poly(A) tails are recognized by poly(A) binding proteins (Goss and Kleiman, 2013).

After these processing events have been completed, the mRNA will have m^7G-cap, a coding sequence that is marked with EJCs if spliced, and a 3' untranslated region (UTR) followed by a poly(A) tail. Additionally, the mRNA will be bound by a cohort of proteins (CBC, RNA binding proteins) that designate the mRNP competent for export to the cytoplasm. Importantly, if mRNA fails to undergo one or more of these processing events it is retained in the nucleus and degraded by the nuclear exosome (Houseley et al., 2006).

Export of mRNA through the NPC

Proper gene expression relies on the successful completion of the nuclear processing events to form the mature export competent mRNP. Of the total pre-mRNA that is generated during transcription, only a small fraction, the mature mRNA, is used by the cell. The remaining RNA in the nucleus, which includes excised introns, aberrantly processed, or broken mRNAs, are potentially dangerous to the cell if exported to the cytoplasm. For this reason, the process of export of mRNA through the NPC is highly regulated and intertwined with the nuclear processing events. This in turn allows for the regulated recruitment of transport receptors only to the mature fully processed mRNAs (Kohler and Hurt, 2007).

Although some RNAs utilize the Ran-dependent Kap export pathways, the vast majority of mRNAs utilize the evolutionarily conserved nuclear export factors NXF1 (in humans) or Mex67 (in *S. cerevisiae*) (Gruter et al., 1998; Segref et al., 1997). *S. cerevisiae* and human cells use at least two different mechanisms to recruit Mex67/NXF1 to the mRNA. In *S. cerevisiae*, Mex67 can be recruited to the mRNA via association with the Serine-Arginine (SR) rich protein Npl3. Npl3 is thought to associate with the mRNA in a phosphorylated state. Further, dephosphorylation of Npl3 stimulates Mex67 recruitment to the mRNA (Gilbert and Guthrie, 2004; Gilbert et al., 2001). In human cells, the mRNA recruitment of NXF1 is also regulated by phosphorylation cycles of SR-proteins (Huang et al., 2003; Huang et al., 2004). Acting in a mechanism that is independent of SR-proteins, a complementary route for Mex67/NXF1 recruitment occurs by interaction with the RNA binding protein Yra1 or ALY, respectively (Strasser and Hurt, 2000; Stutz et al., 2000). Both Yra1 and ALY are part of the transcription-export

complex (TREX) (Strasser et al., 2002). Recruitment of the TREX complex to the mRNP is dependent on 5'capping and splicing processing events (Cheng et al., 2006).

The mature mRNP that contains the transport receptor Mex67/NXF1 is then capable of being exported through the NPC to the cytoplasm. Much of the information that is known about the actual translocation event of the mRNP through the NPC has been documented using high-resolution microscopy techniques. The export of the mRNP was first observed from static images taken by electron microscopy of mRNPs from insect Balbiani Ring genes (Mehlin et al., 1992). This seminal work demonstrated that the mRNP undergoes structural transitions as it docks, translocates, and is released from the NPC. This work also observed that mRNPs are dynamic structures that gain and lose specific proteins during transcription, processing, and export (Kiseleva et al., 1997; Mehlin et al., 1995; Zhao et al., 2002). Building on this, recent signal molecule microscopy analysis has resolved the kinetics of mRNA export in living mammalian cells (Grunwald and Singer, 2010; Mor et al., 2010). Taken together, these studies propose a model for mRNA export that is distinguished by four fundamental events: (1) the mRNP docks with the nuclear face of NPC, (2) translocation of the mRNP through the channel of the NPC, (3) docking of the mRNP at cytoplasmic face of the NPC, and (4) release of the mRNP into the cytoplasm (Figure 1.3).

A critical event that occurs during the terminal steps of every nucleocytoplasmic transport event is the removal of the transport receptor from the cargo in the destination compartment, thus imposing directionality of the transport event. As introduced above, Kap mediated transport relies upon modulation of the nucleotide state (GTP-bound versus GDP-bound) of the small GTPase Ran to promote cargo disassembly at the correct

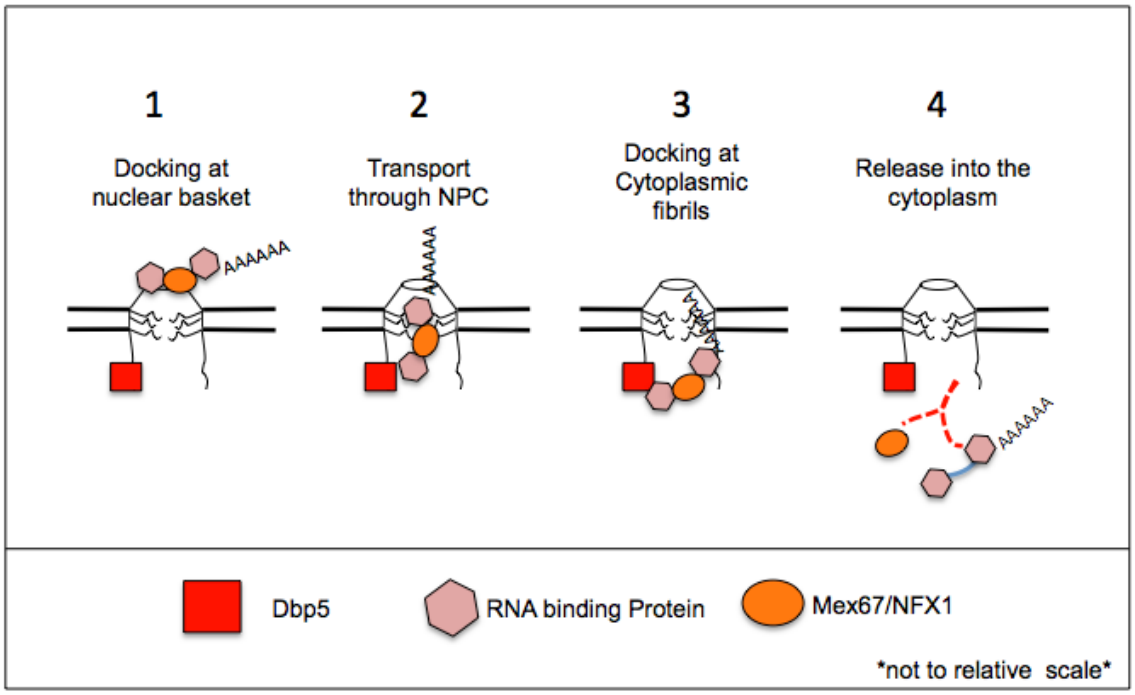

Figure 1.3: Fundamental events during mRNA export. It has been proposed that mRNA export is distinguished by four fundamental events: (1) docking of the mRNP at the nuclear basket (2) translocation of the mRNP through the NPC (3) docking of the mRNP at the cytoplasmic face (4) removal of the transport factor from the mRNP and subsequent release into the cytoplasm.

time and place (Weis, 2003). Removal of the Mex67/NXF1 transport receptor from the mRNP in the cytoplasm occurs via a distinct molecular mechanism that is independent of Ran activity (Kohler and Hurt, 2007).

The transport receptor Mex67/NXF1 is actively removed from the mRNP at the cytoplasmic face of the NPC by the protein Dbp5, a member of the DEAD-box helicase family (Lund and Guthrie, 2005; Snay-Hodge et al., 1998). In *S. cerevisiae*, Dbp5 temperature sensitive alleles have strong accumulation of poly(A)$^+$ RNA at non-permissive growth temperatures, suggesting that Dbp5 plays an essential role during mRNA export (Snay-Hodge et al., 1998; Tseng et al., 1998). Further, Dbp5 localizes to the cytoplasmic face NPC by interaction with the amino terminal domain of Nup159 (Weirich et al., 2004a). Prior studies have documented that Dbp5 functions during mRNA export by dissociating RNA binding proteins and transport receptors from the mRNP (Tran et al., 2007). Removal of these factors at the cytoplasmic face of the NPC in turn imposes the directionality of the export event. A further introduction of DEAD-box proteins and Dbp5 activity at the NPC is presented below. First, a brief introduction to protein translation in the cytoplasm is provided.

Translation of mRNA in the cytoplasm

The conversion of DNA to RNA to protein is essential for all aspects of life. A key aspect of this paradigm is the ability of the cell to convert the sequence information stored in the mRNA into the synthesis of a new protein molecule. To accomplish this task, the information stored in the mRNA nucleotide sequence must be 'translated' into a different information medium (i.e. amino acids). The primary sequence of the RNA

nucleotides is decoded as groups of three consecutive nucleotides called codons. Each codon specifies an amino acid or a stop to the translation process. The codons themselves do not directly recognize the amino acids, rather adapters called transfer RNAs (tRNAs) are used. tRNAs are covalently linked to the amino acids after base pairing directly with the triplet-nucleotide codon on the mRNA. The process of translation of the mRNA occurs in the ribosome, a large macromolecular complex that is made of many different proteins and several different RNA molecules. The overall mechanism of eukaryotic translation is highly conserved and involves a complicated array of different proteins. This process can be divided into three phases: initiation, elongation, and termination (Kapp and Lorsch, 2004). A basic introduction of the primary factors involved in translation initiation and translation termination is provided below.

The current model of translation initiation begins with the formation of the preinitiation complexes (PICs). Here a ternary complex, which contains eukaryotic initiation factor-2 (eIF2), GTP, and the initiator Met-tRNA$_i^{Met}$, bind to the 40S small ribosomal subunit to form the 43S PIC. The 43S PIC is loaded onto the 5' m^{7}G cap of the mRNA in a reaction that is promoted by the CBP, poly(A) binding protein (PAB), and eIF4F complex (Hinnebusch, 2014). Importantly, the binding requirement for CBP and PAB allows the translation machinery to ascertain that both ends of the mRNA are intact before beginning protein synthesis. After binding to the 5' cap the 43S PIC scans the mRNA for an AUG start codon. Upon recognition of the AUG start codon and base-pairing with the initiator Met-tRNA$_i^{Met}$, the eIFs dissociate from the 43S PIC complex,

allowing the 60S large ribosomal subunit to bind forming the 80S initiation complex (Hinnebusch, 2014).

During translation elongation, the 80S initiation complex translocates down the mRNA in 3 nucleotide stepwise movements. These movements in turn allow codon base pairing with cognate tRNA and the addition of amino acids to the growing protein polypeptide (Dever and Green, 2012). The end of the protein-coding message is designated by the presence of stop codons (UAA, UAG, or UGA) within the mRNA sequence. Stop codons are recognized by the ribosome by base pairing with release factor 1 (eRF1), which in turn signals to the ribosome to stop translation and release the polypeptide chain and mRNA molecule (Dever and Green, 2012; Nakamura and Ito, 2003).

DEAD-box proteins

Regulation of the life cycle of messenger RNA-protein (mRNP) complexes is essential for proper gene expression. One family of enzymes, the DEAD-box proteins (DBPs), is intricately involved in these mechanisms and acts in nucleotide-dependent processes, such as RNA duplex unwinding and mRNP remodeling (altering the protein composition of an mRNP) (Jankowsky, 2011a; Jankowsky and Bowers, 2006; Linder, 2006; Rocak and Linder, 2004). DBPs are found in all classes of organisms from bacteria through higher plants and animals (Cordin et al., 2006; Rocak and Linder, 2004). By definition, DBPs contain nine canonical amino acid sequence motifs (I-VI, Ia, Ib, Q) that presumably confer similar enzymatic activities to all of the family members (Figure 1.4), although only a subset have been studied at the enzymological level (Linder, 2006).

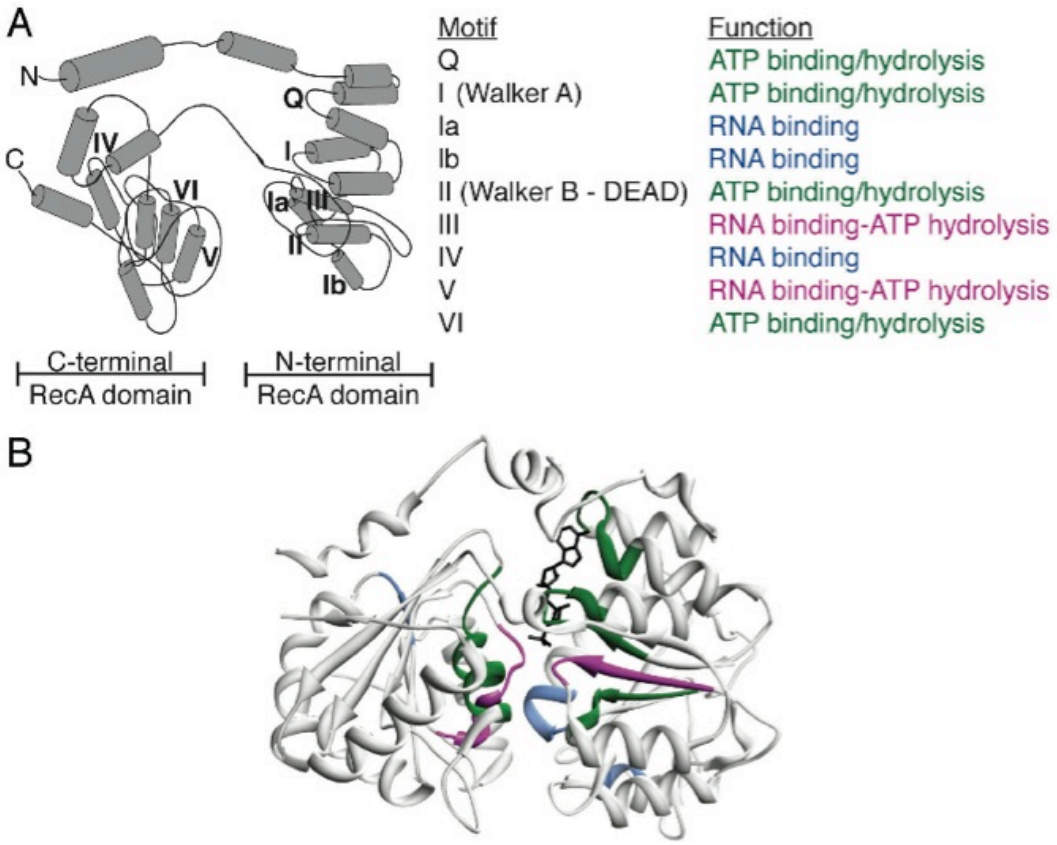

Figure 1.4 Structural organization of a DEAD box protein. (A) Topology model of the RecA-like helicase domains of a generic DEAD-box protein. The positions of the conserved sequence motifs within the labeled RecA helicase domains are indicated with Roman numerals. (B) Structure of human Dbp5 bound with ATP analog (black) [PDB 3GOH] (Collins et al., 2009). Highlighted conserved sequence motifs include those involved in nucleotide binding and hydrolysis (Green); RNA binding and ATP hydrolysis (Pink); RNA binding (Blue).

The high-resolution protein structures of several DBPs are known, and while they share many structural features, there are also important emerging differences (Jankowsky and Fairman, 2007a; Schutz et al., 2010). Common biochemical characteristics shared by DBPs include ATP binding and hydrolysis activity whereby ATP is converted to ADP and inorganic phosphate in an RNA-dependent manner (Jankowsky and Fairman, 2007a). Structurally, DBPs have two RecA-like domains (subdomain 1: N-terminal RecA domain, and subdomain 2: C-terminal RecA domain) that are joined by a flexible linker (Figure 1.4) (Cordin et al., 2006). Most of the conserved motifs line the central cleft between the two domains and provide for conserved ATP binding and hydrolysis activities (Figures 1.4A and 1.4B) (Jankowsky and Fairman, 2007b). The RNA substrate specificity and unique binding sites for potential co-factors and protein-protein interactions occur through less conserved regions, including N- and C-terminal extensions (Schutz et al., 2010). Interestingly, the unique regions are likely key to the different functions amongst the family members. However, for DBPs that perform the same function in different organisms, the regions outside the canonical motifs show considerable conservation (Cordin et al., 2006).

DEAD-box proteins catalyze rearrangements of both RNA-RNA and RNA-protein complexes through helicase and remodeling activities, respectively (Jankowsky, 2011a). Both of these enzymatic activities harness distinct structural changes that occur during the nucleotide cycle. It is unclear, however, if these activities share similar or distinct molecular mechanisms. Until recently, it was thought that all DEAD-box proteins require the ATP hydrolysis event for both duplex unwinding and RNP remodeling. For several DBPs, this mechanism is not true: DEAD-box proteins eIF4A,

Msn16, and Ded1 require ATP binding but not hydrolysis to promote RNA duplex unwinding. Surprisingly, it was demonstrated that ATP hydrolysis occurs primarily to recycle the enzyme for additional rounds of helicase activity (Chen et al., 2008; Liu et al., 2008).

Several studies have analyzed the *in vitro* ability of DBPs to remove proteins from RNA (Bowers et al., 2006; Fairman et al., 2004; Jankowsky et al., 2001; Tran et al., 2007). Several DBPs tested reportedly required ATP hydrolysis to remove proteins from RNA (Bowers et al., 2006; Fairman et al., 2004). In contrast, it has been demonstrated that DBP's remodeling activity can occur independent of ATP hydrolysis. The RNA binding protein Nab2 is released from the mRNP both *in vitro* and *in vivo* by the DEAD-box protein Dbp5 (Noble et al., 2011; Tran et al., 2007). Further, these studies demonstrated that a conformational change that occurs in the transition from the Dbp5-ATP form to the Dbp5-ADP form is required for the remodeling of the mRNP. Importantly, for Dbp5, this conformational change can be functionally driven in vitro by conversion from the nucleotide-free form of Dbp5 to the ADP-bound form (Noble et al., 2011; Tran et al., 2007). Analysis of the x-ray crystal structures of Dbp5 shows that the RNA binding interface is dramatically changed by the transition from the ATP to the ADP state (Collins et al., 2009; Montpetit et al., 2011). Such a change in the RNA binding site during the transition from binding ATP to binding ADP may represent a shared mechanism utilized by many DBPs to remodel RNPs.

Gle1 is a multifunctional regulator of gene expression

The DEAD-box proteins enzymes drive mRNP remodeling through ATP hydrolysis-induced conformational changes that alter the DBP binding to RNA and coincidently RNA-protein interactions (Folkmann et al., 2011; Jankowsky, 2011b; Jankowsky and Bowers, 2006; Jankowsky and Fairman, 2007b; Rocak and Linder, 2004). Factors that regulate DBP nucleotide cycles are speculated to exist, and a few have been reported, including ones for two eukaryotic initiation factors (eIF4A for eIF4AIII) (Ballut et al., 2005; Grifo et al., 1984; Nielsen et al., 2009; Rogers et al., 2001a; Wolf et al., 2010b; Yang et al., 2003b). One such regulatory co-factor is a protein called Gle1. By directly regulating the ATPase activity of distinct DBPs at different stages of RNA metabolism, Gle1 is positioned as a global modulator of gene expression (Alcazar-Roman et al., 2006; Bolger and Wente, 2011; Weirich et al., 2006).

A convergence of recent studies has revealed detailed models of Gle1 action at the NPC during mRNA export (Alcazar-Roman et al., 2006; Folkmann et al., 2013; Folkmann et al., 2011; Hodge et al., 2011b; Montpetit et al., 2011; Noble et al., 2011; Tran et al., 2007; Weirich et al., 2006). Historically, studies to characterize these regulatory roles have focused on the human (h) Gle1 and *Saccharomyces cerevisiae* (y) Gle1 orthologues (Figure 1.5) (Murphy and Wente, 1996; Watkins et al., 1998). Further studies have also identified additional Gle1 orthologues in *S. pombe*, *A. thaliana* and *D. rerio* (Braud et al., 2012; Jao et al., 2012; Moon et al., 1998). Conservation of Gle1 polypeptides was first demonstrated by multiple sequence alignment of orthologues from fungi to mammals (Alcazar-Roman et al., 2010; Watkins et al., 1998). Additionally, analysis of yGle1 and hGle1 chimeras has demonstrated a striking degree of functional

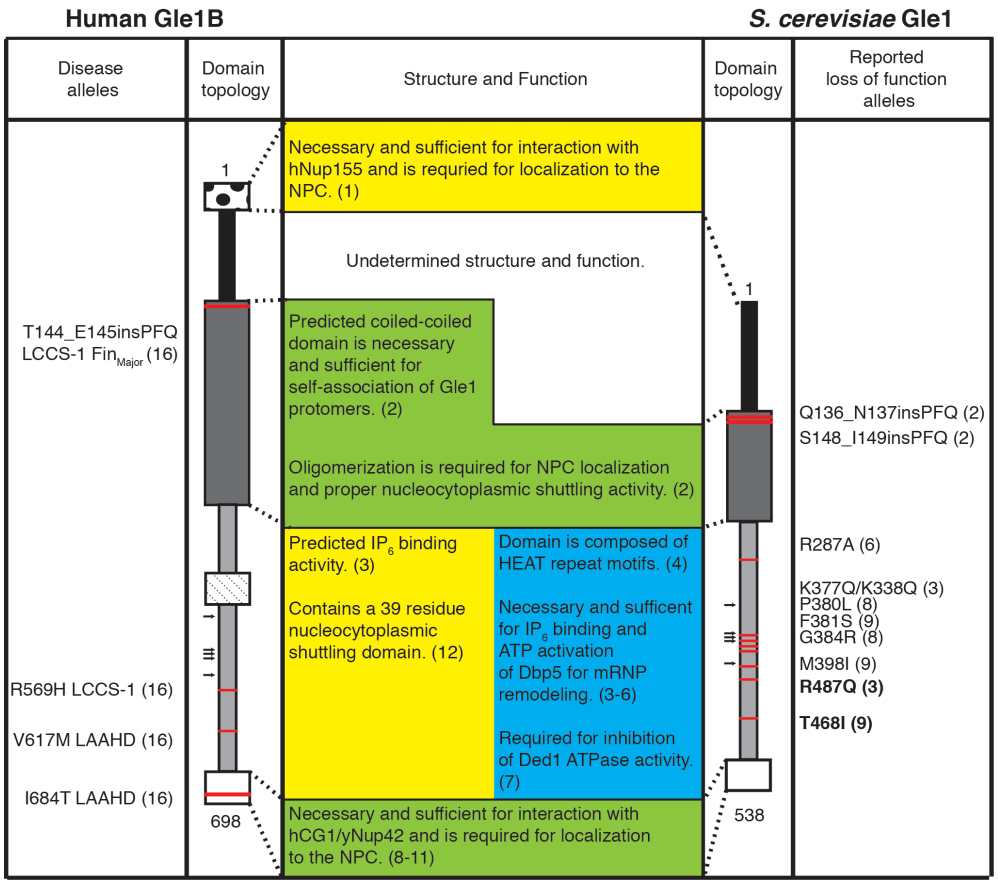

Figure 1.5: Functional and structural domains of Human (Left) and *S. Cerevisiae* (Right) Gle1 proteins. Red dashes indicate the relative position of indicated *gle1* alleles. Black arrows mark the location of the conserved IP_6-coordinating residues. References cited: (1) Rayala et al., 2004 (2) Folkmann et al., 2013 (3) Alcazar-Roman et al., 2010 (4) Montpetit et al., 2011 (5) Tran et al., 2007 (6) Weirich et al., 2006, Alcazar-Roma et al., 2010 (7) Bolger and Wente, 2011 (8) Murphy and Wente, 1996 (9) Stutz et al., 1997 (10) Strahm et al., 1999 (11) Kendirgi et al., 2005 (12) Kendirgi et al., 2003 (13) Nousianinen et al., 2008.

complementation, providing further evidence of conservation (Watkins et al., 1998). Overall, a highly complementary approach utilizing the strengths of both human and yeast model systems has built a rich molecular and cellular understanding of Gle1's roles during gene expression (Alcazar-Roman et al., 2010; Bolger et al., 2008; Bolger and Wente, 2011; Folkmann et al., 2013; Hodge et al., 2011b; Kendirgi et al., 2003; Kendirgi et al., 2005a; Montpetit et al., 2011; Murphy and Wente, 1996; Noble et al., 2011; Rayala et al., 2004; Watkins et al., 1998; Weirich et al., 2006). While technical restraints have limited a completely parallel or duplicative analysis in both these model systems, each has provided essential insight into the Gle1 function. Specifically, x-ray crystallographic and biochemical analysis of yGle1 have yielded valuable details of molecular interactions, whereas the use of human cell lines has provided insight into the cellular dynamics of hGle1. Although studies have highlighted potential subtle differences between orthologues, the high degree of sequence and functional conservation infers that Gle1 proteins across different phyla operate via a common molecular paradigm.

Identified in a *S. cerevisiae* synthetic lethal screen with a *nup100Δ* mutant strain, Gle1 (GLFG lethal mutant complementation group 1) was originally documented as an essential mRNA export factor (Murphy and Wente, 1996). Several studies in human cells have since demonstrated that the function in mRNA export is fully conserved (Kendirgi et al., 2003; Kendirgi et al., 2005a; Watkins et al., 1998). Overall, the domain topology of hGle1B and yGle1 is generally shared (Figure 1.5), although alternative splicing produces two hGle1 isoforms: hGle1B is larger and spans 1-698 amino acid residues, whereas hGle1A lacks the proximal carboxyl (C)-terminal domain (from 655 to 698 residues) (Kendirgi et al., 2003). Both yGle1 and hGle1B localize at steady state to

the nuclear rim and specifically to the NPC; however, diffuse cytoplasmic pools are also observed (Kendirgi et al., 2003; Murphy and Wente, 1996; Strahm et al., 1999). Nucleocytoplasmic shuttling activity is conferred for hGle1 by a 39 amino acid C-terminal region (Kendirgi et al., 2003). While this primary amino acid motif is not conserved in yGle1, immuno-EM analysis shows yGle1 is localized to both sides of the nuclear envelope, suggesting that it also shuttles between the two cellular compartments (Miller et al., 2004).

Targeting of Gle1 to the nuclear rim for mRNA export is achieved through interactions with specific NPC nucleoporins (Nups) on the cytoplasmic fibrils. At its C-terminus, yGle1 binds to yNup42. Likewise, the Nup42 human homologue hCG1 binds the C-terminal domain specific to hGle1B (Figure 1.2) (Kendirgi et al., 2005a; Murphy and Wente, 1996; Rayala et al., 2004; Strahm et al., 1999; Stutz et al., 1997). Indeed, the hGle1A isoform that lacks the hCG1 binding region shows minimal steady state nuclear rim localization and is predominantly cytoplasmic (Kendirgi et al., 2005a). Via a unique amino (N)-terminal 30 amino acid binding site, hGle1 also interacts with hNup155 (Figure 1.2) (Rayala et al., 2004). A third domain that plays an essential role in Gle1 function and NPC dynamics is a shared predicted coiled-coil domain located in the N-terminal half (Figure 1.2). Acting at the terminal step of export, Dbp5 and Gle1 localize to the NPC cytoplasmic face of the NPC through distinct Nup interactions: hDbp5 with hNup214 (yNup159), and hGle1 with hCG1 (yNup42) and hNup155, respectively (Kendirgi et al., 2005a; Murphy and Wente, 1996; Rayala et al., 2004; Schmitt et al., 1999; Strahm et al., 1999; Stutz et al., 1997; Weirich et al., 2004b). Prior studies have documented an important role for the small molecule inositol hexakisphosphate (IP_6) in

both mRNA export and translation termination. Specifically, IP_6 plays the critical role of bridging the interaction between Gle1 and Dbp5 (Alcazar-Roman et al., 2010; Montpetit et al., 2011; Noble et al., 2011).

Previous studies have documented that yGle1 also functions in the cytoplasm to regulate translation (Bolger et al., 2008). Specifically, yGle1 in conjunction with IP_6 activates yDbp5's ATPase activity to remodel the mRNP of the translation termination complex (Alcazar-Roman et al., 2010; Bolger et al., 2008). Additionally, yGle1 has a role in translation initiation, acting in this process independently of IP_6 and Dbp5. Here, yGle1 inhibits the ATPase activity of the DBP Ded1, enabling Ded1 to properly control start site selection (Bolger and Wente, 2011). While a direct role for hGle1 in translation initiation or translation termination has not been documented to date, it has been shown that hGle1 directly interacts with eIF3f, a subunit of the translation initiation machinery (Bolger et al., 2008; Bolger and Wente, 2011; Rayala et al., 2004). This suggests that the function of Gle1 in translation is also conserved.

Taken together, these studies have documented that the protein Gle1 is positioned to impact gene expression at several stages. Interestingly, causal mutations in the human *GLE1* gene have been linked to several human diseases, and the work presented here seeks to elucidate the molecular mechanisms that underpin these disease states. First, a molecular model for Gle1 regulation of Dbp5 during mRNA export at the NPC will be provided.

Mechanism of mRNP export

Understanding how DBPs cycle through stages of nucleotide binding, hydrolysis, and release of products is fundamental to revealing their molecular mechanisms of action. Recent work from our lab and others has made significant progress towards understanding the molecular details for the nucleotide cycle of Dbp5 at the NPC during mRNA export. Taken together, a model has been proposed whereby the nucleotide cycle of Dbp5 has distinct stages (Noble et al., 2011). This is consistent with the proposed mechanism of several other nucleotide-dependent hydrolytic enzymes that are RNA or DNA helicases and is strongly supported by evidence for both *S.cerevisiae* and human Dbp5 indicating distinct nucleotide-dependent protein conformations (Collins et al., 2009; Fan et al., 2009; Henn et al., 2008; Klostermeier, 2011; Noble et al., 2011; Tran et al., 2007).

Further, there is now substantial evidence that Dbp5 protein interaction partners play direct roles in modulating its nucleotide cycle (Alcazar-Roman et al., 2006; Montpetit et al., 2011; Noble et al., 2011; Weirich et al., 2006). Gle1 bound to IP_6 enhances ATP binding by wild-type Dbp5 approximately 2-4 fold, which could account for some of the reported 5-6 fold stimulation of ATPase activity by Gle1-IP_6 (Alcazar-Roman et al., 2006; Noble et al., 2011; Weirich et al., 2006). A dominant negative (DN) Dbp5 protein (Dbp5-R369G) with severely diminished RNA binding inhibits yeast cell growth and mRNA export by sequestering Gle1 (Hodge et al., 2011a). Suggesting that RNA binding functions to release Gle1 from Dbp5. Interestingly, Dbp5 bound to ATP analog, AMP-PNP, has enhanced interaction with Gle1 (Alcazar-Roman et al., 2010). This implies that while Gle1-IP_6 stabilizes ATP binding, at the same time ATP stabilizes

the Dbp5-Gle1-IP_6 interaction, resulting in an overall priming of Dbp5 for ATP hydrolysis. Cooperative binding enhancement for RNA and ATP has also been shown for other DBPs (Burtey et al., 2007; Polach and Uhlenbeck, 2002; Theissen et al., 2008). Taken together, this suggests a mechanism for Gle1-IP_6 stimulation of Dbp5 ATPase activity whereby Gle1-IP_6 binds to Dbp5 to enhance ATP binding, which then facilitates RNA binding to Dbp5. RNA binding to Gle1-Dbp5-ATP complex releases Gle1 from Dbp5. Overall, Gle1-IP_6 promotes the likelihood of ATP hydrolysis. It is possible that Gle1- IP_6 also functions to inhibit ATP release.

Recent work has shown that following ATP hydrolysis, the bound ADP is not efficiently released from full-length yeast Dbp5 (Noble et al., 2011). The release of ADP is critical to allow re-cycling of Dbp5. Strikingly, it was documented that the N-terminal domain (NTD, residues 2-387) of Nup159 acts to promote Dbp5 release of ADP *in vitro* through direct protein-protein interaction (Noble et al., 2011). These *in vitro* biochemical results are directly supported by predictions based on recent x-ray crystallographic structures of complexes assembled from combinations of Δ90dbp5L327V protein, Δ243gle1H337R protein, IP_6, ADP, and nup159NTD (Montpetit et al., 2011). When bound to nup159NTD, the relative position of the Dbp5 N-terminal RecA-like domain changes along with alterations in specific residues of the nucleotide binding pocket (Montpetit et al., 2011). This provides a potential mechanism for promoting release of ADP from the nucleotide binding site in the Dbp5 interdomain cleft (Montpetit et al., 2011). Below a molecular paradigm for function mRNP export at the NPC is proposed.

Targeting of the mRNP to the NPC nuclear face and through the NPC central channel is dependent upon the mRNA export factors Mex67 and Mtr2. By interacting

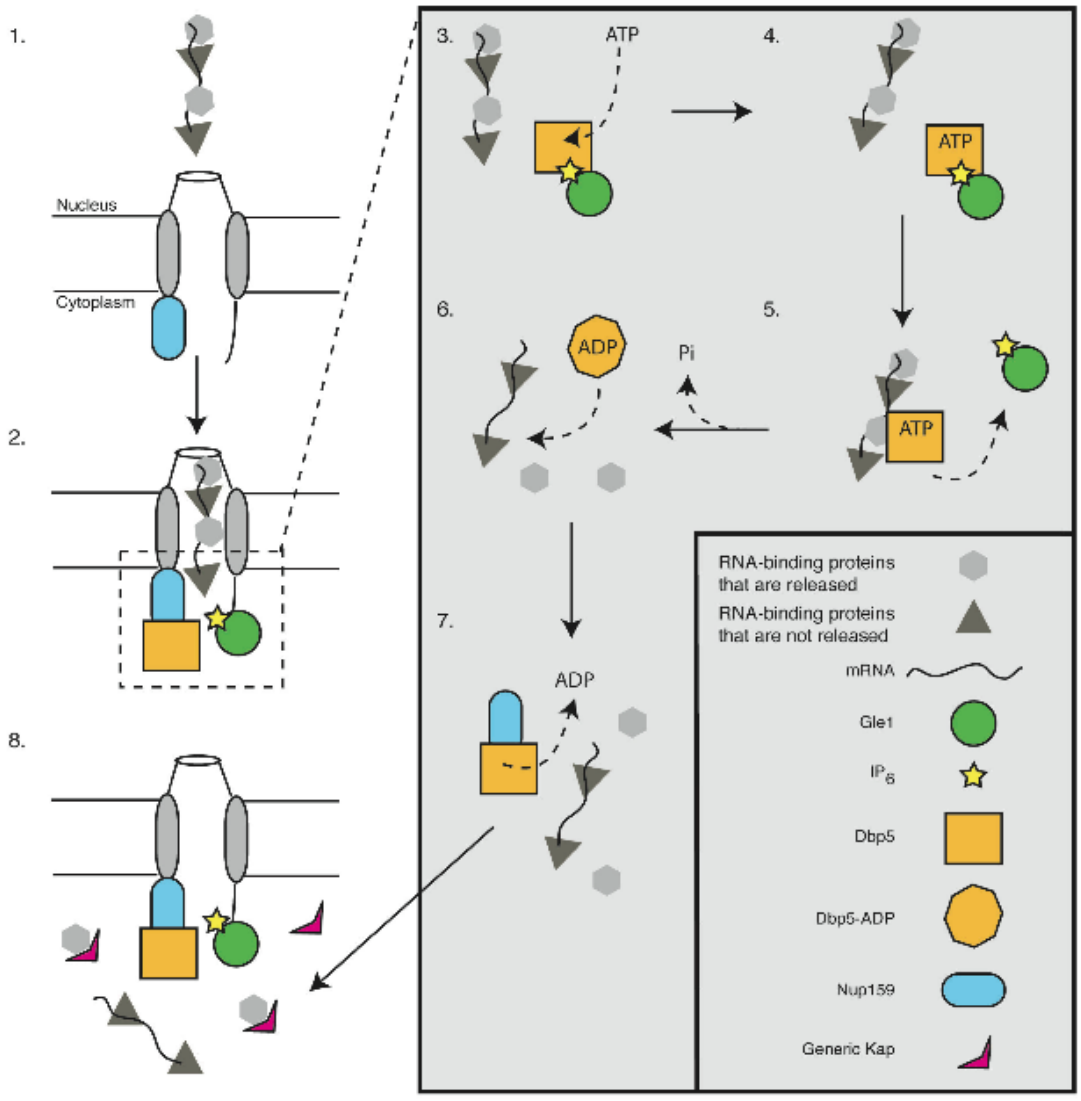

Figure 1.6 Working model for Dbp5/Gle1-IP6/Nup159 mRNA export cycle. During export, the mRNP exits the NPC where it encounters both Gle1-IP6 and Dbp5 at the cytoplasmic fibrils (Steps 1–2). Gle1-IP6 binds Dbp5 and enhances ATP loading (Steps 3–4). The ATP/Dbp5/Gle1-IP6 complex then binds to the mRNP, which stimulates both the release of Gle1-IP6 and the ATP hydrolysis event (Step 5). The change from ATP to ADP triggers a conformational change that drives both the remodeling of the mRNP and release of the mRNA from Dbp5 (Step 6). Dbp5-ADP is then recycled by interaction with Nup159 to release ADP (Step 7), and positioning for binding to Gle1 to begin the cycle again. The released RNA-binding proteins bind to cytoplasmic karyopherins for import back into the nucleus (Step 8).

with both the mRNP and Nups, Mex67 directly facilitates the translocation (Figure 1.6, Step 1). For the terminal export step (Figure 1.6, Step 2), the essential sequence of events that occur at the NPC cytoplasmic face are linked to precise, localized activation of Dbp5 ATPase activity by Gle1-IP_6. Taken together, the *in vitro* and *in vivo* data highlight a mechanism for efficient cycling of both Gle1 and Dbp5 at NPCs (Figure 1.6, Steps 1-8). During export, when the mRNP exits the NPC (Steps 1-2), it encounters both Gle1 and Dbp5 at the cytoplasmic fibrils (Step 2). Gle1 binds to Dbp5 and mediates ATP loading (Step 3). The ATP/Dbp5/Gle1 complex then binds to RNA (Steps 4-5). Binding to RNA stimulates the ATP hydrolysis event, release of Gle1, and displacement of a protein from the mRNP (Steps 5-6). It is unclear if these events happen sequentially or simultaneously. The hydrolysis event triggers a conformational change within Dbp5 (as it goes from ATP-bound to ADP-bound) and this drives remodeling of the mRNP via changes in the RNA binding pocket (Steps 5-6). Dbp5-ADP is then recycled by interaction with Nup159 to release ADP (Step 7). With the overlapping RNA and Nup159 binding sites on Dbp5, the NPC plays a critical role in regulating remodeling cycles. Overall, such a mechanism would allow a single Dbp5 molecule to remain at the pore and thereby to perform multiple remodeling events (Figure 1.6).

Gle1 dysfunction in LCCS-1 and LAAHD pathogenesis

Proper eukaryotic gene expression requires multiple highly orchestrated events centering on the fate of the transcribed mRNA. An extensive and growing catalogue of human diseases are caused by alterations in components of gene expression. Further, given the numerous proteins involved in gene expression, it is likely that more additional

causal mutations will be identified in factors involved in this complex process. It has become clear that perturbations at different steps during gene expression lead to a wide variety of disease pathologies, and that the range of tissues and organs that are influenced also varies. Although the causative genetic alterations are known, the molecular mechanisms underlying these deleterious diseases are poorly understood. Thus, future studies are needed to further dissect the cellular and molecular basis of these disease mutation perturbations. This, in turn, will provide novel insights into the functions of the affected proteins, and the process of gene expression in general.

Lethal Congenital Contracture Syndrome-1 (LCCS-1) is a fetal motor neuron disease, with an estimated incidence of 1:25,000 births in Finland (Nousiainen et al., 2008). An embryonic lethal form of arthrogryposis multiplex congenita (AMC), LCCS-1 pathology is distinguished by total immobility of the fetus. Underlying this phenotype is a lack of anterior horn motor neurons, atrophy of the ventral spinal cord and nearly absent skeletal muscles (Hall, 1985; Herva et al., 1985). In 2008, Nousiainen and colleagues reported a sequence analysis of genomic DNA from LCCS-1 cases that revealed a causal link between the disease and mutation of the *hGLE1* gene. In 51 of 52 cases, the *h-gle1* alleles were homozygous for a single A>G mutation in the third intron of the gene. This homozygous condition is termed *gle1-Fin*$_{Major}$ for its high incidence in the Finnish population, and the mutation generates an illegitimate splice acceptor site that adds nine additional nucleotides to the coding sequence. As such, the *gle1-Fin*$_{Major}$ allele results in an in-frame insertion of a proline-phenylalanine-glutamine (PFQ) tripeptide in the essential N-terminal coiled-coil domain of hGle1 (Figure 1.2) (Nousiainen et al., 2008). Studies of the *gle1-Fin*$_{Major}$ developmental phenotype in a zebrafish model of Gle1

depletion point to apoptosis of the neuronal precursors as the origin of LCCS-1 motoneuron defects (Jao et al., 2012). However, these zebrafish studies also reveal both neurogenic and non-neurogenic developmental defects with *GLE1* depletion, for which expression of the wild type *hGLE1* rescues but *gle1-Fin$_{Major}$* does not. From this work, LCCS-1 is likely not a motor neuron specific disease, but rather all organ precursors are probably impacted (Jao et al., 2012).

In addition to the LCCS-1 pathogenesis for those with homozygous *Fin$_{Major}$* alleles (designated here as LCCS-1^{Fin}), two other mutations have been identified in *hGLE1* with links to the related disease lethal arthrogryposis with anterior horn cell disease (LAAHD) (Nousiainen et al., 2008). LAAHD exhibits a similar but overall milder pathology compared to LCCS-1^{Fin}, with the fetus typically surviving for a short period after birth (Vuopala et al., 1995). In all known LAAHD cases, patients were compound heterozygous for the *Fin$_{Major}$* mutation and an additional point mutation in the region encoding the C-terminal domain of hGle1. Fifty percent of LAAHD cases screened contained a G>A substitution at nucleotide 1849 in exon 13, converting the encoded valine to a methionine (V617M). The remainder of cases contained a T>C substitution at nucleotide 2051 of exon 16, resulting in an isoleucine to threonine substitution (I684T). Interestingly, a third case of compound heterozygosity with a C-terminal mutation occurred in a single patient whose symptoms were categorized as LCCS-1 (termed here LCCS-1^{Het}). This mutation was observed at nucleotide 1706 in exon 12, encoding a histidine in place of an arginine at residue 569 (R569H) (Nousiainen et al., 2008). Each of these three amino acid substitutions (V617M, I684T, and R569H) apparently imparts very different features to the altered protein at their respective position. However, no

studies have been conducted to investigate their perturbations.

Concluding remarks

Nuclear export of mRNAs and their subsequent translation are essential steps in the gene expression pathway and impact all aspects of cell physiology. There is a growing body of evidence suggesting that dysfunctional mRNA metabolism contributes directly to human disease pathology (Cooper et al., 2009; Hurt and Silver, 2008; Renoux and Todd, 2012). This idea is further supported by the genetic linkage of mutant human *GLE1* alleles to the fetal human diseases: LCCS-1 and LAAHD. The work presented here couples fundamental basic science discovery with insights into human disease pathology. In short, we present critical insights into (1) understanding of fundamental principles of NPC structure and function during mRNA export, and (2) defining the cellular and molecular mechanisms underlying two lethal human disease states.

Chapter II

Gle1 functions during mRNA export in an oligomeric complex that is altered in human disease LCCS-1

Introduction[1]

Dysregulation of messenger (m)RNA metabolism has emerged as a significant factor in human disease pathologies, with proper control of mRNA transcription, processing, nuclear export, translation and turnover being critical to cellular homeostasis, signaling, division, and differentiation (Cooper et al., 2009; Hurt and Silver, 2008; Renoux and Todd, 2012). Gle1 is an essential multi-functional protein, conserved from yeasts to humans, that plays a direct role in both mRNA export and translation (Bolger et al., 2008; Murphy and Wente, 1996; Watkins et al., 1998). Mutations in the human (h) *GLE1* gene are responsible for the autosomal recessive Lethal Congenital Contracture Syndrome-1 (LCCS-1) disease (Nousiainen et al., 2008). LCCS-1 is a severe *in utero* form of a heterogeneous group of disorders, termed arthrogryposis multiplex congenita (AMC), that occur in 1 of 3000 human births worldwide (Hall, 1985). LCCS-1 disease pathology is characterized by lack of anterior horn motor neurons and severe atrophy of ventral spinal cord, along with joint and jaw deformities (Herva et al., 1985). Recent work indicates the pathological basis of this disease is attributed to a reduction in Gle1 activity causing the apoptosis of proliferative organ precursors during early development

---

This chapter is adapted from "Gle1 functions during mRNA export in an oligomeric complex that is altered in human disease. Andrew W. Folkmann, Scott E. Collier, Xiaoyan Zhan, Aditi, Melanie D. Ohi, Susan R. Wente. Cell, 2013 155:582-593"

(Jao et al., 2012). However, in LCCS-1, the primary molecular defects in hGle1 cellular roles were unknown.

Previous studies have revealed multiple aspects of Gle1 structure and function in the budding yeast (y) *Saccharomyces cerevisiae* and human cells (Figure 2.1A, 2.1B). The C-terminal domains have extensive conservation, with 27% identical and 27% similar residues found between the regions by reported sequence alignments (from residues 250-538 for yGle1 and 360-659 for hGle1) (Watkins et al., 1998). Further, both have significant spans in their N-terminal regions that are predicted to form coiled-coil structures (Watkins et al., 1998). For mRNA export, hGle1 docks at the nuclear pore complex (NPC) through interactions with the NPC proteins hNup155 and hCG1 (yNup42 for yGle1) (Kendirgi et al., 2005a; Murphy and Wente, 1996; Rayala et al., 2004; Strahm et al., 1999; Stutz et al., 1997). hGle1 is also dynamic and its shuttling between the nucleoplasm and cytoplasm is essential for efficient mRNA export in human cells (Kendirgi et al., 2003). Although humans have a single copy of the *hGLE1* gene, there are at least two alternatively spliced isoforms (hGle1A and hGle1B) (Kendirgi et al., 2003). Whereas hGle1B has distinct steady state localization at the NPC, the hGle1A isoform lacks the C-terminal hCG1-binding domain and is predominantly cytoplasmic. Thus, there are potentially distinct subcellular pools of hGle1A and hGle1B that might reflect multiple roles in gene expression.

During mRNA export and translation, yGle1 regulates the RNA-dependent ATPase activities of specific DEAD-box proteins (DBPs); thus, controlling the action of these DBPs in nucleotide-dependent unwinding of RNA duplexes and/or remodeling of

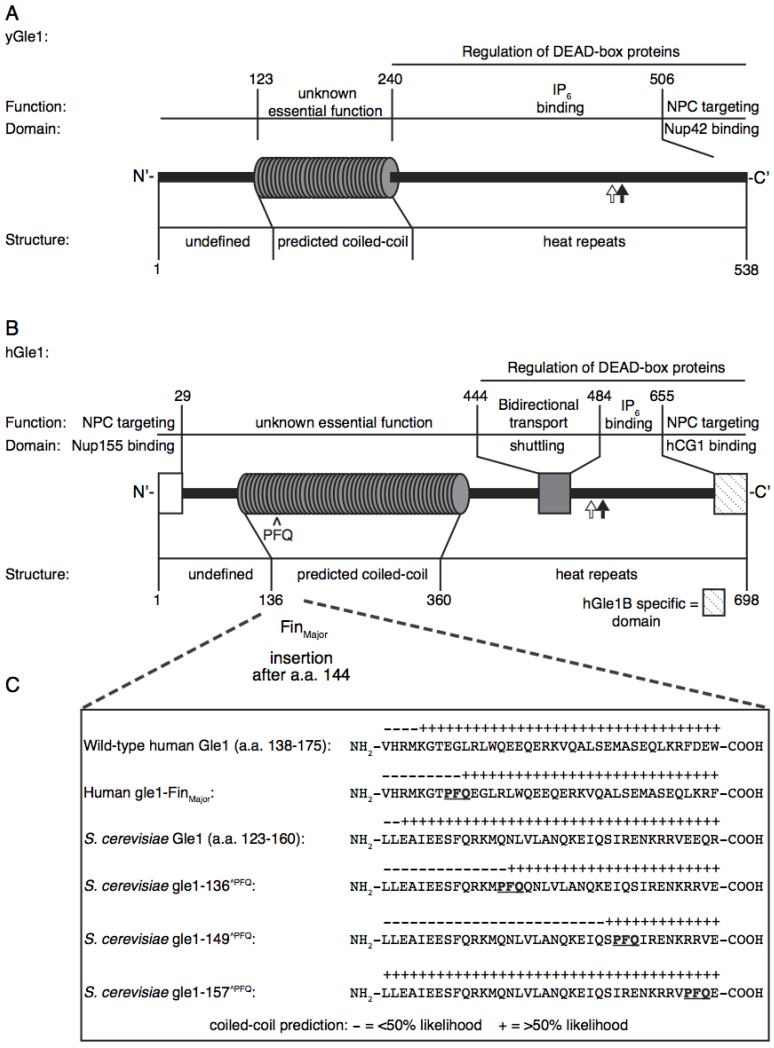

Figure 2.1: Conserved structural and functional elements of Gle1 from *S. cerevisiae* and humans. (A) Diagram depicting functional and structural domains in *S. cerevisiae* (y)Gle1. Black arrow represents the position of the y-*gle1-4* mutation (G382R) (Watkins et al., 1998). White arrow marks the location of conserved IP_6-coordinating residues K377 and K378 (Alcazar-Roman et al., 2010). (B) Diagram depicting functional and structural domains in human (h)Gle1B (adapted from Kendirgi et al., 2005). "PFQ" denotes location of the Fin_{Major} insertion after amino acid 144 in the predicted coiled-coil domain (Nousiainen et al., 2008). Black arrow represents the homologous position (Q548) of the residue mutated in y-*gle1-4* (Watkins et al., 1998). White arrow marks the location of conserved IP_6-coordinating residues K526 and K527 (Alcazar-Roman et al., 2010). (C) Paircoil2-generated structure predictions of Gle1 polypeptide sequences, showing the structural effect of h-gle1-Fin_{Major} and y-gle1 engineered PFQ insertions. (+) indicates >50% probability of coiled-coil structure. PFQ insertions locations are designated by bold underlined typeface.

the mRNA-particle (mRNP) protein composition (Alcazar-Roman et al., 2006; Bolger et al., 2008; Bolger and Wente, 2011; Weirich et al., 2006). Efficient yGle1 function at the NPCrequires inositol hexakisphosphate (IP_6,) binding (Alcazar-Roman et al., 2010; York et al., 1999), and together yGle1-IP_6 triggers Dbp5-dependent mRNP remodeling events required for directional export through NPCs (Tran et al., 2007). Conserved residues in both yGle1 and hGle1 are critical for IP_6 binding and Dbp5 activation (Figure 2.1A-B) (Alcazar-Roman et al., 2010; Montpetit et al., 2011). In translation termination, yGle1-IP_6 directly interacts with Sup45 (eRF1) and is thought to activate Dbp5 for RNP remodeling to promote Sup35 (eRF3) association (Bolger et al., 2008). During translation initiation, yGle1 and hGle1 interact with eIF3 proteins, and yGle1 is known to modulate a different DBP, Ded1, for efficient start site recognition (Bolger et al., 2008; Bolger and Wente, 2011). Thus, Gle1 serves as a multifunctional effector of distinct steps in the gene expression pathway.

The major LCCS-1 causative mutation in *hGLE1* is designated Fin_{Major}, and is a single nucleotide substitution that alters a splice site acceptor in the third intron (Nousiainen et al., 2008). This results in a three amino acid residue insertion (proline-phenylalanine-glutamine, PFQ) in the N-terminal coiled-coil domain of hGle1. LCCS-1 patients are typically homozygous for the Fin_{Major} mutation, whereas heterozygotes show no reported phenotype (Nousiainen et al., 2008). As noted above, the C-terminal domain of hGle1 is linked to DBP regulation, nucleocytoplasmic shuttling, and IP_6 binding (Alcazar-Roman et al., 2010; Kendirgi et al., 2003; Montpetit et al., 2011; Weirich et al., 2006). The N-terminal coiled-coil domain is also essential *in vivo* (Watkins et al., 1998); however, putative protein interaction partners for the coiled-coil domain have not been

defined. It is also unclear whether the coiled-coil domain is involved in mRNA export and/or translation or how it is functionally perturbed in human LCCS-1 disease.

Here we investigated the function of the coiled-coil domain, and in doing so defined the underlying mechanism for LCCS-1 at the molecular level. We show that the coiled-coil domain is critical for Gle1 self-association. Moreover, both hGle1 oligomerization and mRNA export functions are perturbed with the Fin_{Major} protein. For yGle1, the coiled-coil domain is specifically required for mRNA export and not translation. These data reveal a novel step in the mRNA export pathway and provide direct evidence for a defect in hGle1 regulation of mRNA export at the NPC as the molecular mechanism causing the human LCCS-1 disease.

Materials and methods

HeLa cell culture and immunoblotting

HeLa cells were cultured in complete medium (DMEM, Gibco) supplemented with 10% FBS (Atlanta Biologicals) at 37 °C in 5% CO_2. Transient transfections of GFP expression vectors were performed using Fugene6 (Promega) according to manufacturer's instructions. For siRNA experiments, cells were first transfected with a scrambled siRNA or siRNA targeting *hGLE1* using HiPerFect (Qiagen). For live cell imaging experiments, cells were plated in 35mm No. 1.5 glass bottom dishes (Mattek). Before imaging, culture medium was replaced with phenol red-free DMEM (Gibco) supplemented with 10% FBS and 25mM HEPES. For paraformaldehyde fixation, cells were plated on No. 1.5 round coverslips in a 24 well plate (Fisher). For immunoblots, HeLa cells were processed as described (Bolger et al., 2008). Protein bands were visualized with a Li-COR scanner.

Yeast culture methods

Yeast strains were grown at indicated temperatures in either YPD (2% peptone, 2% dextrose, 1% yeast extract) or selective minimal media lacking appropriate amino acids and supplemented with 2% dextrose, and 5-fluoroorotic acid (5-FOA, US Biological) as needed at 1.0 mg/ml.

Translation termination

Translation termination experiments using the tandem β-galactosidase-luciferase reporters were performed as described (Alcazar-Roman et al., 2010; Bolger et al., 2008).

Biochemical analysis of recombinant proteins

MBP-TEV-yGle1(241-528), MBP-TEV-yGle1, MBP-TEV-y-gle1-136$^{\wedge PFQ}$, MBP-TEV-y-gle1-149$^{\wedge PFQ}$, and GST-Dbp5 were purified as described (Tran et al., 2007). The GST-hGle1(1-362), MBP-hGle1(1-362), and MBP-h-gle1(1-365)-Fin$_{Major}$ were expressed in E. coli BL21-RIL (DE3) cells (Stratagene). Bacteria were lysed by sonication in buffer (200mM NaCl, 20mM Tris, pH 7.5), and the soluble fraction was used for affinity chromatography with either amylose resin (New England Biolabs) or glutathione-coupled sepharose (GE Healthcare) according to manufacturer recommendations. Size exclusion chromatography with a S200 column (GE Healthcare) was used to further isolate complexes. PK/LDH-coupled ATPase assays (Noble et al., 2011), soluble binding assays (Kendirgi et al., 2005), and SVAU analysis (Roberts-Galbraith et al., 2010) were performed as described. Velocity scans were analyzed using Sedfit (version 14.0) (Schuck and Rossmanith, 2000). Size distributions were determined for a confidence level of p = 0.95, a resolution of n = 200, and sedimentation coefficients between 0 and 80 S.

Live cell microscopy

All images were processed with ImageJ (NIH) or Adobe Photoshop CS6. Wild-type *S. cerevisiae* (W303) with plasmids harboring either *y-GLE1-GFP* (pBRR118b) or *y-gle1-136$^{\wedge PFQ}$-GFP* (pSW3779) were imaged as described (Noble et al., 2011) using a microscope (BX50; Olympus), Olympus 100×/1.3 UPlanF1 oil immersion objective, and digital charge coupled device camera (Orca-R2; Hamamatsu). For HeLa cells, photo-acceptor bleaching and sensitized emission FRET microscopy experiments were conducted on a confocal microscope (LSM710, Zeiss) using a Zeiss 40×/1.1 C-Apochromat water objective. Photo-acceptor bleaching was performed on HeLa cells co-transfected with: (1) pSW3775 (*Cer-hGLE1B*) and pSW3774 (*Venus-hGLE1B*), (2) mCerulean3-C1 and pSW3774, or (3) pSW3977 (*Venus-hGle1B(362-698)*) and pSW3775. Cell volume was bleached by exciting at 514 nm throughout the targeted region, and FRET efficiency was calculated. For sensitized emission FRET measurements, HeLa cells were co-transfected with either pSW3775 and pSW3774 or mCerulean3 and pSW3774. A normalized FRET (NFRET) signal for indicated regions was determined using standard methods. FRAP was performed on untreated HeLa cells co-transfected with *Pom121-mCherry* and either *GFP-hGLE1B* (pSW1831), *GFP-Fin$_{Major}$* (pSW3903), or *GFP-h-gle1BΔCC* (pSW3976), or on *hGLE1* siRNA treated HeLa cells co-transfected with *Pom121-mCherry* and either siRNA-resistant *GFP-hGLE1B^{R}* (pSW3908), *GFP-Fin$_{Major}{}^{R}$* (pSW3945), or *GFP-h-gle1BΔCC* (pSW3976). All FRAP microscopy experiments were conducted on a confocal microscope (LSM710, Zeiss) using a Zeiss 40×/1.1 C-Apochromat water objective configured for time-lapse acquisition. Bleaching was achieved by exciting at 488 nm throughout the region.

Electron microscopy

Uranyl formate stained samples were prepared as described (Ohi et al., 2004). Samples were imaged on a FEI Morgagni electron microscope operated at an acceleration voltage of 100 kV. Images were recorded at a magnification of 22-36,000x and collected using a 1K x 1K CCD camera (ATM). To prepare samples in vitrified ice, a holey carbon grid (Quantifoil Micro Tools GmbH, Germany) was glow-discharged and used to adsorb gel-filtration purified human Gle1 particles. Grids were blotted and frozen in liquid ethane using a Vitrobot (FEI, Hillsboro, OR). Vitrified specimens were imaged under low-dose conditions at a nominal magnification of 100,000x at defocus values ranging from –3 to –5 μm using a Gatan cryo-transfer holder in a FEI Tecnai 200 kV electron microscope equipped with a field emission electron source (FEI, Hillsboro, OR) and 4K x 4K Gatan Ultrascan CCD.

Yeast two hybrid assays

Yeast two hybrid analysis was performed as described (Clontech, Protocol #PT3024-1). Briefly, PJ69-4A yeast transformed with the indicated G_{BD} an G_{AD} fusion proteins were grown in selective media to an A_{600} of ~0.8 OD units, pelleted and suspended in assay buffer (60mM Na_2HPO_4, 40mM NaH_2PO_4, 10mM KCl, 1mM $MgSO_4$, pH 7.0). Cells were lysed using freeze thaw cycles (4X). β-galactosidase activity was detected using ortho-nitrophenyl-β-galactoside as a substrate and measuring absorbance at 420 nm. Activities reported were normalized to G_{BD}-hGle1B b-galactosidase levels.

Immunoblotting

For western blotting, HeLa cells were lysed in 1% NP-40, 150mM NaCl, 50mM Tris pH 7.5, and protease inhibitors. Samples were resuspended with SDS buffer, separated by

SDS-PAGE, transferred to nitrocellulose, and immunoblotted with anti-hGle1 (Jao et al., 2012), anti-GFP (Molecular Probes), or anti-Actin (Sigma) antibodies. Secondary antibodies conjugated with infrared dyes were visualized with the Li-Cor Odyssey scanner (Lincoln, NE).

***In situ* hybridization**

S. cerevisiae cells were grown and processed as described (Wente and Blobel, 1993). To localize poly(A)$^+$RNA in HeLa cells, cells were fixed seventy-two hours post siRNA treatment and processed as described (Watkins et al, 1998). Both human and yeast cells were incubated for 2 hr with 1 ng/µl Cy3-conjugated oligo d(T) in hybridization buffer containing 125 µg/ml tRNA, 0.5 mg/ml ssDNA and 1% BSA. DNA was stained with 0.1 µg/ml DAPI. Yeast cells were mounted for imaging in 90% glycerol and 1 mg/ml *p*-phenylenediamine, pH 8.0 (Sigma-Aldrich), with human in ProLong Gold Antifade media (Invitrogen). Wide field images were acquired using a microscope (BX50; Olympus) equipped with a motorized stage (Model 999000, Ludl), Olympus 100×/1.3 UPlanF1 objective (Yeast samples) or Olympus 40×/1.3 UPlanF1 objective (HeLa samples), and digital charge coupled device camera (Orca-R2; Hamamatsu). Images were processed with ImageJ (NIH) or Adobe Photoshop CS6. The mean Cy3 intensity was determined for the nuclear and cytoplasmic compartment of individual GFP positive cells. Nuclear/cytoplasmic (N/C) ratios were calculated and plotted on a column vertical scatter plot for indicated conditions.

siRNA depletion and rescue experiments

Allstars Negative Control siRNA and *hGLE1* siRNA (5'CAGCGCGTGAAGCAAGCAGAA-3') were purchased from Qiagen. For all siRNA

depletion experiments, HeLa cells were reverse transfected with 20nM of indicated siRNAs using HiPerFect (Qiagen) reagent following manufacturer's instructions. For live cell imaging experiments, sixty hours post *hGLE1* siRNA treatment, cells were transfected with siRNA resistant ("R") *GFP-hGLE1B*^{R}, *GFP-Fin*$_{Major}^{R}$, or *GFP-h-gle1BΔCC* expression vectors using Fugene 6 reagent (Promega). Seventy-two hours post siRNA treatment, cells were analyzed by FRAP microscopy. For *in situ* hybridization experiments, twenty-four hours post siRNA treatment, cells were transfected with *GFP*, *GFP-hGLE1B*^{R} or *GFP-Fin*$_{Major}^{R}$ expression vectors using Fugene 6 reagent (Promega). Seventy-two hours post siRNA treatment, cells were processed for detection of poly(A)$^{+}$RNA by *in situ* hybridization.

Results

Gle1 self-associates *in vitro* via its coiled-coil domain

To date no protein interaction partners for the Gle1 coiled-coil domain have been reported. Since coiled-coil domains are often utilized to mediate homotypic interactions, we speculated that Gle1 might self-associate. To test this, a series of *in vitro* biochemical experiments were conducted with recombinant purified proteins. First, for *in vitro* soluble binding assays, a glutathione-S-transferase (GST)-tagged N-terminal region of hGle1 (residues 1-362; GST-hGle1(1-362)) was expressed and purified from bacteria. GST-hGle1(1-362) or GST alone was incubated with [^{35}S]methionine-labeled hGle1(1-362) generated with an *in vitro* rabbit reticulocyte lysate system and glutathione-Sepharose beads. Bound [^{35}S]-hGle1(1-362) was eluted and analyzed by SDS-PAGE and autoradiography. An increased level of [^{35}S]-hGle1(1-362) was bound with GST-

hGle1(1-362) as compared to GST alone (Figure 2.2A). This suggested that the coiled-coil domain is sufficient to mediate self-association.

As an independent assessment of Gle1 self-association, sedimentation velocity analytical ultracentrifugation (SVAU) was employed. For this, recombinant maltose-binding-protein (MBP)-hGle1(1-362) was purified from bacteria (Figure 2.2B). MBP-hGle1(1-362) protomer itself has a predicted molecular mass of 0.084 MDa. Strikingly, MBP-hGle1(1-362) sedimented in a series of distinct peaks corresponding to at least eight species with high relative molecular masses ranging from 0.096 MDa to 2.0 MDa (Figure 2.3A). As controls, we examined purified MBP alone and a purified recombinant yGle1 polypeptide for the C-terminal domain (residues 241-538; yGle1(241-538)) by SVAU. For both, a single peak of low molecular mass was observed at 0.044 and 0.040 MDa, respectively (Figure 2.3C-D). Overall, the N-terminal coiled-coil domain of hGle1 was both necessary and sufficient to form large *in vitro* complexes potentially representing higher order oligomers. Next, the oligomeric state of recombinant MBP-h-gle1(1-365)-Fin_{Major} was analyzed by SVAU. Similar to wild-type, MBP-h-gle1(1-365)-Fin_{Major} sedimented in a series of distinct peaks ranging from 0.097 MDa to 1.9 MDa (Figure 2.3B). Thus, the Fin_{Major} protein also self-associated and formed oligomeric complexes.

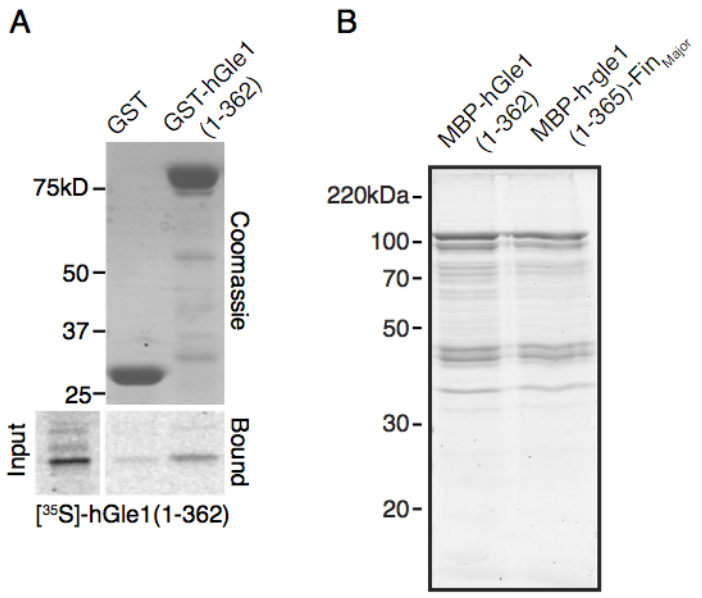

Figure 2.2: The coiled-coil domain of hGle1 is sufficient to mediate self-association (A) hGle1 self-associates *in vitro.* Soluble binding is shown for ^{35}S-labeled hGle1(1-362) incubated with either recombinant GST or GST-hGle1(1-362). Proteins were visualized by Coomassie staining and autoradiography. Gels were analyzed by densitometry to quantify the GST and ^{35}S gel band intensities. There is a 1.6-fold enrichment for ^{35}S-hGle1(1-362) with GST-hGle1(1-362) versus GST alone. (B) Coomassie staining of affinity-purified recombinant MBP-hGle1(1-362) and MBP-h-gle1(1-365)-Fin$_{Major}$ are shown, resolved by SDS-PAGE.

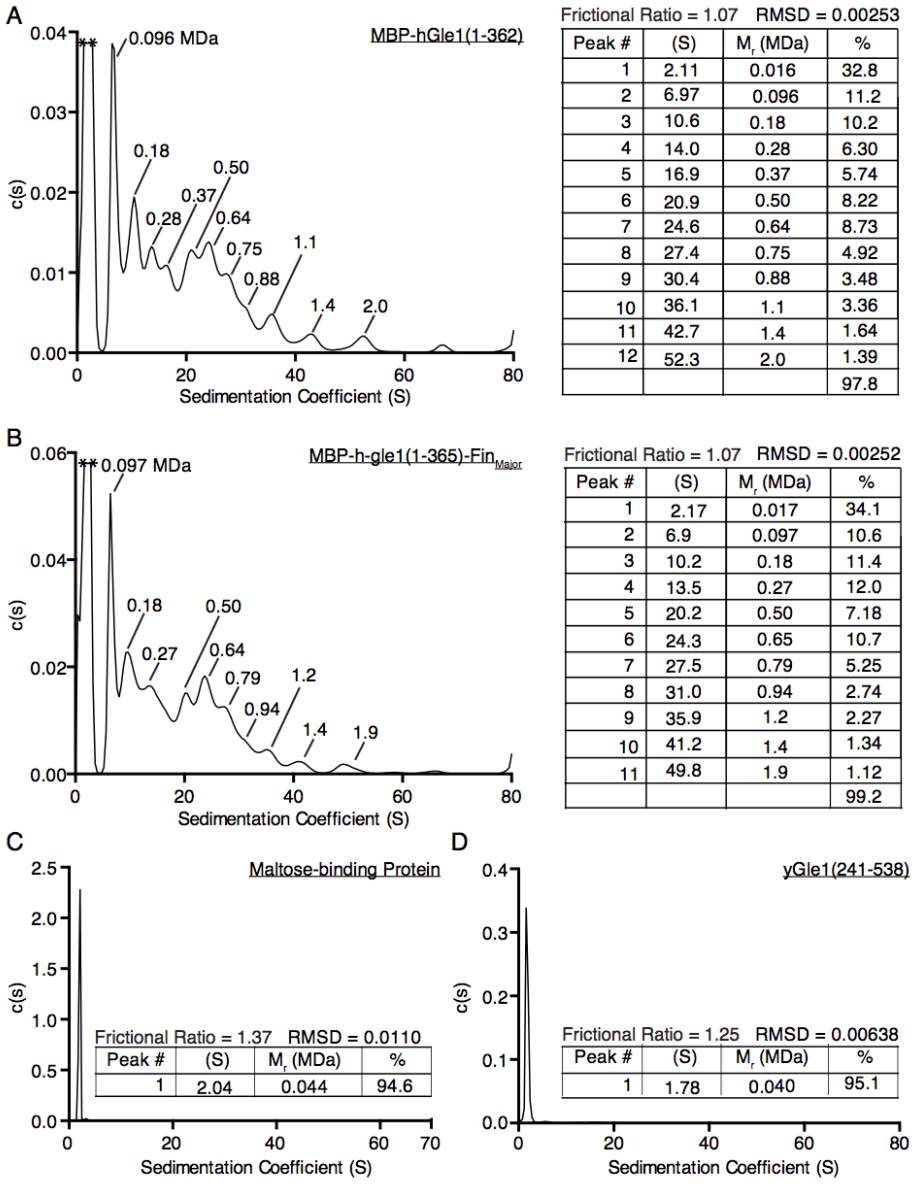

Figure 2.3: hGle1 forms large oligomeric complexes (A-B) hGle1 adopts a variety of higher order oligomeric states *in vitro*. Sedimentation velocity analytical ultracentrifugation (SVAU) was performed on recombinant (A) MBP-hGle1(1-362) and (B) MBP-h-gle1(1-365)-Fin_{Major}. A representative trace demonstrating the formation of higher order oligomeric complexes is shown. ** indicates the presence of a MBP-tagged degradation product. Determined molecular masses and percent abundance are given for indicated peaks. (C-D) The coiled-coil domain is required for Gle1 self-association. SVAU was performed on recombinant (C) MBP and (D) yGle1(241-538). Representative traces are shown. Determined molecular masses and percent abundance are given for indicated peak.

hGle1 oligomers form disk structures that are disorganized with Fin_{Major}

To gain insight into the hGle1 oligomer structure, the high molecular mass MBP-hGle1(1-362) complexes were analyzed using negative stain electron microscopy (NegEM). Purified, recombinant MBP-hGle1(1-362) samples at ~0.5 mg/ml were further fractionated by size exclusion chromatography. NegEM revealed that MBP-hGle1(1-362) formed ring/disk structures, as shown in a representative field (Figure 2.4A) and the montage of individual ring/disks (Figure 2.4B). Measurements of the diameter for 500 particles ranged from ~15 nm to 60 nm, with an average size of 25.8 nm (standard deviation of 6.64 nm) (Figure 2.4F). To further investigate the structures, cryo-electron microscopy (cryo-EM) was conducted, allowing preservation of native protein structure and eliminating negative staining artifacts. The cryo-EM images showed that MBP-hGle1(1-362) oligomers adopted a disk-like shape in solution (Figure 2.4G).

We next examined recombinant MBP-h-gle1(1-365)-Fin_{Major} protein by NegEM. MBP-h-gle1(1-365)-Fin_{Major} also formed disk-shaped particles; however, these appeared structurally disorganized compared to wild-type disks (Figure 2.4C-D). Fields of particles from independent purifications were compared and individual particles binned into three distinct structural categories: (1) aggregates, (2) disordered disks, and (3) round disks (Figure 2.4E). A significantly greater proportion of the MBP-h-gle1(1-365)-Fin_{Major} particle samples were disordered disks. We concluded that the PFQ-insertion perturbs the *in vitro* oligomeric complex.

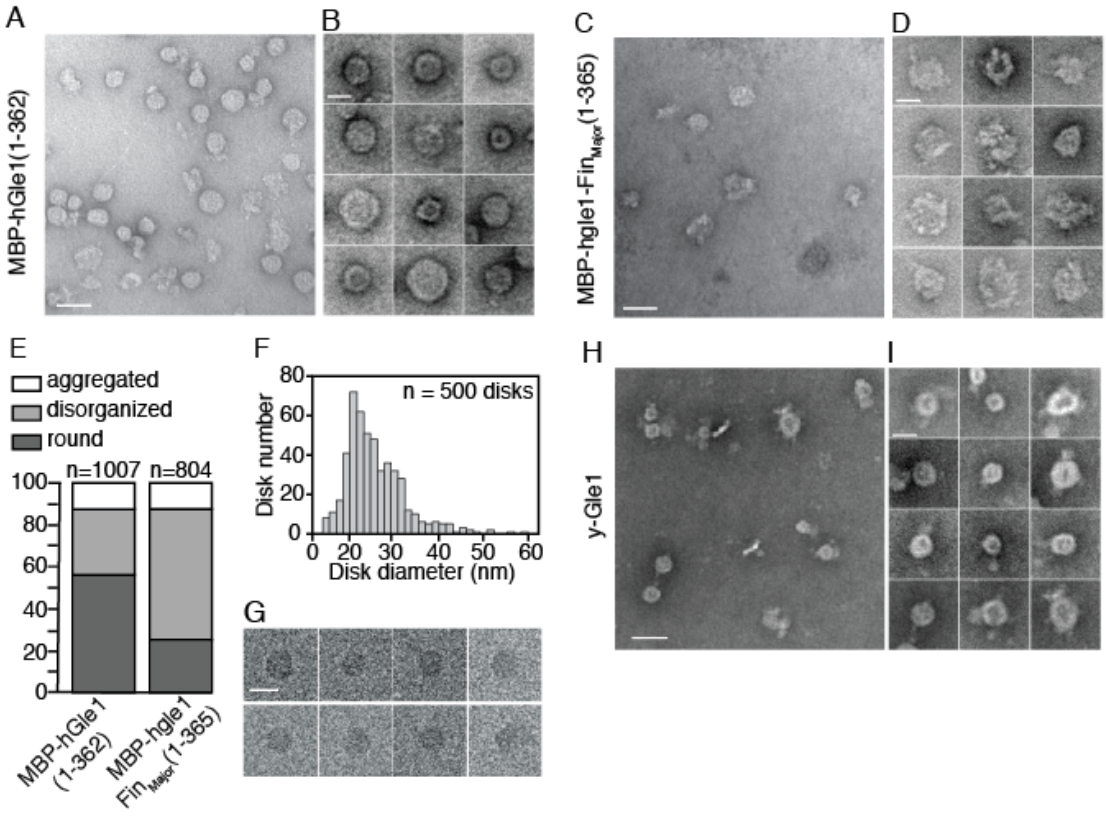

Figure 2.4: Gle1 oligomers form disk structures (A-B) hGle1 forms large circular structures. (A) Representative EM image for purified MBP-hGle1(1-362). Bar, 50 nm. (B) Gallery of individual MBP-hGle1(1-362) particles. Bar, 25 nm. (C-E) Fin_{Major} particles are malformed and disorganized. (C) Representative EM image of MBP-h-gle1(1-365)-Fin_{Major}. Bar, 50 nm. (D) Gallery of individual MBP-h-gle1(1-365)-Fin_{Major} particles. Bar, 25 nm. (E) Quantification of particle morphology for MBP-hGle1(1-362) and MBP-h-gle1(1-365)-Fin_{Major} samples, categorized as aggregates, disorganized, or round. (F) hGle1 particles vary in diameter. Histogram of the measured diameter of MBP-hGle1(1-362) particles. (G) hGle1 oligomeric particles form disk-like structures. CryoEM images of MBP-hGle1(1-362) disk-shaped structures in vitrified ice. Bar, 25 nm. (H-I) Oligomeric disk structures are conserved through evolution. (H) Representative EM image of recombinant yGle1. Bar, 50 nm. (I) Gallery of individual yGle1 particles. Bar, 25 nm.

Gle1 oligomerization is structurally conserved

We hypothesized that recombinant yGle1 would also form disk-like oligomeric structures. To investigate this, recombinant untagged full-length yGle1 was purified and further fractionated by size exclusion chromatography. By negative stain EM, similar to MBP-hGle1(1-362), yGle1 formed disk-like structures (Figure 2.4H-I). Importantly, as isolation of untagged full-length hGle1 was technically not possible, analysis of full-length, untagged yGle1 provided strong evidence that disk structure formation was intrinsic to Gle1 and not an artifact of either the MBP tag or an isolated N-terminal domain. Moreover, the structural characteristics of the oligomer were conserved between yGle1 and hGle1.

hGle1 self-associates in living cells

To test whether hGle1 self-associates in human cells, Forster resonance energy transfer (FRET) microscopy was used. Plasmids expressing hGle1B tagged with mVenus (Venus) or mCerulean3 (Cer3) were co-transfected into HeLa cells. Twelve hours post-transfection, FRET measurements were made in living cells using photo-acceptor bleaching FRET microscopy (Figure 2.5A). Strikingly, a FRET interaction of Cer3-hGle1B and Venus-hGle1B was detected in the cytoplasm (9.19% FRET efficiency) and in the nucleoplasm (5.85% FRET efficiency). In comparison, the percent FRET efficiency between Cer3 alone and Venus-hGle1B was low (<1.25%) in both the cytoplasm and nucleoplasm. As an additional control, a Venus fusion protein for only the hGle1B C-terminal region (residues 362 to 698) was tested. Only low FRET efficiency (<2.0%) for both the nucleoplasm and cytoplasm was detected with co-

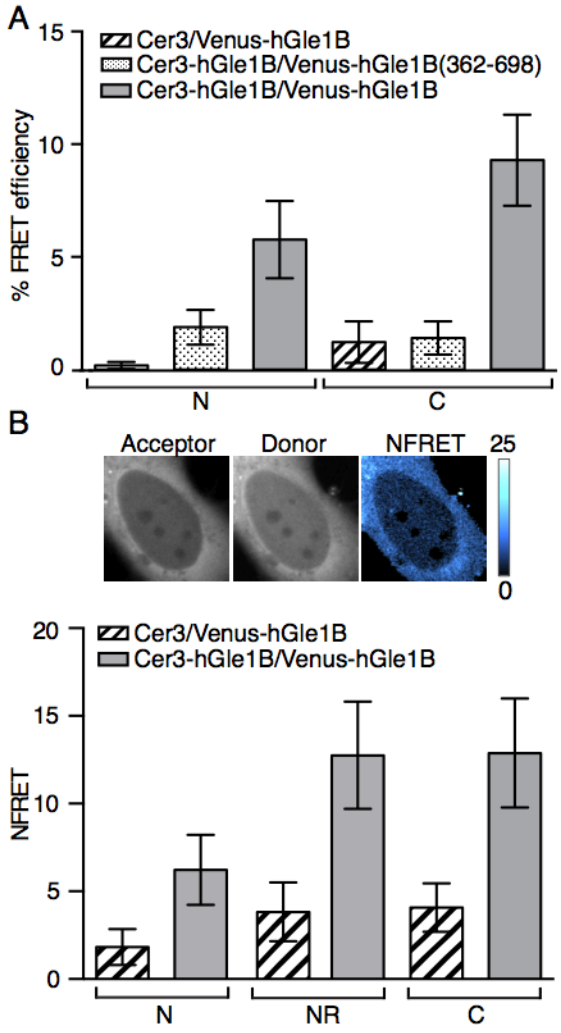

Figure 2.5: hGle1B self-associates in living cells (A) hGle1B self-associates in living cells. Analysis of hGle1B interactions by acceptor photobleaching FRET microscopy in HeLa cells expressing the indicated fluorescent protein FRET pairs. FRET efficiencies of indicated regions were measured. Nucleoplasm and cytoplasm are designated by "N" and "C", respectively. Error bars represent mean $\pm$ 95% confidence interval (CI) with $n \geq 20$ cells from two independent experiments. (B) hGle1B self-associates at the nuclear rim. Analysis of sensitized emission FRET at the nuclear rim in HeLa cells expressing the indicated proteins. Shown are representative images of Venus-hGle1B (acceptor), Cer-hGle1B (donor) and the normalized FRET (NFRET) intensity map signal, *top*. Bar, 10μm. Bar graph depicts the NFRET signal for indicated regions, *bottom*. Nucleoplasm, cytoplasm, and nuclear rim are abbreviated as "N","C", and "NR", respectively. Error bars for each condition represent mean $\pm$ 95% CI with $n \geq 15$ cells from at least two independent experiments.

expression of Cer3-hGle1B and Venus-hGle1B(362-698) (Figure 2.5A). Thus, the coiled-coil domain was required to mediate hGle1B self-association in living cells.

During the acceptor bleaching event (~50 seconds), subtle movement of the nuclear rim prevented accurate FRET measurements using the photo-acceptor bleaching method. Thus, sensitized emission FRET measurements were made. In cells expressing Cer3-hGle1B and Venus-hGle1B, we observed a normalized FRET (NFRET) signal in the cytoplasm (12.9), nucleoplasm (6.22), and at the nuclear rim (12.8) (Figure 2.5B). In cells expressing Cer3 and Venus-hGle1B cells, low NFRET (<4.08) signal was detected in all respective locations (Figure 2.5B). Together, these results indicated that hGle1 has the capacity to self-associate, at a minimum, as a dimer pair in living cells.

Fin_{Major} perturbs essential hGle1 function in mRNA export

To investigate whether the *Fin_{Major}* phenotype is due to perturbed mRNA export, translation initiation, and/or translation termination, several independent tests were conducted. Our previous studies found that hGle1 localization at the NPC is dependent on interactions with both hNup155 and hCG1 (Kendirgi et al., 2005a; Rayala et al., 2004), and that hGle1 interacts with the translation initiation factor eIF3f (Bolger et al., 2008). Using the yeast two-hybrid assay, G_{BD}-hGle1B and G_{BD}-Fin_{Major} DNA-binding domain (BD) bait proteins were analyzed with respective activation domain (AD) G_{AD}-hCG1, G_{AD}-hNup155, or G_{AD}-eIF3f prey proteins, with b-galactosidase expression as the interaction readout. In all cases, the G_{BD}-Fin_{Major} was similar to wild-type G_{BD}-hGle1B (Figure 2.6A). This suggested that the Fin_{Major} protein was properly folded.

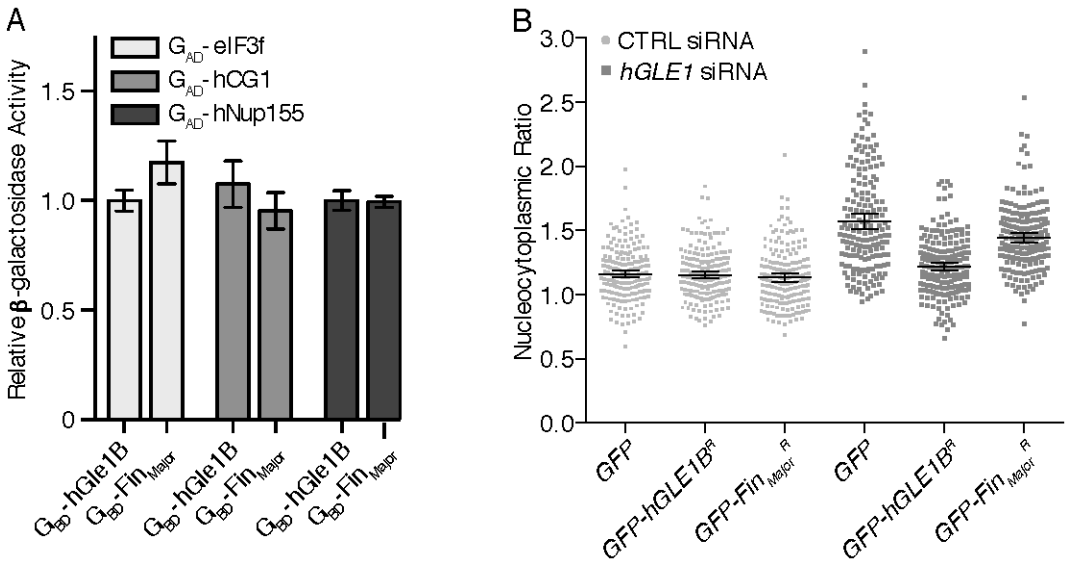

Figure 2.6: Exogenous expression of Fin_{Major} protein does not rescue *hGLE1* siRNA depletion phenotype (A) Known Gle1 yeast two hybrid interactions are intact in *h-gle1-Fin_{Major}* mutant. Shown are yeast two hybrid interactions of G_{AD}-hNup155, G_{AD}-eIF3f, and G_{AD}-hCG1 with either G_{BD}-hGle1B or G_{BD}-hgle1B-Fin_{Major}, each normalized to wild-type G_{BD}-hGle1B β-galactosidase activity. Error bars represent standard error of the mean from 5 independent experiments. (B) Quantification of the nucleocytoplasmic distribution of poly(A)$^+$RNA in CTRL and *hGLE1* siRNA treated cells transfected with plasmids expressing *GFP*, *GFP-hGLE1B^R*, or *GFP-Fin_{Major}^R* . Total poly(A)$^+$RNA was detected by *in situ* oligo (dT) hybridization. The mean Cy3 intensity was determined for the nuclear and cytoplasmic compartment of individual GFP positive cells. Nuclear/cytoplasmic (N/C) ratios were calculated and plotted on a column vertical scatter plot for indicated conditions. Error bars represent mean ± 95% confidence interval with n ≥ 175 cells from three independent experiments.

Furthermore, the hCG1, Nup155 and eIF3f interactions were not perturbed by the PFQ insertion (Figure 2.6A).

Because the LCCS-1 disease is a homozygous recessive condition, we established a siRNA knockdown and add-back, human cell culture model system. As confirmed by immunoblotting, endogenous hGle1 levels were reduced by transfection of a small interfering RNA (siRNA) targeting *hGLE1* (Figure 2.7A, lane 2). As a control, a scrambled siRNA was tested in parallel (CTRL). To assay mRNA export, the cellular distribution of bulk poly(A)$^+$RNA in *hGLE1* and CTRL siRNA cells was monitored by *in situ* hybridization with an oligo (dT) probe. Only cells treated with the *hGLE1* siRNA showed robust nuclear accumulation of poly(A)$^+$RNA (Figure 2.7B).

Rescue of the mRNA export defect was analyzed by expressing either *GFP* alone, a GFP-tagged siRNA-resistant (R) *hGLE1B* gene *(GFP-hGLE1B^R)*, or a GFP-tagged siRNA resistant Fin_{Major} gene (*GFP-*$Fin_{Major}{}^R$). For each trial, the nuclear/cytoplasmic (N/C) ratio of the poly(A)$^+$RNA distribution was determined by measuring fluorescence intensity. For CTRL siRNA with expression of *GFP*, *GFP-hGLE1B^R*, or *GFP-*$Fin_{Major}{}^R$, the mean N/C ratio was ~1.2, with no significant difference between the three conditions. In contrast, the mean N/C ratio for expression of only *GFP* with the *hGLE1* siRNA was ~1.6, reflecting nuclear accumulation. Importantly, expression of GFP-*hGLE1B^R* with the *hGLE1* siRNA rescued the mRNA export defect (mean N/C ratio = 1.2) confirming that the *hGLE1* siRNA phenotype was not due to off-target effects (Figure 2.7B, Figure 2.6B). However, most strikingly, expression of the *GFP-*$Fin_{Major}{}^R$ did not rescue the *hGLE1* siRNA poly(A)$^+$RNA nuclear accumulation defect (mean N/C ratio = 1.5). Immunoblotting confirmed expression of the GFP-

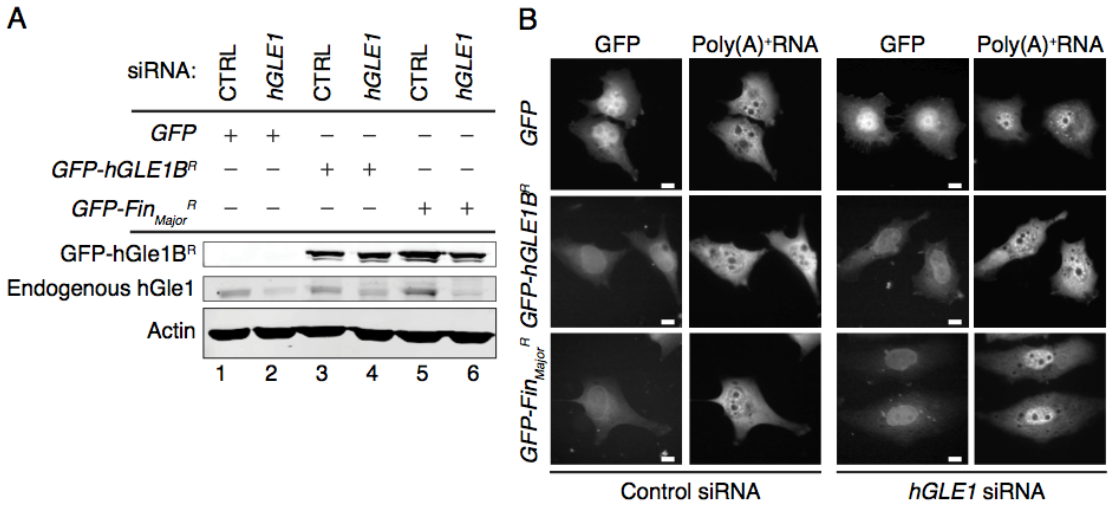

Figure 2.7: Fin_{Major} has a defect in nuclear poly(A)$^+$ RNA export (A) *hGLE1* siRNA treatment depletes endogenous hGle1 protein levels. Immunoblot analysis of hGle1 and actin protein levels in scrambled control (CTRL) or *hGLE1* siRNA-treated HeLa cells transfected with the indicated GFP-tagged proteins. (B) Nuclear poly(A)$^+$ RNA accumulation in *hGLE1* siRNA treated cells expressing the indicated GFP-tagged proteins, detected by *in situ* oligo-dT hybridization and direct fluorescence microscopy. See Figure S2.6B for quantification of the nucleocytoplasmic distribution of poly(A)$^+$ RNA.

hGle1B^{R} (Figure 2.7A, lane 4) and GFP-Fin$_{Major}$^{R} (Figure 2.7A, lane 6) proteins. Moreover, similar to GFP-hGle1B^{R}, the GFP-Fin$_{Major}$^{R} localized to the nuclear rim in both the *CTRL* and *hGLE1* siRNA cells (Figure 2.7B). Thus, we concluded that Fin$_{Major}$ is defective for function in mRNA export.

Fin$_{Major}$ mimic insertions in yGle1 specifically alter mRNA export function

Robust assays for Gle1 roles in translation initiation and translation termination have to date been established only in the yeast *S. cerevisiae* model. In addition, due to protein solubility issues, reconstitution of Gle1-IP$_6$ activation of Dbp5 has only been possible with the *S. cerevisiae* proteins. Thus, to further analyze the potential perturbations of Fin$_{Major}$ function in mRNA export, we conducted a series of experiments with yGle1. First, to directly test whether the yGle1 N-terminal region impacts Dbp5 activation, purified recombinant MPB-yGle1 proteins were assayed for *in vitro* Dbp5 ATPase stimulation. As reported, the C-terminal region of yGle1 (residues 241-538; Δ240Gle1) with IP$_6$ is sufficient for stimulating Dbp5's ATPase activity (Figure 2.8) (Weirich et al., 2006). In side-by-side assays, the relative stimulation activity level for full-length yGle1 and y-Δ240Gle1were similar (Figure 2.8). Thus, *in vitro* activation Dbp5 did not require a functional yGle1 N-terminal coiled-coil domain.

Based on the sequence and structural homologies and the fact that the hGle1 coiled-coil domain can partially complement the role of the yGle1 domain (Watkins et al., 1998), we designed Fin$_{Major}$ mimic insertions in yGle1 for tests of *in vivo* function. *In silico* analysis with the Paircoil2 coiled-coil prediction program showed that insertion of a three amino acid PFQ motif after amino acid 136 or 149 in yGle1 would potentially

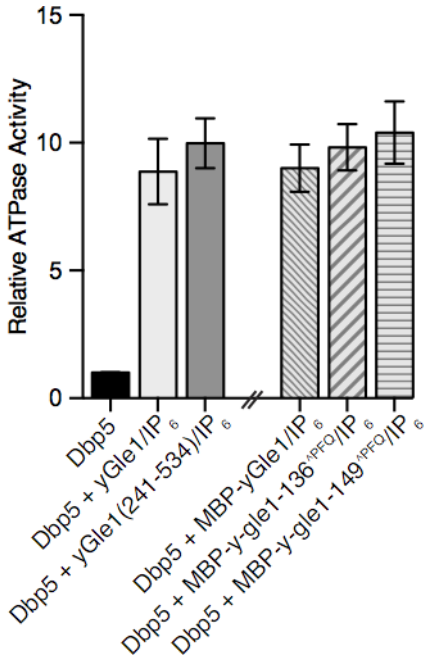

Figure 2.8: Stimulation of Dbp5's ATPase activity *in vitro* does not require coiled-coil domain**.** y-gle1$^{\wedge PFQ}$ proteins stimulate Dbp5 ATPase activity *in vitro.* Graph depicts Dbp5 ATPase activities for purified recombinant wild-type yGle1 and altered y-gle1 proteins, normalized to Dbp5 alone. Standard error of the mean was calculated from 3 independent experiments.

disrupt coiled-coil formation in a manner that would effectively mimic the structural effects of the PFQ found after residue 144 in the Fin_{Major} protein (Figure 2.1C, Table 1-2) (Nousiainen et al., 2008). Importantly, the modeling analysis also predicted regions of the yGle1 coiled-coil domain that should be impacted less by a PFQ insertion. For example, adding PFQ after amino acid 157 in yGle1 was not predicted to change the potential for the region to form a coiled-coil (Figure 2.1C, Table 2). Based on this, *y-gle1-136$^{\wedge PFQ}$*, *y-gle1-149$^{\wedge PFQ}$*, and *y-gle1-157$^{\wedge PFQ}$* mutants were generated. The mutant strains showed no growth defects compared to wild-type *yGLE1*, indicating no global folding defects for the proteins (Figure 2.9A). Moreover, purified recombinant MBP-y-gle1-136$^{\wedge PFQ}$ and MBP-y-gle1-149$^{\wedge PFQ}$ proteins activated Dbp5 to the same relative level as wild-type MBP-yGle1 (Figure 2.8). In addition, live cell direct fluorescence microscopy of yeast cells showed that the GFP-tagged y-gle1$^{\wedge PFQ}$ proteins localized predominantly at the nuclear rim in a similar manner to wild-type GFP-yGle1 (Figure 2.9D) and GFP-Fin_{Major} in HeLa cells (Figure 2.7B).

Next, synthetic fitness defects were tested for double mutants generated from the pairwise combination of the respective *y-gle1$^{\wedge PFQ}$* mutants with mRNA export and/or translation mutants. This included several mRNA export specific mutants (*nup100Δ*, *nup42Δ*, *rat7-1(nup159)*), a translation initiation mutant (*nip1-1*), a translation termination mutant (*sup45-2*), and two mutants with defects in both mRNA export and translation termination (*rat8-2(dbp5)* and *ipk1Δ*) (Bolger et al., 2008; Murphy and Wente, 1996; Stutz et al., 1997). The *y-gle1-157$^{\wedge PFQ}$* mutant did not have synthetic fitness defects in any of the tested double mutants (Figure 2.9B, 2.10A, 2.10B), correlating with the prediction that it would not perturb the coiled-coil region.

> 50% probability of forming coiled-coil domain | < 10% probability of forming coiled-coil domain

***S. cerevisiae* wild-type Gle1**					***S. cerevisiae* gle1-136$^{\wedge PFQ}$**				
Position	**Residue**	**Register**	**P-value**	**Score**	**Position**	**Residue**	**Register**	**P-value**	**Score**
120	T	g	0.29049	-3.04	110	L	d	0.50957	-7.88
121	A	a	0.29049	-3.04	111	L	e	0.50957	-7.88
122	P	b	0.29049	-3.04	112	D	f	0.50957	-7.88
123	L	c	0.07643	4.35	113	N	g	0.50957	-7.88
124	L	d	0.04931	6.23	114	A	a	0.50957	-7.88
125	E	e	0.04931	6.23	115	K	b	0.50957	-7.88
126	A	f	0.04931	6.23	116	N	c	0.50957	-7.88
127	I	g	0.04931	6.23	117	S	d	0.50957	-7.88
128	E	a	0.03041	0.11	118	N	e	0.50957	-7.88
129	E	b	0.0147	10.66	119	A	f	0.50957	-7.88
130	S	c	0.01472	10.66	120	T	g	0.50957	-7.88
131	F	d	0.01472	10.66	121	A	a	0.50957	-7.88
132	Q	e	0.01472	10.66	122	P	b	0.50957	-7.88
133	R	b	0.01437	10.73	123	L	c	0.36269	-4.72
134	K	c	0.01437	10.73	124	L	d	0.31032	-3.51
135	M	d	0.01437	10.73	125	E	e	0.31032	-3.51
136	Q	e	0.01437	10.73	126	A	f	0.31032	-3.51
137	N	f	0.01437	10.73	127	I	g	0.31032	-3.51
138	L	g	0.01437	10.73	128	E	a	0.3024	-3.32
139	V	a	0.01437	10.73	129	E	b	0.23742	-1.67
140	L	f	0.01268	11.14	130	S	c	0.23742	-1.67
141	A	g	0.00985	11.96	131	F	d	0.22157	-1.23
142	N	a	0.00792	12.64	132	Q	e	0.19536	-0.45
143	Q	b	0.00576	13.59	133	R	f	0.19405	-0.42
144	K	c	0.00536	3.81	134	K	g	0.19307	-0.38
145	E	d	0.00381	14.79	135	M	a	0.19397	-0.38
146	I	e	0.00247	15.98	136	P	b	0.19397	-0.38
147	Q	f	0.00168	17.02	137	F	c	0.0537	5.87
148	S	g	0.00168	17.02	138	Q	d	0.02889	8.3
149	I	a	0.00168	17.02	139	Q	b	0.0188	9.83
150	R	b	0.00168	17.02	140	N	c	0.0188	9.83
151	E	c	0.00168	17.02	141	L	d	0.01764	10.05
152	N	d	0.00168	17.02	142	V	e	0.01764	10.05
153	K	e	0.00168	17.02	143	L	f	0.01268	11.14
154	R	f	0.00168	17.02	144	A	g	0.00985	11.96
155	R	g	0.00168	17.02	145	N	a	0.00792	12.64
156	V	a	0.00168	17.02	146	Q	b	0.00576	13.59
157	E	b	0.00168	17.02	147	K	c	0.00536	13.81
158	E	c	0.00168	17.02	148	E	d	0.00381	14.79
159	Q	d	0.00168	17.02	149	I	e	0.00247	15.98
160	R	e	0.00168	17.02	150	Q	f	0.00168	17.02

Table 1: Paracoil2 secondary structure prediction
Shown are the secondary structure predictions for respective yGle1 polypeptide sequences with the program Paracoil2 (McDonnel et al., 2006). The scores represent the pairwise residue probabilities for each amino acid to reside in a coiled-coil domain (Berger et al. 1995). Residues highlighted in red have greater than 50% likelihood of residing in a coiled-coil domain (score ≥3.24). Residues highlighted in gray have less than a 10% likelihood of contributing to a coiled-coil domain (score ≤-5.04).

> 50% probability of forming coiled-coil domain | < 10% probability of forming coiled-coil domain

***S. cerevisiae* gle1-149^PFQ**					***S. cerevisiae* gle1-157^PFQ**				
Position	**Residue**	**Register**	**P-value**	**Score**	**Position**	**Residue**	**Register**	**P-value**	**Score**
120	T	G	0.29049	-3.04	120	T	g	0.29049	-3.04
121	A	A	0.29049	-3.04	121	A	a	0.29049	-3.04
122	P	B	0.29049	-3.04	122	P	b	0.29049	-3.04
123	L	c	0.29049	-3.04	123	L	c	0.07643	4.35
124	L	d	0.29049	-3.04	124	L	d	0.04931	6.23
125	E	e	0.29049	-3.04	125	E	e	0.04931	6.23
126	A	f	0.29049	-3.04	126	A	f	0.04931	6.23
127	J	g	0.29049	-3.04	127	I	g	0.04931	6.23
128	E	a	0.29049	-3.04	128	E	a	0.04931	6.23
129	E	b	0.29049	-3.04	129	E	b	0.04931	6.23
130	S	c	0.29049	-3.04	130	S	c	0.04931	6.23
131	F	d	0.29049	-3.04	131	F	d	0.04931	6.23
132	Q	e	0.28522	-2.91	132	Q	e	0.04931	6.23
133	R	f	0.27602	-2.68	133	R	f	0.04931	6.23
134	K	g	0.27602	-2.68	134	K	g	0.04931	6.23
135	M	a	0.27602	-2.68	135	M	a	0.04931	6.23
136	Q	b	0.27602	-2.68	136	Q	b	0.04931	6.23
137	N	c	0.27602	-2.68	137	N	c	0.04931	6.23
138	L	d	0.27602	-2.68	138	L	d	0.04931	6.23
139	V	e	0.27602	-2.68	139	V	e	0.04931	6.23
140	L	f	0.27602	-2.68	140	L	f	0.04931	6.23
141	A	d	0.22016	-1.18	141	A	g	0.04931	6.23
142	N	e	0.2201	-1.18	142	N	a	0.04931	6.23
143	Q	f	0.21631	-1.07	143	Q	b	0.04931	6.23
144	K	g	0.21631	-1.07	144	K	c	0.04931	6.23
145	E	a	0.21631	-1.07	145	E	d	0.04931	6.23
146	I	b	0.1628	0.59	146	I	e	0.04931	6.23
147	Q	c	0.08813	3.71	147	Q	f	0.04931	6.23
148	S	d	0.07374	4.51	148	S	g	0.04931	6.23
149	P	e	0.04161	6.91	149	J	a	0.04931	6.23
150	F	f	0.00264	15.81	150	R	b	0.04931	6.23
151	Q	g	0.00132	17.65	151	E	c	0.04931	6.23
152	I	a	0.00132	17.65	152	N	d	0.04931	6.23
153	R	b	0.00132	17.65	153	K	e	0.04931	6.23
154	E	c	0.00132	17.65	154	R	f	0.06717	4.93
155	N	d	0.00132	17.65	155	R	g	0.07031	4.72
156	K	e	0.00132	17.65	156	V	a	0.07031	4.72
157	R	f	0.00132	17.65	157	P	g	0.08078	4.10
158	R	g	0.00132	17.65	158	F	g	0.00872	12.34
159	V	a	0.00132	17.65	159	Q	a	0.00395	14.68
160	E	b	0.00132	17.65	160	E	b	0.00183	16.80

Table 2: Paracoil2 secondary structure prediction
Shown are the secondary structure predictions for respective yGle1 polypeptide sequences with the program Paracoil2 (McDonnel et al., 2006). The scores represent the pairwise residue probabilities for each amino acid to reside in a coiled-coil domain (Berger et al. 1995). Residues highlighted in red have greater than 50% likelihood of residing in a coiled-coil domain (score ≥3.24). Residues highlighted in gray have less than a 10% likelihood of contributing to a coiled-coil domain (score ≤-5.04).

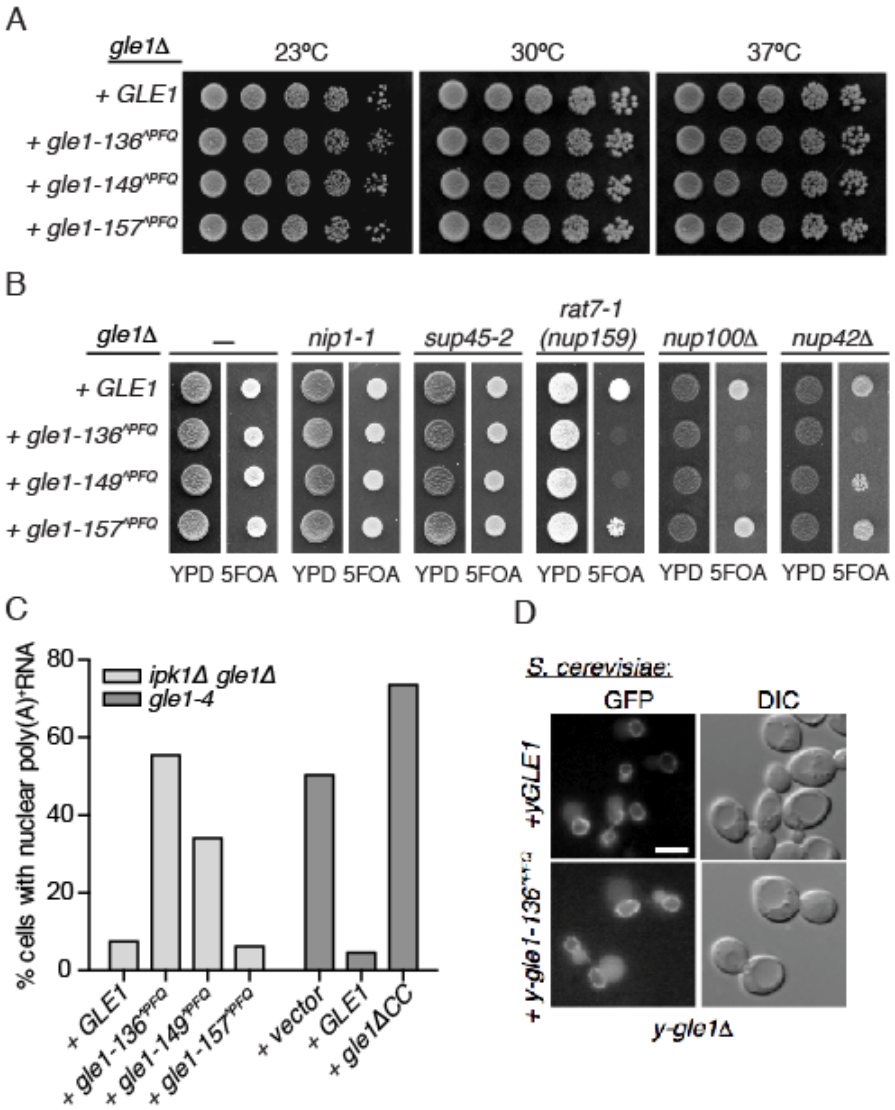

Figure 2.9: The Fin_{Major} mimic y-gle1$^{\wedge PFQ}$ alleles have specific defects in mRNA export (A) *y-gle1$^{\wedge PFQ}$* mutants exhibit no growth defect. Growth of the indicated strains in 5-fold serial dilution on YPD was monitored at the temperatures shown. (B) *y-gle1$^{\wedge PFQ}$* mutants display genetic interactions with mRNA export mutants. Strains bearing the indicated mutation in combination with *y-gle1Δ* harboring a *y-gle1$^{\wedge PFQ}$-LEU* plasmid and a *yGLE1/URA3* plasmid were monitored for growth at 23°C. Failure to grow on synthetic complete media containing 5-FOA indicates synthetic lethality. (C) The yGle1 PFQ insertions that mimic Fin_{Major} perturb mRNA export, and *y-gle1ΔCC* expression does not rescue export defects. Nuclear accumulation of poly(A)$^+$ RNA was detected by *in situ* oligo-dT hybridization following a shift to 37°C for 2 hours (*ipk1Δ y-gle1Δ)* or 1 hour (*y-gle1-4*). Calculations were based on >100 cells/condition. (D) y-gle1-136$^{\wedge PFQ}$ protein localizes to the nuclear rim. A *y-gle1Δ* strain, carrying plasmids harboring vectors expressing either *yGLE1-GFP* or *y-gle1-136$^{\wedge PFQ}$-GFP* were examined by live-cell direct fluorescence microscopy. Bar, 5 μm.

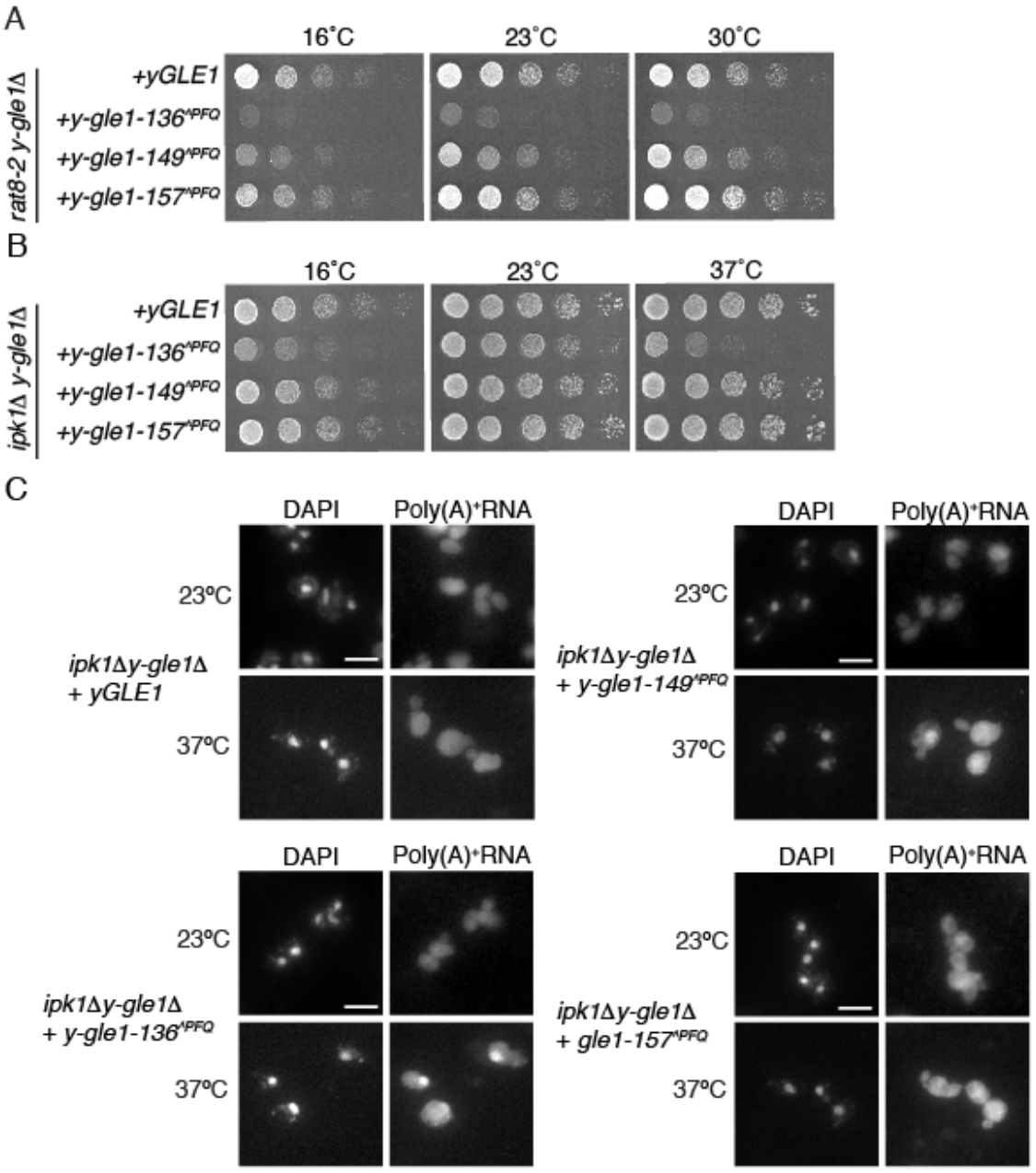

Figure 2.10: Synthetic growth defects are observed in double mutants of *y-gle1*$^{\wedge PFQ}$ with RNA export mutants (A) Synthetic growth defects are observed in double mutants of *y-gle1*$^{\wedge PFQ}$ with *rat8-2 (dbp5).* 5-fold dilutions of the indicated strains were spotted onto YPD and monitored for growth at 16, 23, and 30°C. (B) Synthetic growth defects are observed in double mutants of *y-gle1*$^{\wedge PFQ}$ with *ipk1Δ.* 5-fold dilutions of the indicated strains were spotted onto YPD and monitored for growth at 16, 23, and 37°C. (C) An *ipk1Δ y-gle1Δ* strain carrying plasmids harboring either *yGLE1*, y-*gle1-136*$^{\wedge PFQ}$, *y-gle1-149*$^{\wedge PFQ}$, or *y-gle1-157*$^{\wedge PFQ}$ were analyzed by *in situ* hybridization, under conditions of 23° growth or shift to 37° for 2 hrs. Bar, 5μm.

Strikingly, the *y-gle1-136$^{\wedge PFQ}$* and *y-gle1-149$^{\wedge PFQ}$* mutants had no effect when combined with either *nip1-1* or *sup45-2*. However, the *y-gle1-136$^{\wedge PFQ}$* and *y-gle1-149$^{\wedge PFQ}$* mutants were synthetically lethal when combined with the *nup100Δ* or the *rat7-1(nup159)* mutant (Figure 2.9B). The *y-gle1-136$^{\wedge PFQ}$* was also synthetically lethal with *nup42Δ* (Figure 2.9B). This revealed a separation of function with the *y-gle1-136$^{\wedge PFQ}$* and *y-gle1-149$^{\wedge PFQ}$* mutants having defects in mRNA export and not in translation.

In combination with the *ipk1Δ* or the *rat8-2(dbp5)* mutant, only the *y-gle1-136$^{\wedge PFQ}$* allele showed synthetic growth defects compared to the single mutants (Figure 2.10A-B). Given that *ipk1Δ* double mutants were viable at the permissive growth temperature and Ipk1 (for IP_6 production) is required for both mRNA export and translation termination (Bolger et al., 2008), the *y-gle1$^{\wedge PFQ}$ ipk1Δ* mutants were excellent candidates for assaying functional effects. After shifting to the nonpermissive growth temperature of 37°C, a significant percentage of the *y-gle1-136$^{\wedge PFQ}$ ipk1Δ* and the *y-gle1-149$^{\wedge PFQ}$ ipk1Δ* cells showed nuclear poly(A)$^{+}$RNA accumulation; whereas, the *y-gle1-157$^{\wedge PFQ}$ ipk1Δ* cells did not exhibit a defect (Figure 2.9C and 2.10D). Next, a plasmid-based reporter assay was used to assess translation termination. By monitoring for production of tandem β-galactosidase/luciferase proteins that are separated by either a stop codon, a stem-loop, or no stop codon in their intervening linker, the level of stop codon read-through was determined (Stahl et al., 1995). As reported (Bolger et al., 2008; Alcazar-Roman et al., 2010), the *ipk1Δ* single mutant had ~25% read-through. In comparison, no enhanced defects in termination efficiency were detected for any of the *ipk1Δ y-gle1$^{\wedge PFQ}$* double mutants (Figure 2.11A). As an independent test for translation initiation, we investigated whether expression of a *y-gle1ΔCC* mutant (with an internal

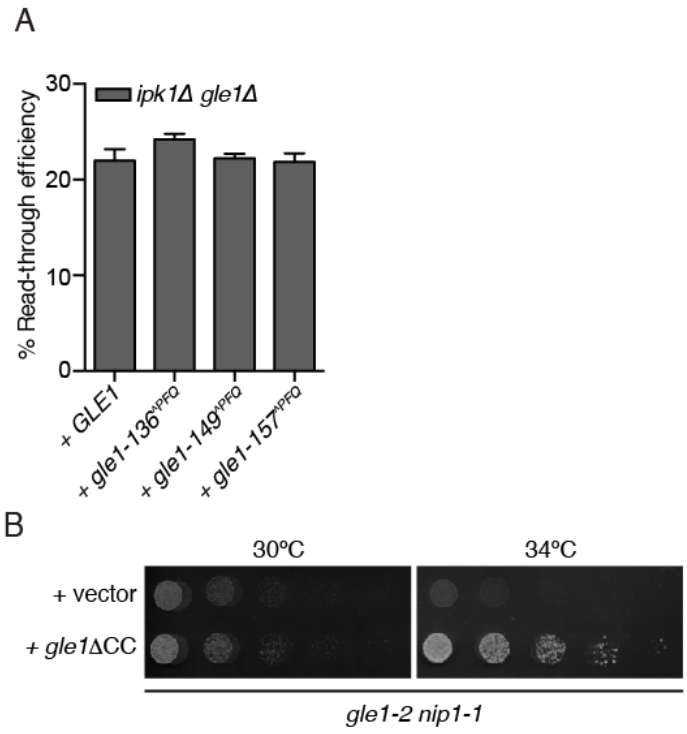

Figure 2.11: The *y-gle1*$^{\wedge PFQ}$ mutants do not exhibit defects in translation (A) *y-gle1*$^{\wedge PFQ}$ mutants exhibit no defect in translation termination. Ratios of luciferase and b-galactosidase activities were determined and read-through efficiency expressed as the percentage from the reporter with a stop codon inserted in-frame into the linker region between the tandem b-galactosidase and luciferase coding sequences (denoted the TMV reporter) compared to the reporter lacking a stop codon (the TQ control) (Stahl et al., 1995). Standard error of the mean was calculated from 3 independent experiments. (B) *y-gle1ΔCC* rescues the temperature sensitivity of *y-gle1-2 nip1-1*. Growth of serially diluted strains on –LEU media was monitored at the indicated temperatures.

in-frame deletion of the sequence encoding the coiled-coil domain) suppressed the growth defects linked to translation initiation in the *y-gle1-2 nip1-1* mutant (Figure 2.11B). This was indeed observed. In contrast, *y-gle1ΔCC* expression did not rescue the mRNA export defect in *y-gle1-4* cells (Figure 2.9C). Thus, *y-gle1*$^{\wedge PFQ}$ mutants that mimic Fin_{Major} had specific defects in mRNA export that correlated with the *Fin*$_{Major}$ results.

yGle1 oligomerization is required *in vivo*

We previously showed that expression of a chimeric yeast-human Gle1 protein rescues temperature sensitive growth properties of a *y-gle1-4 S. cerevisiae* mutant (Watkins et al., 1998). Specifically, when the sequence encoding the essential coiled-coil domain of yGle1 is deleted (*y-gle1ΔCC*), it can be replaced by an in-frame fragment encoding the coiled-coil domain of hGle1 (*+hGLE1 CC*) (Figure 2.12). We further tested a Fin_{Major} coiled-coil (*+Fin*$_{Major}$ *CC*) chimera and it rescued growth of the *y-gle1-4* strain at 30°C to a similar level as the hGle1-CC chimera. However, neither the hGle1-CC nor the Fin_{Major}-CC chimera complemented a lethal *y-gle1Δ* mutant. This indicated that the *y-gle1ΔCC+hGLE1-CC* was not fully functional and in the context of the chimera, the hGle1-CC domain was potentially perturbed in a manner similar to Fin_{Major}. Building on this, we investigated if swapping in a heterologous oligomerization domain would complement functionality *in vivo*. Expression of a chimeric protein with the coiled-coil region of yGle1 swapped for that of the well-characterized transcription factor Gcn4 (O'Shea et al., 1991) (*+GCN4*) partially rescued the temperature sensitive *y-gle1-4*

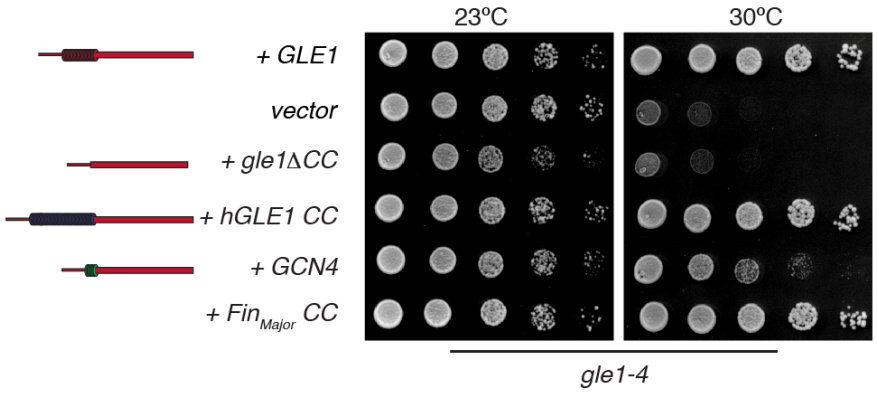

Figure 2.12: Oligomerization of Gle1 is required for function *in vivo*. Mutant y-*gle1-4* strains harboring plasmids expressing *yGLE1*, vector only, *y-gle1ΔCC*, *y-gle1ΔCC+hGLE1-CC, y-gle1ΔCC+GCN4,* or *y-gle1ΔCC+Fin$_{Major}$-CC* were monitored for growth in 5-fold serial dilution on -LEU media at the temperatures shown. (Left) Schematic representation of the coiled-coil chimeric proteins with yGle1 (red), Gcn4 (yellow), hGle1 (Green), and Fin$_{Major}$ (Green with white bar indicating PFQ insertion).

phenotype (Figure 2.12), revealing that oligomerization is important for yGle1 function *in vivo*.

Nucleocytoplasmic shuttling of Fin_{Major} is inhibited

Proper hGle1 nucleocytoplasmic shuttling is critical for mRNA export and requires a unique 39-amino acid span in the C-terminal region (Figure 2.1B) (Kendirgi et al., 2003). Given that Fin_{Major} was defective in mRNA export and oligomer structure but still showed steady state localization at the nuclear rim (Figure 2.7), we examined GFP-Fin_{Major} dynamics in living cells using fluorescence recovery after photobleaching (FRAP). Due to the homozygous recessive *Fin_{Major}* disease phenotype, experiments were conducted in HeLa cells with and without *hGLE1* siRNA treatment (as in Figure 2.7). Nuclei of cells transiently expressing a respective GFP-tagged protein were photobleached and the nuclear GFP fluorescence was monitored over time (Figure 2.13 and 2.14). The FRAP data sets were fit with a one-phase exponential association model. Importantly, the relative $t_{1/2}$ for wild-type GFP-hGle1B nuclear signal after FRAP in untreated HeLa cells (Figure 2.13A and 2.13C) was 12.3 min and correlated with our previous measurements by fluorescence loss in photobleaching (Kendirgi et al., 2003). When GFP-Fin_{Major} was assayed by FRAP in untreated cells, the $t_{1/2}$ was not significantly different from wild-type GFP-hGle1B (Figure 2.13A and 2.13C). This was expected due to the homozygous recessive nature of the LCCS-1 disease pathology (Nousiainen et al., 2008). FRAP analysis of wild-type GFP-hGle1B^R in *hGLE1* siRNA treated cells showed similar shuttling dynamics ($t_{1/2}$ 10.3 min) as compared to the presence of endogenous hGle1 (Figure 2.13B and 2.13D). However, strikingly, the shuttling

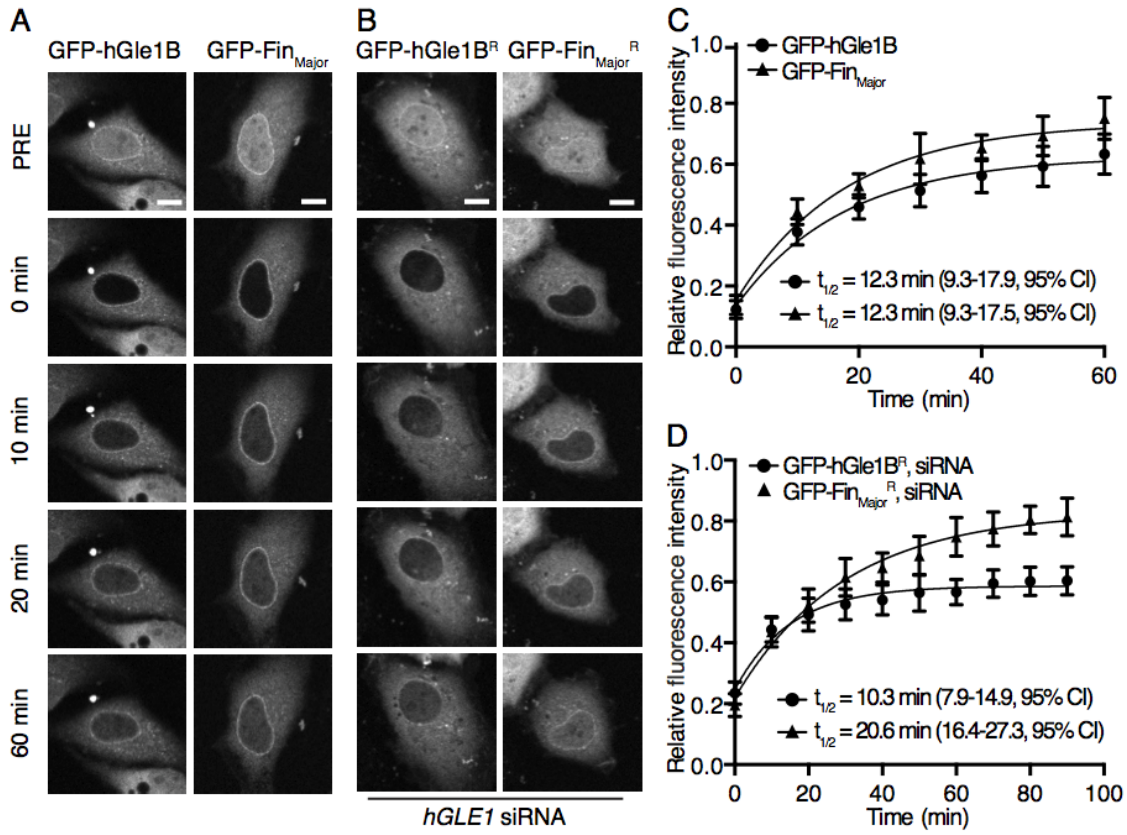

Figure 2.13: Nucleocytoplasmic shuttling dynamics are altered for the LCCS-1 Fin_{Major} disease protein (A-B) Fin_{Major} has altered nuclear shuttling activity. (A) FRAP analysis of HeLa cells expressing *GFP-hGLE1B* and *GFP-Fin*$_{Major}$. (B) FRAP analysis of *hGLE1* siRNA-treated HeLa cells expressing siRNA-resistant *GFP-hGLE1B*^{R} or *GFP-Fin*$_{Major}^{R}$. Bar, 10μm. (C-D) Recovery curves of the experimentally determined bleached region, fit with a one-phase association model. Error bars represent mean ± 95% CI with n ≥ 12 cells from 3 independent experiments.

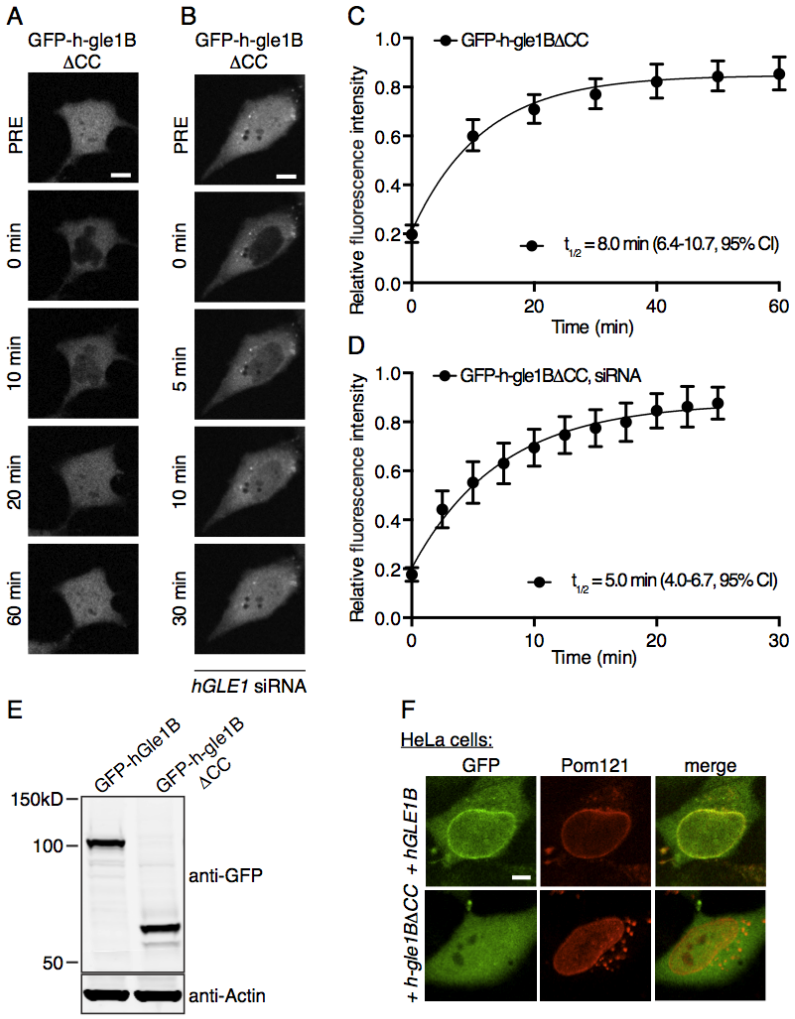

Figure 2.14: The coiled-coil domain is required for localization to the nuclear rim (A-B) Deletion of the coiled-coil domain alters hGle1 nuclear shuttling activity. (A) HeLa cells expressing *GFP-h-gle1BΔCC* were analyzed by FRAP microscopy. Representative FRAP time series images for GFP-tagged h-gle1BDCC is shown. Bar, 10µm. (B) FRAP analysis of *hGLE1* siRNA-treated HeLa cells expressing GFP-h-gle1BDCC. Representative FRAP time series images are shown. Bar, 10µm. (C-D) Recovery curves of the experimentally determined bleached region, fit with a one-phase association model. Error bars represent mean ± 95% confidence interval with n ≥ 9 cells from three independent experiments. (E) Immunoblotting for GFP-hGle1B and GFP-h-gle1BDCC was performed with total HeLa cell lysates from respectively transfected cultures, and shows approximately equivalent expression levels relative to the actin levels in each respective lysate. (F) Deletion of the coiled-coil domain of hGle1 perturbs localization to the nuclear rim. HeLa cells expressing *mCherry-Pom121* and either *GFP-hGLE1B* or *GFP-h-gle1BΔCC* were visualized by direct fluorescent microscopy. Bar, 10 µm.

dynamics of GFP-Fin_{Major}^{R} were significantly slower ($t_{1/2}$ 20.6 min) in *hGLE1* siRNA treated cells (Figure 2.13B and 2.13D). In sum, as in the LCCS-1 disease state, when expressed as the only hGle1 in the siRNA treated cells, Fin_{Major} had inhibited nucleocytoplasmic shuttling. Thus, the defect in mRNA export was potentially due to the altered Fin_{Major} oligomer structural state impacting nucleocytoplasmic shuttling.

hGle1 requires the coiled-coil domain for NPC localization

The hGle1 coiled-coil domain alone is not sufficient for nuclear rim localization (Kendirgi et al., 2005a). To test if the coiled-coil domain has a role in NPC localization independent of hNup155 and hCG1, we examined the subcellular localization of respective GFP-tagged protein lacking the coiled-coil domain (gle1ΔCC) in HeLa or *S. cerevisiae* cells. HeLa cells were co-transfected with plasmids expressing Pom121-mCherry and either GFP-hGle1B or a GFP-h-gle1BΔCC. As reported, direct fluorescence microscopy in living cells revealed that GFP-hGle1B localized robustly to the nuclear rim overlapping with mCherry-Pom121 (Figure 2.14F) (Kendirgi et al., 2003). In contrast, the nuclear rim signal intensity for GFP-h-gle1BΔCC was markedly reduced. Immunoblotting showed similar expression levels for both GFP-tagged proteins (Figure 2.14F).

If the coiled-coil domain function is conserved, we predicted yGle1 localization to NPCs would also require the coiled-coil domain. In *S. cerevisiae,* plasmids expressing either wild-type yGle1-GFP or ygle1ΔCC-GFP were transformed into wild-type haploid

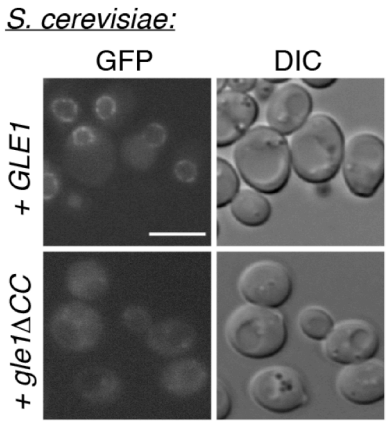

Figure 2.15: The coiled-coil domain of yGle1 is required for localization to the nuclear rim. Wild-type strains expressing GFP-yGle1 or GFP-ygle1ΔCC were grown to mid-log phase at 23°C and visualized by direct fluorescence microscopy. Bar, 5 μm.

cells. By live cell fluorescence microscopy, yGle1-GFP localized to the nuclear rim (Figure 2.15) (Strahm et al., 1999). However, similar to EGFP-hgle1BΔCC, ygle1ΔCC-GFP was not enriched at the nuclear rim. Thus, in both human and *S. cerevisiae* cells, the coiled-coil domain was necessary for proper nuclear rim and NPC localization (Figure 2.15).

We next examined if the deletion of the coiled-coil domain influenced the dynamics of Gle1 in the cell. FRAP analysis revealed that GFP-h-gle1BΔCC shuttled faster than wild-type in both untreated ($t_{1/2}$ 8.0 min versus 12.3 min; Figure 2.14C and 2.13C) and *hGLE1* siRNA treated ($t_{1/2}$ 5.0 min versus 10.3 min; Figure 2.14D and 2.13D) cells. Overall, the hGle1 oligomeric state modulated both NPC localization and nucleocytoplasmic dynamics.

Discussion

In this report, we document a novel requirement for Gle1 self-association during mRNA export and uncover molecular defects underlying a lethal human disease LCCS-1. Our results show that wild-type Gle1 protomers form discrete multimers and higher-order disk structures *in vitro*, with evidence for dimer formation happening in living cells. This self-association occurs through the essential Gle1 coiled-coil domain wherein the LCCS-1 Fin_{Major} disease alteration resides. Importantly, disk structures formed with the Fin_{Major} coiled-coil domain are more disordered and malformed. Moreover, in HeLa cells, the Fin_{Major} protein is defective in mRNA export and has slowed nucleocytoplasmic shuttling. We propose that LCCS-1 disease pathology is due to perturbations in Gle1 oligomerization and shuttling that disrupt efficient nuclear export of mRNA at NPCs.

Coiled-coil domains are often utilized to mediate the formation of biological homo and hetero-oligomeric complexes and directly impact protein function (Burkhard et al., 2001). We speculate that the Fin_{Major} is a distinct perturbation of the hGle1 oligomeric structure compared to the h-gle1-ΔCC that does not oligomerize. This is based on the different effects on nucleocytoplasmic shuttling and steady state NPC localization. Fin_{Major} shuttles slower and is detected at the nuclear rim, contrasted with h-gle1-ΔCC which shuttles faster and is not rim localized. Thus, oligomerization might regulate Gle1 residence time at the NPC, and hGle1 interactions with hNup155 and hCG1 could potentially facilitate Gle1 self-association. It is striking that the Fin_{Major} analogous alleles in *S. cerevisiae* (*y-gle1^PFQ*) specifically disrupt mRNA export function but not yGle1 roles in translation initiation or termination, and that expressing *y-gle1ΔCC* rescues translation initiation. Thus, proper Gle1 self-association might only be strictly required at the NPC.

Our *in vitro* studies reveal that Gle1 forms large oligomeric disk structures with an average diameter of 25.8 nm (Figure 2.3). This was surprising, and such structures have not been previously reported with other isolated NPC associated factors. It is tempting to speculate that these disk structures might be present in the NPC, which measures ~105 nm in total diameter (Maimon et al., 2012). However, there are no reports of such an NPC-associated disk-like particle in the published structural studies of NPCs in intact cells, or of isolated NPCs or nuclear envelopes (Frenkiel-Krispin et al., 2010; Kiseleva et al., 2004; Maimon et al., 2012; Yang et al., 1998). In intact cells, the electron density of such a disk might not be detected via tomography approaches. It is also possible that the Gle1 oligomer dissociates (partially or fully) during NPC or nuclear

envelope isolation. Further studies are needed to investigate these possibilities, and to determine the stoichiometry within the Gle1 oligomer *in vitro* and *in vivo*. Additionally, the presence of Gle1 binding partners *in vivo* will likely play important structural and/or regulatory roles affecting how Gle1 self-associates. Overall, using FRET microscopy, we observed hGle1 self-association in living cells (Figure 2.5) and can conclude that, at a minimum, a dimer interaction exists at the NPC.

Gle1/IP_6 function at the NPC cytoplasmic face triggers Dbp5-mediated mRNP remodeling and facilitates directional mRNA export through the NPC (Alcazar-Roman et al., 2006; Tran et al., 2007; Weirich et al., 2006). As part of the Dbp5 ATPase cycle, release of ADP from Dbp5 is mediated by Nup159 binding at the NPC cytoplasmic face (Noble et al., 2011). Interestingly, Nup159 protomers dimerize by interaction with Dyn2 (Stelter et al., 2007). Thus, both Dbp5 modulators at the NPC (Gle1 for ATP loading and ATPase activation, and Nup159 for ADP release) are at least dimers at the NPC.

As the C-terminal yGle1 domain is sufficient *in vitro* for stimulating Dbp5 ATPase activity, there are at least two working models by which Gle1 self-association might function in mRNA export. First, oligomerization might promote Gle1 enrichment at the NPC and generate a self-organized platform of multiple C-terminal Gle1 domains. This, in turn, could allow stimulation of the same Dbp5 molecule multiple times, or multiple Dbp5 molecules simultaneously, to promote efficient mRNP remodeling and directional mRNA export. Preliminary support for this model can be drawn from the y-gle1ΔCC+GCN4 chimera complementation results, wherein the Gcn4 coiled-coil domain facilitates assembly of parallel aligned dimers (O'Shea et al., 1991).

Alternatively, self-association might allow multiple distinct interactions with individual protomers in a Gle1 oligomer. Based on structural analysis of the yGle1 C-terminal domain (Montpetit et al., 2011), it is possible that the binding interfaces for Dbp5 and Nup42 are mutually exclusive. Thus, Gle1 self-association would allow a dimer (or higher order oligomers) to coincidentally bind the NPC and activate Dbp5 for mRNA export. Our ongoing studies will be aimed at investigating the Nup and Dbp5 binding interfaces on the oligomeric complex.

This work implicates Gle1 dysregulation of Dbp5's mRNP remodeling activity during mRNA export as the key molecular pathological event in LCCS-1. As the RNA-binding protein composition of an mRNP dictates both its regulation and function during gene expression (Muller-McNicoll and Neugebauer, 2013), altered mRNP remodeling during mRNA export likely has global cellular impacts. In addition to LCCS-1, human genetic linkage analysis has identified additional *GLE1* causal mutations that result in the lethal arthrogryposis with anterior horn cell disease (Nousiainen et al., 2008). Further, recent deep sequencing studies report *gle1* mutant alleles in other human diseases (Al-Qattan et al., 2012; Tzschach et al., 2012). For these diseases, it is unclear whether or how hGle1 has cell type specific effects. Indeed, our studies of *GLE1* depletion in zebrafish show potential impacts on multiple proliferative organ precursors (Jao et al., 2012). With Gle1 uniquely positioned to modulate mRNP composition through regulation of multiple DBPs (Alcazar-Roman et al., 2006; Bolger and Wente, 2011; Weirich et al., 2006), we speculate that disruption of specific Gle1 mechanistic steps in export and/or translation results in different pathological outcomes.

Defective oligomerization of the SMN protein has been causally linked to some cases of Spinal Muscular Atrophy (SMA) (Lorson et al., 1998; Pellizzoni et al., 1999). In this case, defects in SMN oligomerization cause ineffective assembly of the small nuclear (sn)RNPs and disruption of pre-mRNA splicing (Shpargel and Matera, 2005; Wan et al., 2005). Our analysis of Gle1 self-association extends this paradigm for perturbations of RNP effector oligomerization, and highlights altered mRNP remodeling as a new molecular disease mechanism. Taken together, this work provides new evidence for the cellular mechanism underlying the lethal human LCCS-1 disease, and impacts the broader understanding of the involvement of defective NPCs, altered mRNA transport and misregulated gene expression in human disease.

Chapter III

Structure-function analysis defines molecular perturbations that underpin Gle1 dysfunction in disease pathology

Introduction[2]

Proper eukaryotic gene expression requires multiple, highly orchestrated events centering on the fate of the transcribed messenger RNA (mRNA): from transcription to translation to degradation. At the core of this regulation are RNA binding proteins (RBPs) that associate with each mRNA transcript to form a messenger ribonucleoprotein (mRNP) complex. Throughout its lifecycle, each mRNP undergoes a series of dynamic changes to its RBP composition that mediate specific functions such as splicing, nuclear export, translation, and degradation (McKee and Silver, 2007; Muller-McNicoll and Neugebauer, 2013). Considering elaborate networks of RNA/protein and protein/protein interactions are coordinated to regulate RNA metabolism, it is expected that perturbing these interactions can have complex, if not pleiotropic, cellular phenotypes. Indeed, alterations in RBPs or factors that influence RBP function have been linked to many human disease states (Cooper et al., 2009; Hurt and Silver, 2008; Renoux and Todd, 2012). These pathologies cover a broad spectrum of tissues, organs, age onset, and severity of phenotype. Although causative biochemical and cellular alterations are known

---

This chapter is adapted from "Insights into mRNA export-linked molecular mechanisms of human disease through a Gle1 structure-function analysis. Adv. Biol. Regul. 2014 54:74-91."

for some of these genetic linkages, the molecular mechanisms underlying many such deleterious diseases are poorly understood.

During the mRNA life cycle, mRNP compositional changes are dictated by the active binding and release of specific RBPs in a process collectively termed RNP remodeling. In several cases, this process is mediated by members of the RNA-dependent ATPase family termed DEAD-box proteins (DBP). The DBP enzymes drive mRNP remodeling through ATP hydrolysis-induced conformational changes that alter the DBP binding to RNA and coincidently RNA-protein interactions (Folkmann et al., 2011; Jankowsky, 2011b; Jankowsky and Bowers, 2006; Jankowsky and Fairman, 2007b; Rocak and Linder, 2004). Interestingly, some DBPs require a protein cofactor to stimulate and regulate their activity (Alcazar-Roman et al., 2006; Ballut et al., 2005; Bolger and Wente, 2011; Korneeva et al., 2005; Nielsen et al., 2009; Rogers et al., 2001b; Weirich et al., 2006; Wolf et al., 2010a; Yang et al., 2003a). This chapter focuses on the essential, conserved protein Gle1 that is required for modulating distinct DBPs during mRNA export and translation.

Gle1 is an essential mRNA export factor in eukaryotes with docking sites on specific nuclear pore complex (NPC) proteins (Nups), including Nup42 in yeast and hCG1 and Nup155 in human cells(Kendirgi et al., 2005b; Rayala et al., 2004). At the cytoplasmic NPC face, Gle1 bound to inositol hexakisphosphate activates Dpp5, an essential DEAD-box protein(Alcazar-Roman et al., 2006; Weirich et al., 2006). During nuclear export, the conversion of Dbp5 from the ATP to the ADP bound state triggers the remodeling of exported mRNA-protein complexes (Tran et al., 2007). This remodeling

event is thought to function as a molecular ratchet imposing directionality on nuclear export (Stewart, 2007).

In addition to the pools of Dbp5 and Gle1 functioning at the NPC, both proteins are also found in the cytoplasm. Consistent with this localization, others have reported a role for Dbp5 in translation termination (Gross et al., 2007). Prior studies have demonstrated that Gle1-IP_6 activates yDbp5 to remodel the mRNP termination complex. Furthermore, Gle1 also functions during translation initiation (Bolger et al., 2008). In this role, yGle1 regulates the ATPase activity of the DEAD-box protein Ded1 (Bolger and Wente, 2011)). Unlike the mechanism of regulation for Dbp5, Gle1 acts to inhibit the ATPase activity of Ded1. Taken together, these studies document that the Gle1 acts as a multifunctional regulator that couples mRNA export to the process of translation

Sequence analysis of genomic DNA from LCCS-1 patient cases identified a causal mutation that generates an illegitimate splice acceptor site within the third intron of the gene *GLE1*. This specific mutation (FIN_{Major}) results in an insertion of three amino acid residues (PFQ) in the amino-terminal domain of hGle1 (Figure 1.6). Two other mutations have been identified in *hGLE1* with links to the related disease lethal arthrogryposis with anterior horn cell disease (LAAHD) (Nousiainen et al., 2008). LAAHD exhibits a similar but overall milder pathology compared to LCCS-1. In all known LAAHD cases, patients were compound heterozygous for the Fin_{Major} mutation and an additional point mutation in the region encoding the C-terminal domain of hGle1 (V617M, and I684T) (Figure 1.6). Interestingly, a third case of compound heterozygosity with a C-terminal mutatio n occurred in a single patient whose symptoms were categorized as LCCS-1 (termed here LCCS-1^{Het}). Similar to the LAAHD cases, this patient was compound heterozygous for

the Fin_{Major} mutation and an additional point mutation in the region encoding the C-terminal domain (R569H). No studies have been conducted to investigate the potential perturbations caused by these alterations.

Given the pleotropic effects of the disease pathology, we speculated that hGle1 dysfunction resulting from these mutations could be impacting any one or all of the known Gle1 functions. Having determined the molecular defects caused by Fin_{Major} (Folkmann et al., 2013), we investigated the structural and functional perturbations contributed by the C-terminal domain LAAHD and LCCS-1^{Het} disease mutations. As detailed below, sequence and structural comparisons suggested that these changes alter the stability of the C-terminal HEAT repeat domain, hCG1 binding and mRNA export function. Moreover, analysis of the steady-state localization of these *h-gle1* mutants further revealed a disruption in steady state localization to the nuclear rim. Thus, these mutants are likely defective in mRNA export. This is consistent with our previous finding that the Fin_{Major} PFQ-insertion disrupts the function of Gle1 in mRNA export at the NPC.

Results

Homology model of human Gle1B C-terminal domain allows visualization of potential structural characteristics

Each of the mutations contributing to compound heterozygous LAAHD and LCCS-1^{Het} phenotypes occur in the sequence encoding the C-terminal domain of hGle1 (Nousiainen et al., 2008). Previous studies have documented that this domain is necessary and sufficient both for ATPase stimulation of Dbp5 and for binding IP_6 (Alcazar-Roman

et al., 2006; Montpetit et al., 2011; Weirich et al., 2006). To gain insight into the functional perturbations contributed by the V617M and I684T modifications in LAAHD as well as the single R569H compound heterozygous case of LCCS-1^{Het}, we examined the spatial location of the disease variants in the context of the C-terminal HEAT repeat folds. To date, an atomic level structural model for any domain of hGle1 has not been reported. However, the crystal structure of the yGle1 C-terminal domain was recently determined (Montpetit et al., 2011), and the yeast C-terminal domain structure is primarily composed of HEAT repeat motifs. To investigate the conservation between yGle1 and hGle1 C-terminal domains, we conducted a regional sequence alignment for the core region lying between 480-627 for hGle1 and 331-478 for yGle1. This analysis demonstrated a primary sequence identity of 33% and similarity of 57%, excluding loop regions between helices (data not shown). Based on this sequence conservation, we concluded that the crystal structure of yGle1 is a suitable template structure to produce a basic homology model of the hGle1 C-terminal region for the purpose of hypothesis generation.

To generate the model, the amino acid sequence of hGle1(371-627) was submitted to the Phyre-2 protein fold recognition server (Kelley and Sternberg, 2009). The server produced three models of greater than 60% confidence in fold homology. As predicted from the sequence conservation between hGle1 and yGle1, the highest scoring model resulted from the threading of hGle1 sequence through the published structure of y-D241gle1^{H337R} [PDB 3PEU]. With a reported confidence of 100% and r.m.s.d of 0.7Å, the model predicts that the amino acid sequence of hGle1(371-627) produces an all

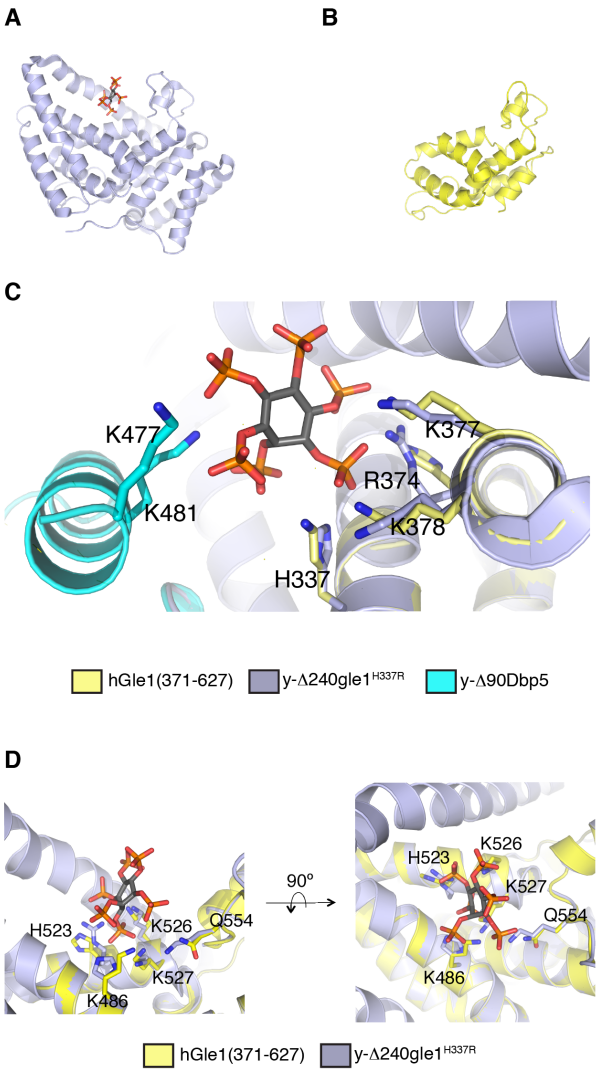

Figure 3.1: Identification of putative IP_6 coordinating residues in hGle1. (A) Structure of y-D243gle1^{H337R} (GRAY) [PDB 3PEU] is shown. (B) A homology model for hGle1(371-627) (YELLOW) was generated based on the crystal structure of y-D243gle1^{H337R} [PDB 3PEU] using the structure prediction server Phyre-2 (Keley and Sternberg, 2009). (C-D) This model was constructed by superposing the hGle1(371-627) model onto the y-D243gle1^{H337R} molecule within the y-D90dbp5/y-D243gle1^{H337R} complex (PDB 3PEU). IP_6 is rendered as a gray stick molecule with orange phosphate and red oxygen atoms. Nitrogen atoms in Gle1 structures are in blue. (C) Conserved IP_6-coordinating polar residues in yGle1 and yDbp5 are labeled. (D) Conserved polar residues in hGle1 are labeled. Methods: Structural analysis and generation of the figure images was done using the program PyMOL (Schrödinger, Inc).

alpha-helix HEAT repeat fold comparable to that of y-D241gle1^{H337R} (Figure 3.1A-B). The two additional models were generated based on published structures of eIF4G [PDB 2VSX and PDB 1HU3]. The eIF4G structure is composed in part of several HEAT repeat motifs, further supporting the fold recognition represented in the hGle1 model (Marcotrigiano et al., 2001). Taken together, these data indicated that the C-terminal domain of hGle1 is likely comprised of all alpha-helix HEAT repeats.

The yGle1 protein binds to IP_6 via positively charged residues located on the Dbp5/yGle1 binding interface (Alcazar-Roman et al., 2010; Montpetit et al., 2011). In the yGle1 crystal structure, the polar residues His-337/Arg-374/Lys-377/Lys-378 interact with the phosphate groups of IP_6 (Montpetit et al., 2011). Prior reports have documented that these IP_6 coordinating residues are conserved throughout evolution (Alcazar-Roman et al., 2010; Montpetit et al., 2011). We searched for additional polar contacts within the yGle1 structure by examining residues that were within 6Å of the IP_6 phosphate groups. This analysis identified Lys-401 as an additional IP_6 coordinating residue for yGle1. Importantly, structural superposition of the hGle1 model onto the yGle1-IP_6-yDbp5 co-crystal structure (PDB ID 3PEU) revealed spatial conservation of this polar charge with residue Gln-554 in the hGle1(371-627) model (Figure 3.1D). By analysis of the multiple sequence alignment, we found that the hGle1 residue Gln-554 is located at position n+1 from yGle1 residue Lys-401 (Figure 3.2C). We speculate that this residue provides additional contacts for coordinating IP_6 (Figure 3.1C-D). Interestingly, the multiple sequence alignment also revealed that several insect and plant Gle1 proteins did not show charge conservation for the identified IP_6 coordinating residues (His-337/Arg-374/Lys-377/Lys-378/Lys-401) (Figure 3.2A-C). These data suggested that some Gle1 proteins

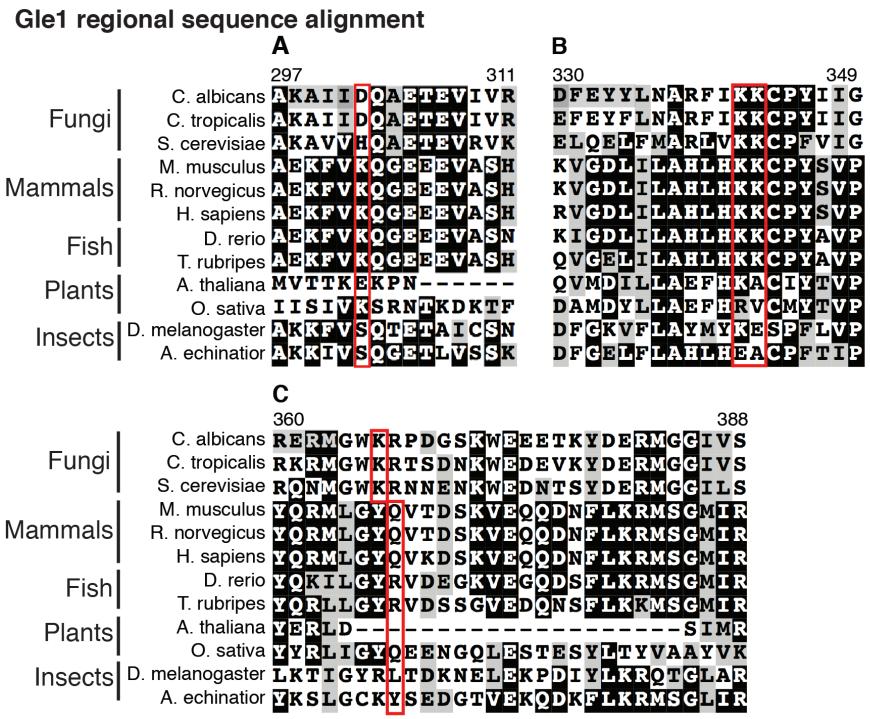

Figure 3.2: Charge conservation of the IP_6 coordinating residues in Gle1 is observed in some organisms (A-C) Sequence alignment of conserved region of the C-terminal domain of Gle1 from selected fungal and metazoan species. (A) Red box indicates position of yGle1-H337 and hGle1-K486 residues. (B) Red box indicates position of yGle1-R374/K377/K378 and hGle1-H523/K526/K527 residues. (C) Red box indicates position of yGle1-K401 and hGle1-Q554 residues.

might have diverged to have different requirements for IP_6 binding or might coordinate IP_6 via different positively charged residues. Future studies are needed to distinguish between these possibilities.

Structural superposition of the hGle1 model onto the yGle1-IP_6-yDbp5 co-crystal structure (PDB ID 3PEU) further revealed an apparent high degree of structural complementarity for the hGle1 model with the Dbp5 and IP_6 binding interface that was experimentally determined for yGle1 (Figure 3.1C-D). This molecular visualization supports our working hypothesis that hGle1 might coordinate the negatively charged IP_6 molecule using conserved or highly similar molecular contact points. Biochemical experiments designed to examine the effects of charge substitutions (and other mutational analysis) of the IP_6 binding site are needed to validate the hypothesis that yeast and human proteins recognize IP_6 in a common binding model.

Substitution of histidine at Arg-569 of hGle1 is predicted to disrupt a putative intramolecular salt-bridge

Sequence alignment analysis revealed that the hGle1 Arg-569 residue altered in LCCS-1^{Het} is highly conserved throughout evolution; however, the functional significance of this residue was unclear. The Arg-569 residue is located in the helical core of the C-terminal domain structure near the Dbp5-Gle1 interface (Figure 3.3B). The homologous residue in yGle1 is Arg-417. To understand the structural and functional significance of this position, we mapped Gle1 evolutionary sequence conservation onto

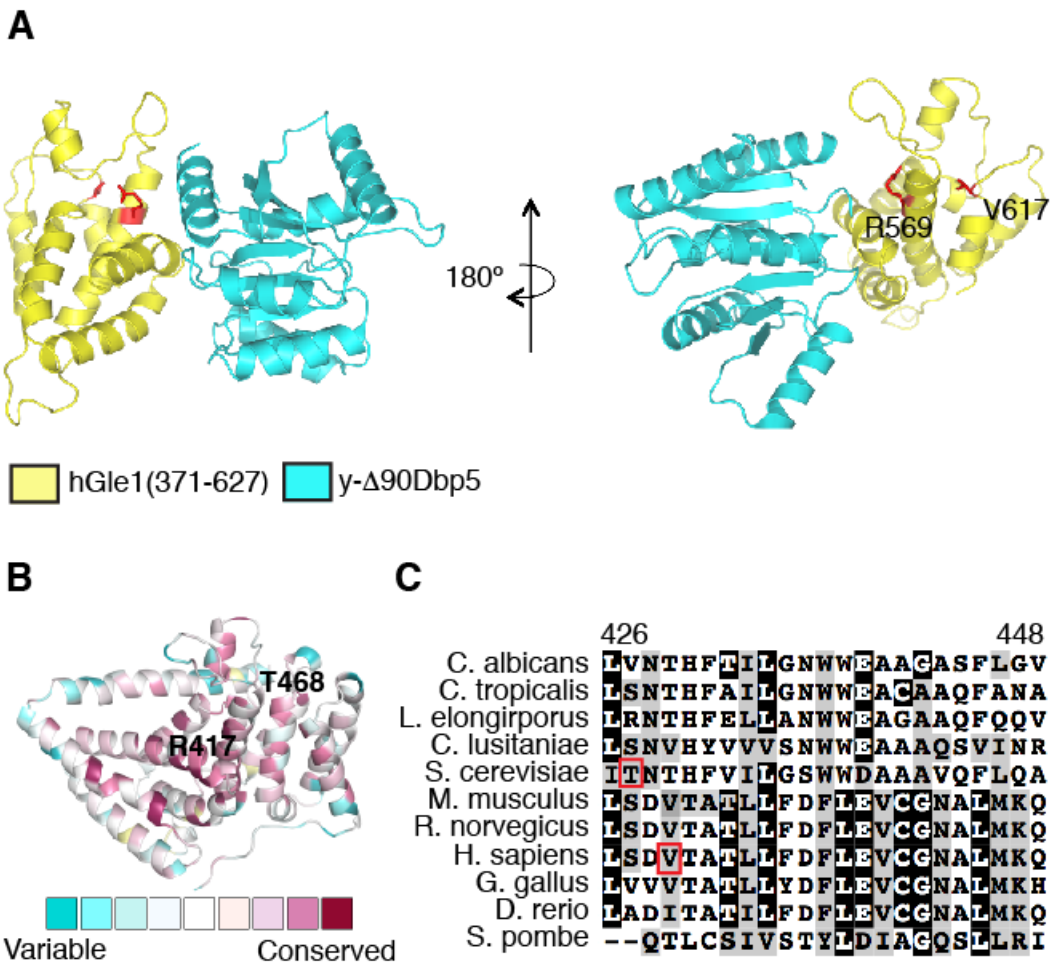

Figure 3.3: hGle1 homology model defines conserved structural characteristics (A) This model was constructed by replacing the y-Δ243gle1^{H337R} molecule within the y-Δ90dbp5/y-Δ243gle1^{H337R} complex (PDB 3PEU) with the homology model of hGle1(371-627). (B) The results of the analysis of the y-Δ241gle1^{H337R} by the ConSurf server are shown. The Gle1 structure is represented by a ribbon model, colored by the following conservation scale: dark purple residues are the most conserved; white residues are the average on the conservation scale; cyan residues are variable. (C) Sequence alignment of conserved region of the C-terminal domain of Gle1 from selected fungal and metazoan species. Sequences were aligned with ClustalX , shaded with Boxshade 2.1. Red boxes denote the positions of Thr-468 and Val-617 residues in yeast and human Gle1 respectively. Methods: Structural analysis and generation of the figure images was done using the program PyMOL (Schrödinger, Inc). Multiple sequence alignment analysis was done using the ClustalX , and shaded with Boxshade 3.21

the surface of the Δ241gle1^{H337R} structure using the Consurf server (Ashkenazy et al., 2010; Glaser et al., 2003; Landau et al., 2005). This analysis demonstrated that the residues comprising the contact points for the core of the yGle1 C-terminal domain were also the most highly conserved evolutionarily, with yGle1 Arg-417 positioned centrally in the conserved region (Figure 3.3B,3.4A). While the polar side-chain of this Arg-417 conserved residue might be important for folding and/or stability of the heat repeat was located near both the Dbp5 and IP_6 binding interfaces, it did not make direct contact with either of these molecules in the crystal structure. Thus, we hypothesized that this tertiary motif. Further, the high degree of sequence conservation suggested that the yGle1 Arg-417 polar side-chain might form intramolecular electrostatic interactions with surrounding polar residues. Indeed, a highly conserved negative polar side-chain of Glu-340 was located within 3 Å of the Arg-417 side-chain (Figure 3.4A). This data indicated that the Arg-417 likely forms a hydrogen bond with the Glu-340 residue. Furthermore, the homologous residues in hGle1 were conserved identically (Arg569/Glu-489). The high degree of sequence conservation at these positions inferred that the intramolecular hydrogen bond might also be conserved in hGle1. Taken together, we speculated that this intramolecular hydrogen bond is a conserved determinant for the proper folding of the C-terminal domain of Gle1. Preliminary support for this model with respect to yGle1 can be found in a previous study, which reported that substitution of Glutamine at Arg-417 in yGle1 resulted in the recombinant protein being insoluble (Alcazar-Roman et al., 2010). If the intramolecular salt-bridge is indeed conserved in hGle1, we further posit that substitution of histidine at Arg-569 would disrupt this interaction and lead to instability or misfolding of the hGle1 C-terminal domain.

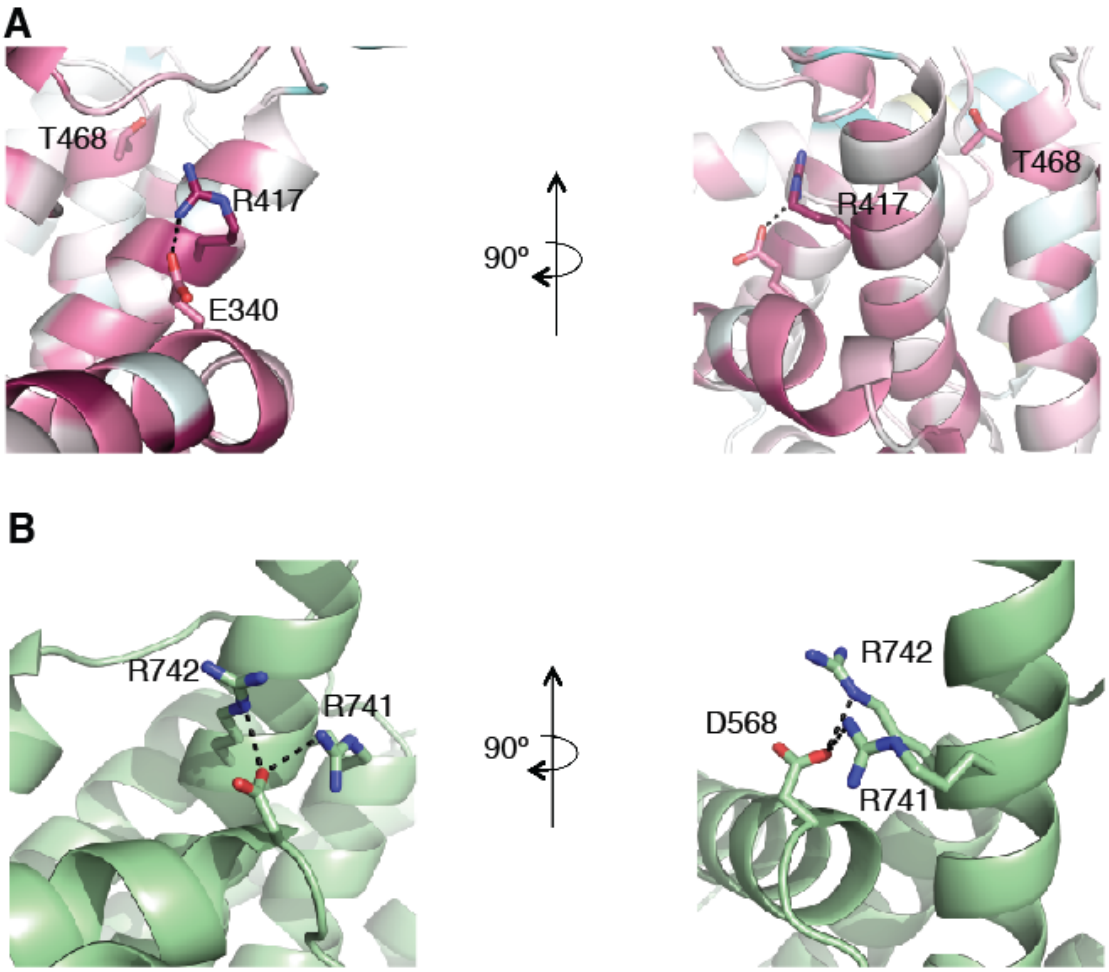

Figure 3.4: Conservation of intramolecular salt-bridge in yGle1 and eIF4G. (A) Conserved residues in y-D243gle1^{H337R} structure are depicted. Dashed line indicated potential hydrogen bond (distance <3Å). (B) Hydrogen bond acceptor and donor residues are indicated in eIF4G structure (PDB 2VSX). Dashed line indicates potential hydrogen bond (distance <3Å). Methods: Structural analysis and generation of the figure images was done using the program PyMOL (Schrödinger, Inc).

eIF4G and Gle1 share critical structural characteristics

Others have shown that the yGle1 C-terminal domain is structurally similar to that of eIF4G (14% identity, 4.1 Å r.m.s.d) (Montpetit et al., 2011). Functionally, Gle1 and eIF4G share homologous roles as co-factors for respective DBPs; Gle1 activates the Dbp5 ATPase for remodeling and eIF4G stimulates eIF4A helicase activity (Korneeva et al., 2005; Noble et al., 2011; Rogers et al., 2001b; Tran et al., 2007). We hypothesized that if yGle1-Arg-417/Glu-340 residues did in fact form an intramolecular salt-bridge bridge critical to the structural integrity of Gle1, a similar hydrogen bonding pair might also be found in the eIF4G helical structure. To test this, a pairwise structural alignment of y-D241gle1^{H337R} (PDB 3PEU) and eIF4G (PDB 2VSX) was conducted using the DaliLite server (Holm and Park, 2000). This structural alignment revealed the presence of a predicted salt-bridge in eIF4G between residues Asp-568, Arg-742 and Arg-741, which are located at a similar position in the HEAT repeat structure to the proposed salt bridge in yGle1 (Figure 3.4B). We concluded that an intramolecular salt-bridge in the core of the HEAT repeat fold is a shared structural determinant for both Gle1 and eIF4G.

We next examined the sequence conservation of the Dbp5 and eIF4A binding interfaces on the respective Gle1 and eIF4G structures. To accomplish this, eIF4G sequence conservation was mapped onto the eIF4G structure (PDB 2VSX) using the Consurf server (Figure 3.5A). Three residues make contacts with eIF4A (Glu-659, Lys-655, Asn-615) (Schutz et al., 2008). In our conservation analysis, we found strong conservation of these residues as well as Lys-611 and Arg-609, forming a cluster of polar contacts at the eIF4A binding interface (Figure 3.5A). In a similar fashion, examination

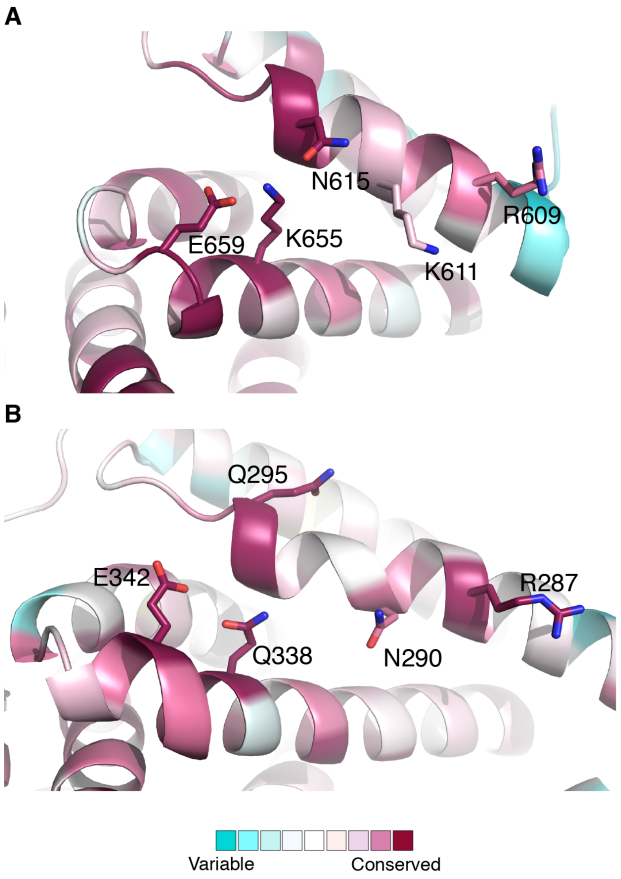

Figure 3.5: Conservation of molecular polar contact points in Gle1 and eIF4G. (A-B) The results of the analysis of the (B) y-D241gle1^{H337R} [PDB 3PEU] and (C) eIF4G [PDB 2VSX] structures by the ConSurf server are shown. A ribbon model is depicted, colored by the following conservation scale, represents the structures: dark purple residues are the most conserved; white residues are the average on the conservation scale; cyan residues are variable. Conserved polar residues for yGle1 and eIF4G are labeled. (C) Sequence alignment of conserved region of the C-terminal domain of Gle1 from selected fungal and metazoan species. Sequences were aligned with ClustalX, shaded with Boxshade 2.1. Red box denotes the position of the Iso-684 hGle1B residue. Methods: Structural analysis and generation of the figure images was done using the program PyMOL (Schrödinger, Inc). Multiple sequence alignment analysis was done using the ClustalX, and shaded with Boxshade 3.21

of the yGle1/yDbp5 interface revealed that the yGle1 structure contained an identical spatial motif of similar polar residues (Gln-295, Lys-287, Glu-342, Gln-338, Asn-290) within its C-terminal domain (Figure 3.5B). This suggested that the binding interfaces for yGle1/yDbp5 and eIF4G/eIF4A share a specific motif of molecular polar contacts. Together, these data further supported the hypothesis that eIF4G and Gle1 have many similar key structural characteristics and might have evolved from a shared ancestral DBP co-factor.

Structural analysis of hGle1 Val-617 reveals linkage to defective mRNA export

We next examined the spatial location within the hGle1(371-629) model of the Val-617 residue changed to methionine in LAAHD. This residue was located near the Dbp5-Gle1 interface but did not make direct contact with Dbp5 (Figure 3.3A). Based on the fold homology, the Val-617 residue was predicted to be positioned directly behind the alpha-helix that contains the Arg-569 residue (Figure 3.3A). One possible explanation for the pathological effects for this mutation could be that substitution of methionine at this position might disrupt the helical packing of the HEAT repeat motifs. Sequence alignment analysis revealed that the hGle1 Val-617 residue was in a similar region to Thr-468 residue in yGle1 (Figure 3.3C). Further, the Thr-468 residue is located behind the helix that contains the hydrogen bond donor residue Arg-417 (Figure 3.3B, 3.4A). Previously, a *y-gle1*^{T468I} mutant was found to be a loss-of-function allele, and this allele was originally identified based on a synthetic lethal genetic interaction in combination with a null mutant for *NUP42* (*nup42D*) (Stutz et al., 1997). Importantly, these results suggested that altering the structure of yGle1 at this position disrupts its function in

mRNA export. We predict that the substitution of methionine at Val-617 results in a loss-of-function phenotype in mRNA export for the *h-gle1*^{V617M} mutant.

The hGle1 Iso-684 residue altered in LAAHD is located in the conserved hCG1 binding domain

Previous reports documented that hGle1 scaffolds to the NPC by binding to both hCG1/Nup42 and Nup155, and more recent works indicates an additional role for the coiled-coil domain and hGle1 self-association (Kendirgi et al., 2005a; Murphy and Wente, 1996; Rayala et al., 2004). These interactions are thought to position Gle1 at the NPC cytoplasmic face to allow for spatial activation of Dbp5's mRNP remodeling activity (Tran et al., 2007). Specifically, residues 559-698 of hGle1B are both necessary and sufficient for the biochemical interaction with hCG1. Deletion of these residues results in the loss steady-state nuclear rim localization and shifts hGle1 localization to the cytoplasm (Kendirgi et al., 2003; Kendirgi et al., 2005a). The Iso-684 residue modified to threonine in LAAHD is located in the middle of this hCG1-binding motif. Further, in our analysis, there is high sequence conservation for a non-polar residue at this position (Figure 3.5C). We hypothesize that substitution of a polar residue for Iso-684 might electrostatically clash with hCG1 residues at the binding interface. Alternatively, a polar residue at this position might cause the hCG1-binding domain to be unfolded. In either case, we concluded that substitution of threonine for Iso-684 probably perturbs the interaction of hGle1B with hCG1.

LAAHD/LCCS-1^{Het} altered proteins do not localize at steady-state to the nuclear rim

Since our *in silico* analysis suggested that all three mutations observed in compound heterozygous cases potentially disrupt the function of hGle1 in mRNA export, we hypothesized that these disease mutants might influence the steady-state localization of Gle1 at the nuclear rim. We compared the subcellular localization of GFP-tagged hGle1 proteins with the respective changes to that of the NPC-associated integral membrane protein Pom121 in HeLa cells. HeLa cells were co-transfected with plasmids expressing Pom121-mCherry and either GFP-hGle1B, GFP-h-gle1B^{R569H}, GFP-h-gle1B^{V617M}, or GFP-h-gle1B^{I684T}. Twelve hours post-transfection, the steady state localization of the GFP-tagged proteins was examined by live cell direct fluorescence microscopy. Wild-type GFP-hGle1B localized to the nuclear rim, overlapping completely with the Pom121-mCherry. In contrast, the steady-state nuclear rim signal intensity for GFP-h-gle1B^{R569H}, GFP-h-gle1B^{V617V}, and GFP-h-gle1B^{I684T} was reduced (Figure 3.6). These data indicated that each of these changes disrupts the function of Gle1 in mRNA export possibly by inhibiting localization to the NPC.

hGle1 is in a stable complex at the nuclear pore complex

Analysis of the steady state localization of the LAAHD and LCCS-1^{Het} mutants suggested that they had altered steady state localization at the NPC. Our prior studies show that hGle1B localizes to the nuclear rim and cytoplasm, and shuttles between the nuclear and cytoplasmic compartments (Kendirgi et al., 2003). Thus, separate pools of Gle1 might exist to function exclusively in either mRNA export or translation. To

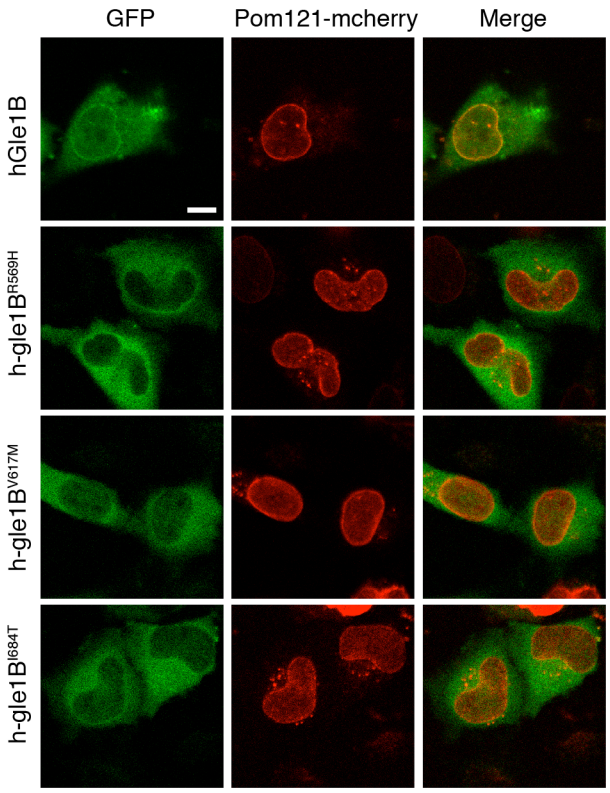

Figure 3.6: LAAHD and LCCS-1^{Het} Gle1 proteins have altered steady-state NPC localization. HeLa cells expressing *POM121-mCherry* and either *GFP-hGLE1B*, *GFP-h-gle1B^{R569H}*, *GFP-h-gle1B^{V617M}*, and *GFP-h-gle1B^{I684T}* were visualized by direct fluorescent live cell microscopy. Bar, 10 µm. Methods: Hela cells were cultured in complete medium (DMEM, Gibco) supplemented with 10% FBS (Alanta Biologicals) at 37 °C in 5% CO_2. Cells were plated in 35mm No. 1.5 glass bottom dishes (Mattek). Transient transfection with indicated plasmids was performed using Fugene6 (Promega) following manufacturer recommendations: *POM121-mCherry* and pSW1831 (*GFP-hGle1B*), pSW3971 (*GFP-h-gle1B^{R569H}*), pSW3972 (*GFP-h-gle1B^{V617M}*), or pSW3973 (*GFP-h-gle1B^{I684T}*). All live-cell direct fluorescence microscopy experiments were performed on a confocal microscope (LSM710, Zeiss, 40X/1.1 C-Apochromat water objective).

investigate the dynamics of Gle1 at the NPC, fluorescence loss after photobleaching (FRAP) microscopy was performed. HeLa cells were co-transfected with plasmids expressing GFP-hGle1B. Twelve hours post-transfection, the nuclear rims of cells transiently expressing GFP-hGle1B were photobleached and the GFP fluorescence was monitored over time. Strikingly, we observed that GFP-hGle1B fluorescence recovered very slowly (Figure 3.7A). This indicated that hGle1 is in a stable complex at the NPC. In a previous FRAP microscopy study of the dynamics for GFP-yDbp5 at the NPC, GFP-yDbp5 was dynamically associated with the nuclear rim ($t_{1/2}$ of recovery ~0.8s) (Hodge et al., 2011b). To see if hDbp5 behaved similarly, we directly next examined the dynamics of GFP-hDbp5 at the nuclear rim using FRAP microscopy. HeLa cells were co-transfected with plasmids expressing GFP-hDbp5. Twelve hours post-transfection, the nuclear rim of cell transiently expressing GFP-hDbp5 was photobleached and the GFP fluorescence was monitored over time. In contrast to GFP-hGle1B, hDbp5 recovered very fast. The FRAP data set was fit with a one-phase exponential association model (Figure 3.7B-C). The relative $t_{1/2}$ for GFP-hDbp5 was ~0.8s which directly correlated with the previous yDbp5 measurement. Overall, Dbp5 more transiently associated with the NPC in comparison to its co-factor Gle1 that was in a more stable complex. The disparity of the dynamics of Dbp5 and Gle1 at the NPC is highly intriguing. One possible explanation is that Gle1 is bound at the NPC in a stable oligomeric complex to ensure a sufficiently high concentration for efficient stimulation of Dbp5's remodeling activity. As such, we predict that Gle1 self-association into oligomeric complexes influences its residence time at the NPC. In addition, given that Gle1 also shuttles between the nucleus

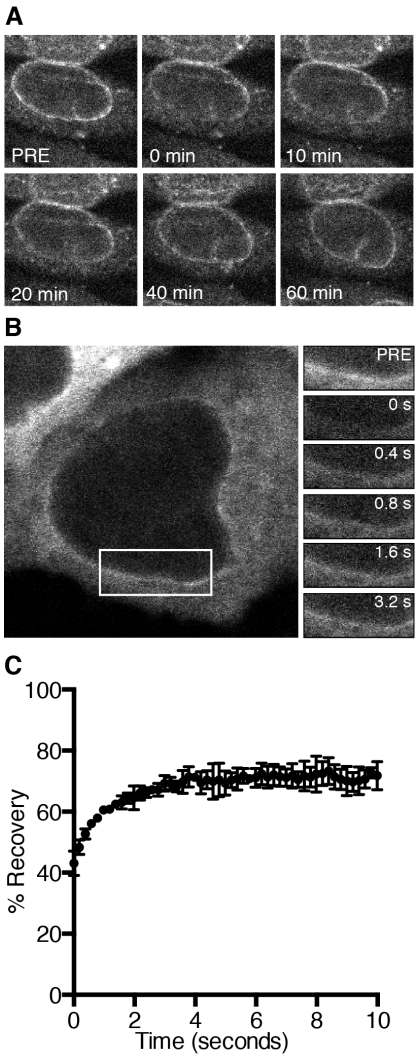

Figure 3.7: Gle1 is a stable component of the NPC. (A) HeLa cells expressing *GFP-hGLE1B* were analyzed by FRAP microscopy. Representative nuclear rim FRAP time series images are shown. Bar, 10 μm. (B) HeLa cells expressing *GFP-hDBP5* were analyzed by FRAP microscopy. Representative nuclear rim FRAP time series images are shown. Bar, 10 μm. White box indicates imaging region of interest for FRAP acquisition (C) FRAP recovery curve experimental determined bleached region, fit with a one-phase association model. Error bars represent mean ± standard deviation with n=5 cells. Methods: HeLa cells were cultured and transfected as in Figure 4. FRAP microscopy experiments were performed on HeLa cells co-transfected with *POM121-mCherry* and either pSW1832, or pSW3253 (*GFP-hDBP5*). The bleaching region of interest (B-ROI) was set to encompass the nuclear rim. Bleaching was achieved by exciting at 488 nM throughout the entire B-ROI (with a LSM710, Zeiss, 40X/1.1 C-Apochromat water objective). Post-bleaching images were acquired every 10 minutes (GFP-hGle1) or 200ms (GFP-hDbp5).

and cytoplasm, there is the potential for different subcellular pools of Gle1 being involved in distinct steps of the mRNA life cycle and gene expression.

Discussion

During normal gene expression, mRNP remodeling events function as distinct transition points that specify both the fate and function the mRNA (Muller-McNicoll and Neugebauer, 2013; Valkov et al., 2012). Here we investigated the potential structural and functional perturbations contributed by the unique changes found in the compound heterozygous LAAHD and LCCS-1^{Het}. Analysis of the steady-state localization in living cells revealed that the GFP-h-gle1B^{R569H}, GFP-h-gle1B^{V617M}, and GFP-h-gle1^{I684T} disease proteins have perturbed nuclear rim localization. Furthermore, specific structural perturbations potentially result. Based on *in silico* analysis, the R569H and V617M alterations might disrupt the overall fold of the Gle1 C-terminal domain; furthermore the I684T is positioned to disrupt Gle1 binding with hCG1. Combined with our recently published biochemical and *in vivo* analysis of the molecular defects caused by Fin_{Major}, we propose a unified model of the molecular disease pathology whereby defective mRNA export at NPCs contributes to both the LCCS-1 and LAAHD disease states. Importantly, dysfunctional remodeling of the mRNP during export has emerged as a new molecular disease mechanism for RNA metabolism-linked disease states.

In addition to the insights from analyzing disease mutants, important information is also gained from comparing conserved and divergent aspects of Gle1 orthologues. Previous sequence alignment and structural analysis suggested that the IP_6 coordinating residues in Gle1 are highly conserved throughout evolution (Alcazar-Roman et al., 2010;

Montpetit et al., 2011). This suggested that the IP_6 molecule was stringently required for Gle1's regulatory activity of Dbp5 in most organisms. Our new sequence alignment data allows for flexibility in this regulatory paradigm. Specifically, we document that that several insect and plant Gle1 proteins do not apparently share the charge conservation for the key IP_6 coordinating residues, suggesting that these proteins could function independent of IP_6. In addition, *S. cerevisiae* yDbp5 utilizes Lys-477 and Lys-481 to coordinate IP_6 binding with yGle1 (Figure 3.1 and 3.8) (Alcazar-Roman et al., 2010). Prior sequence alignment analysis documented that these IP_6 coordinating residues in Dbp5 show moderate charge conservation (Figure 3.8) (Montpetit et al., 2011). It is important to note that the insect Dbp5 proteins examined do not show charge conservation at Lys-477 or Lys-481 positions. This supports our hypothesis that Dbp5/Gle1 might function independent of IP_6 in some cases. It is unclear why the Gle1 and Dbp5 in some organisms might not utilize IP_6. Interestingly, in plant tissues, IP_6 is present at high concentration and is the principal storage form of phosphorus (Raboy, 2001). Thus, it is intriguing to speculate that this high concentration of IP_6 may be deleterious for regulation of Dbp5 and may represent the reason for why Gle1 functions independent of IP_6 in plants. Comprehensive analysis of the sequence conservation of these IP_6 coordinating residues and binding activity in Gle1 is needed across different evolutionary organism kingdoms and phyla to further our understanding.

It had been previously reported that eIF4G and Gle1 share a similar structural fold, suggesting that eIF4G and Gle1 share a similar ancestral DBP co-factor (Montpetit et al., 2011). Importantly, our *in silico* analysis supports and expands upon this conclusion. Specifically, our analysis demonstrates that eIF4G and Gle1 both harbor a

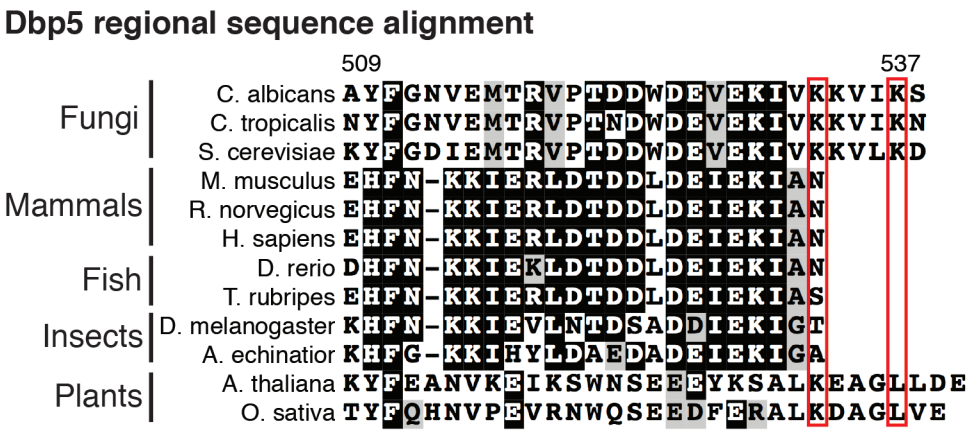

Figure 3.8: Charge conservation of the IP_6 coordinating residues in Dbp5 is observed in some organisms. (A) Sequence alignment of the far C-terminal region in Dbp5 from selected fungal and metazoan species. Red box indicates position of yDbp5-K477/K481 residues.

key intramolecular salt-bridge that has the potential to stabilize the overall HEAT repeat fold. Secondly, despite lack of sequence conservation, eIF4G and Gle1 have maintained similar spatial positioning of conserved polar contacts in the binding interface for their respective DBP interaction partners. This suggests that eIF4G and Gle1 utilize similar molecular contact points to regulate their respective DBP. These are important insights into the structural and functional aspects of DBP co-factors and will aid the identification of other putative co-factors that regulate DBPs and/or additional Gle1/eIF4G-like co-factors.

The pathological phenotypes for LCCS-1 and LAAHD are highly pleiotropic, affecting multiple tissues and organs (Herva et al., 1985; Nousiainen et al., 2008; Vuopala et al., 1995). This is not necessarily unexpected for a case of defective mRNA export, as multiple defects in gene expression are likely to arise from altering such an essential molecular process. However, it is also perplexing that both LAAHD and LCCS-1 pathologies are manifested at a relatively late stage *in utero*; for example, the LCCS-1^{Fin} disease results in fetal lethality at ~32 weeks gestation and not earlier (e.g. early embryonic development) (Herva et al., 1985). Different tissues and cell types might elicit different pathologies depending on specific severity of the perturbation in gene expression. It is intriguing to speculate that less severe changes that perturb Gle1 activity to a lesser extent might have specific phenotypes in adults. Further, given that Gle1 is positioned to influence multiple steps during gene expression, the possibility exists for distinct perturbations of Gle1 functions in mRNA export or translation having different pathological outcomes. It is also possible that only certain subcellular pools of Gle1 are

impacted in discrete diseases, be it the more stable NPC-associated Gle1 oligomers, the cytoplasmic Gle1A form, the nuclear pool, or an actively shuttling population.

Based on the evidence so far, we conclude that the reported disease perturbations of hGle1 in LCCS-1 and LAADH are all impacting mRNA export. It is possible that alleles specific for Gle1 translation roles might have other pathologies. Interestingly, mutations in *hGLE1* have also been linked to a hand and foot dorsalization disease, but both the physiological and molecular underpinnings of this phenotype are yet to be resolved (Al-Qattan et al., 2012). Given the large spectrum of proteins and signaling factors that regulate each gene expression transition point, we predict that aberrant mRNP remodeling will play a role in other RNA metabolism-linked disease states.

Chapter IV

Future directions

Introduction

Causative mutations in RNA metabolism factors have been identified for several human disease states. Although genetic alterations are known, identification of the specific perturbations in gene expression that contribute to disease manifestation has remained unclear (Cooper et al., 2009; Hurt and Silver, 2008; Renoux and Todd, 2012). The conserved mRNA export factor *GLE1* has been causally linked to the disease Lethal-Congenital Contracture Syndrome-1 (LCCS-1)(Nousiainen et al., 2008). The main causative mutation (Fin_{Major}) is the insertion of a Proline Phenylalanine Glutamine (PFQ) peptide sequence within the uncharacterized coiled-coil domain of Gle1. In the first study presented here, biochemical and biophysical approaches demonstrated that Gle1 self-associates to form oligomeric complexes both *in vitro* and *in vivo*. Further, structural analysis revealed that Gle1 oligomers form disk shaped particles that were malformed with the gle1-Fin_{Major} protein. Analysis of the *in vivo* functional significance of self-association revealed a specific requirement for the mRNA export mechanism. In summary, this work identified a novel requirement for Gle1 self-association in mRNA export mechanism that is perturbed in the LCCS-1 disease state.

Mutations in human *GLE1* have also been causally linked lethal arthrogryposis with anterior horn cell disease (LAAHD)(Nousiainen et al., 2008). In the second study, structure prediction and functional analysis provide strong evidence to suggest that the

LCCS-1 and LAAHD disease mutations disrupt the function of Gle1 in mRNA export. Strikingly, direct fluorescence microscopy in living cells reveals a dramatic loss of steady-state NPC localization for GFP-h-gle1 proteins expressed from human *hgle1* genes harboring LAAHD and LCCS-1 mutations. The potential significance of these residues is further clarified by analyses of sequence and predicted structural conservation. This work offers insights into the perturbed mechanisms underlying human LAAHD disease state and emphasizes the potential impact of altered mRNA transport and gene expression in human disease pathology.

Taken together, our work provides the first evidence for the basic molecular mechanism causing the LCCS-1 and LAAHD disease states. The studies presented here however do not address the mechanism of why self-association is important for the function Gle1. Specifically, it is unclear how self-association impacts Gle1's nucleocytoplasmic shuttling activity or steady-state localization to the NPC. Further, the functional mechanism for Gle1 self-association at the NPC remains unresolved. Attaining this mechanistic information is critical for understanding the molecular mechanism of *hGLE1* linked disease pathologies. Thus future studies are needed to investigate the precise biochemical and cellular mechanism(s) of Gle1 self-association during the mRNA export mechanism. These ideas are discussed below.

A**nalysis of Gle1 self-association *in vivo***

Our biophysical analysis of Gle1 self-association in living cells suggested that Gle1 self-associates at least as a dimer in the cytoplasm, nucleoplasm, and at the NPC. The assertion of a 'dimer pair' is based solely on the documented distance constraint

(<10nm) for FRET energy transfer to occur between acceptor and donor molecules (Xia and Liu, 2001). In contrast, our *in vitro* biochemical analysis using SVAU documented that both yeast and human Gle1 proteins form higher order oligomeric complexes. Thus, an important outstanding question is whether Gle1 in living cells forms these higher order oligomeric complexes.

A simple experiment to examine the oligomeric state of Gle1 in living cells would be to use FRAP microscopy on GFP-tagged hGle1 fusion proteins to obtain a translational diffusion coefficient, which in turn would allow for calculation of the molecular mass of the GFP-tagged hGle1 and h-gle1BΔCC molecules (Nenninger et al., 2010). It is difficult with this approach to distinguish between monomers and dimers. However, molecules that exhibit large differences in molecular mass can easily distinguished. Comparison of the determined molecular mass for hGle1B and h-gle1BΔCC would allow for approximation of the oligomeric state of hGle1 in living cells.

Structural analysis of the NPC has documented that the NPC is a ring structure that has eight-fold rotational symmetry that is perpendicular to the nuclear envelope plane (Cronshaw et al., 2002, Rout et al,2000). This symmetry suggests that the NPC is constructed of eight identical building blocks, here termed spokes. Thus, if each spoke contained one Gle1 molecule, one would expect there to be 8 Gle1 molecules total per NPC. If Gle1 were present as a dimer at the NPC, each spoke would have two Gle1 molecules, with a sum total of 16 molecules per NPC.

Prior studies in *S. cerevisiae* have provided estimates for both the total of NPCs and relative number of Gle1 molecules within single yeast cells. Specifically, using quantitative western blotting it is estimated that there are ~1040 molecules of yGle1

within a yeast cell (Ghaemmaghami et al., 2003). Further, it has been documented that a yeast nucleus has ~120 NPCs (Winey et al., 1997). Simple arithmetic (total # Gle1/total # NPC) gives an estimate of ~8 Gle1 molecules per NPC (1 Gle1 molecule per spoke). This calculated estimate of 8 total Gle1 molecules per NPC is not compatible with our hypothesis that a 'dimer pair' of Gle1 is bound at each spoke of the NPC.

There are several possible explanations for this incompatibility: (1) the measurement of yGle1 abundance is incorrect, (2) yGle1 oligomers are asymmetrically disturbed on the 'spokes' of the NPC, or (3) not every NPC contains Gle1 molecules. The measurement of yGle1 abundance was documented in a genome wide analysis study of the yeast proteome. Repeating the measurement using updated technology and reagents is critical first step. yGle1 molecules may be asymmetrically distributed on a subset of spokes, or a subset of NPCs. New super-resolution microscopy techniques allows for the examination of Nup molecules on individual NPCs using light microscopy. Using a similar approach one could examine the distribution of yGle1 molecules on individual NPCs in mutant and wild-type yeast and human cells.

Biochemical and structural analysis of Gle1 self-association *in vitro*

The analysis presented here demonstrates that the coiled-coil domain (aa. 1-362) is both necessary and sufficient for hGle1 self-association *in vitro* and in living cells. It remains unclear however if the entire predicted coiled-coil domain (aa. 120-362) is required to mediate self-association. Alternatively, specific sub-domain(s) may alone be sufficient to mediate this biochemical activity. This hypothesis can examined using by domain mapping the coiled-coil domain using soluble binding assays. In a parallel set of

studies, the identified domains could be analyzed using NegEM and SVAU, and by FRET microscopy. Together, this work will uncover critical biochemical and structural characteristics of hGle1 self-association. Further, the information gained from these experiments can be used to generate mutants to test for functionality using the *hGLE1*-siRNA cell-culture model system. A compelling alternative strategy would be to perform an identical set of studies with yGle1 protein.

Our structural analysis using bacterially expressed recombinant protein documented that yGle1 forms large ordered disk-like structures *in vitro*. The question of whether yGle1 forms these disk-like oligomeric structures *in vivo* remains unanswered. To begin to answer this question, one could assay for the ability of endogenous Gle1 protein to form these disk-like structures. A previous study has generated a strain that expresses a tandem-affinity-purification (TAP) yGle1-fusion protein. Using standard methods TAP-yGle1 protein could be purified from this yeast strain. The elution of TAP-yGle1 could then be analyzed using NegEM. As a control, a TAP-y-gle1ΔCC affinity purification and analysis by NegEM could be done in parallel. Together, this could examine if endogenously expressed yGle1 protein *in vitro* can self-associate to form disk-like oligomeric structures.

In our analysis we documented that MBP-hgle1(1-362) oligomeric disks adopt a variety of different diameters in solution. This observation is supported by our biochemical analysis by SVAU which indicated that the MBP-hgle1(1-362) protein can adopt a variety of oligomeric states in solution. The heterogeneity of protein species within the binding isotherm did not allow for the determination of the precise molecular mass of individual oligomeric complexes by SVAU. Thus, the precise stoichiometry of

hGle1 protomer molecules within an oligomeric disk is unknown. One prediction is that as the diameter of the disk increases, the number of protomer hGle1 molecules increases proportionally. Alternatively, variable structural rearrangements between individual protomer molecules may influence disk diameter. To distinguish between these possibilities it will be important to determine the precise stoichiometry of hGle1 protomer molecules within the oligomeric complex. To accomplish this task, the hGle1 oligomeric structures need to be adequately fractionated to reduce the heterogeneity of protein species in solution. This, in turn, will allow precise determination of molecular mass by SVAU. This fractionation could be accomplished by gel filtration chromatography using a Sephacryl S-1000 column. Individual fractions containing hGle1 disk oligomers of specific size range should then be analyzed using NegEM and SVAU. As mentioned above, a compelling alterative strategy would be to perform an identical set of studies with yGle1 protein.

It is intriguing to speculate that Gle1 interaction partners may somehow directly influence Gle1 self-association. Alternatively, the Gle1 oligomer may function to optimally position binding partners for optimal biochemical activity. To examine these possibilities it will be important for future studies to: (1) determine the location of the Gle1 protein-protein interaction domains on the disk structure, and (2) access the impact of interaction partners on Gle1 self-association. As a starting point, known Gle1 interaction partners should be tested first. At the NPC yGle1 biochemically associates with both Dbp5 and Nup42. Additionally, the protein (Good for dead-box proteins) Gfd1 has been documented to directly interact with the C-terminal domain of yGle1. Gfd1 was originally identified in a multi-copy suppressor of a *dbp5* temperature sensitive allele.

Purified recombinant Dbp5, Nup42, or Gfd1 could be mixed with the yGle1-disk protein solution. Following fractionation by size exclusion chromatography the Gle1/Nup42, Gle1/Dbp5, or Gle1/Dbp5 oligomeric complexes could be examined using NegEM.

Functional significance of Gle1 self-association

An exciting area of future research surrounds the investigation of the fundamental mechanistic role of Gle1 self-association plays during mRNA export at the NPC. There are at least two working models by which self-association might function during the mRNA export mechanism. First, self-association might allow multiple distinct co-incident interactions with NPC components with individual protomers in a Gle1 oligomer. Second, self-association might promote Gle1 enrichment at the NPC and generate a self-organized platform of multiple C-terminal Gle1 domains.

A prior structural analysis using X-ray crystallography has documented the binding interface between yGle1 and Dbp5(Montpetit et al., 2011). Biochemical analysis from our lab has defined the conserved region in hGle1 that is both necessary and sufficient for interaction with hCG1 (yeast Nup42 homologue)(Kendirgi et al., 2005a). Taken together, these structural and biochemical data suggested that the binding interface for Dbp5 and Nup42 on the Gle1 C-terminal domain may be mutually exclusive. Thus, self-association would allow the Gle1 oligomer to bind the NPC (Nup42) and activate Dbp5 coincidentally during mRNA export. In contrast, Dbp5 and Nup42 would not be able to coincidentally bind to a single Gle1 protomer (i.e. y-Δ240Gle1). To test this hypothesis, competition binding experiments using recombinant y-Δ240Gle1, Dbp5, and Nup42 proteins could be conducted. This analysis will provide valuable information on

the possible mechanism of Gle1 oligomerization and the location of the Nup42 binding interface.

Human Gle1 scaffolds to the NPC via biochemical interactions with both Nup155 and hCG1 (Kendirgi et al., 2005a; Rayala et al., 2004). The domains within hGle1 required for these interactions are located in the far N- and C-terminal regions respectively. Prior studies have documented that both these domains are required steady-state localization of hGle1 to the NPC. Importantly, neither of these domains requires the presence of the coiled-coil domain for the biochemical interactions to occur with the respective Nups. Building on this work, we found that deletion of the coiled-coil domain also disrupted hGle1 steady-state localization to the NPC. The altered GFP-hgle1BΔCC protein contains intact Nup155 and hCG1 interaction domains, suggesting that the self-association is critical for hGle1 localization to the NPC.

As mentioned above, prior structural analysis suggested that the binding interface on the C-terminal domain of yGle1 for Dbp5 (DDX19 is human homologue) and Nup42 (hCG1 homologue) may be mutually exclusive. In agreement with this hypothesis, it is intriguing to speculate that the disruption of steady-state localization h-gle1BΔCC protein is due to competition between DDX19 and hCG1 for binding to the hGle1 C-terminal domain. Similar to y-Δ240Gle1, the h-gle1BΔCC protein does not have the biochemical ability to self-associate. One prediction of this hypothesis is that reducing DDX19 binding to the C-terminal domain should restore h-gle1BΔCC steady-state NPC localization. This could be accomplished experimentally by: (1) depleting endogenous levels of DDX19 using siRNA technoglogy, or (2) generating a h-gle11BΔCC^{19MT} protein that does not biochemically interact with DDX19. Using the yDbp5 and yGle1

co-cyrstal as a structural template, conserved polar residues that mediate critical salt-bridge interactions between the hGle1 and DDX19 proteins can be identified (Montpetit et al., 2011). These residues can be altered to generate an h-gle1BΔCC^{19MT}.

An important experimental caveat that is not controlled for in the prior cellular analysis of the hCG1 and Nup155 binding domains is the presence of endogenous untagged hGle1. This analysis was done by exogenous expression of GFP-tagged *hGLE1* variants. The loss of steady-state localization at the nuclear rim with the domain variants may have occurred as a result of a competition with endogenous hGle1 for limiting NPC scaffold interactions. Importantly, our recent analysis of the requirement of the coiled-coil domain was done using our *hGLE1*-siRNA model system. It will be important for future studies to reexamine the requirement of hCG1 and Nup155 binding domains in the *hGLE1*-siRNA model system. This analysis is critical for: (1) proper interpretation of the requirement hCG1/Nup155 scaffolding interactions, and (2) understanding the molecular function(s) self-Gle1 association plays at the NPC.

Our hypothesis that Gle1 functions *in vivo* as a dimer is based on our complementation analysis with the yGle1 chimeric proteins. Specifically, we documented that expression of a chimeric protein with the coiled-coil region of yGle1 swapped for that of the leucine-zipper dimerization domain of the transcription factor GCN4 (*y-gle1ΔCC +GCN4*) partially rescued the temperature sensitive *y-gle1-4* phenotype. This data suggested that a dimer pair of yGle1 could partially rescue the function *in vivo.* This chimeric protein however does not rescue as well as expression of wild-type yGle1. Suggesting that the y-gle1ΔCC+GCN4 protein may lack biochemical attributes that would allow it perform at the same level as wild-type yGle1.

One intriguing possibility is that the wild-type protein rescues better because it can self-associate to form higher order oligomers. To test this hypothesis one could take advantage of the various permutations of GCN4 leucine zipper domain that have been generated. The 30 aa GCN4 leucine zipper domain has been engineered to form parallel tetramer complex in solution. One prediction would that the expression y-gle1ΔCC+GCN4^{tetramer} protein would recue the *y-gle1-4* phenotype better than the y-gle1ΔCC+GCN4 protein or possibly to the same level as wild-type yGle1. Using a similar approach, chimeric h-gle1ΔCC+GCN4 variant proteins can be tested by rescue of functional defects in our *in vitro hGLE1*-siRNA cell culture model.

The functional model that oligomerization promotes a self-organized platform of multiple C-terminal Gle1 domains is based on the *y-gle1ΔCC+GCN4* chimera data, wherein the GCN4 coiled-coil domain facilitates assembly of parallel aligned dimers. In this chimeric protein, the C-terminal domains of yGle1 are orientated in the same direction. One prediction of this model is that the orientation of the yGle1 C-terminal domain within the dimer is critical for functionality *in vivo.* To test this hypothesis directly one could engineer yGle1 to form an anti-parallel dimer. In this case the C-terminal Gle1 domains would be facing in opposing directions. To accomplish this task one could take advantage of the anti-parallel leucine zipper domain from a protein from *Bacillus subtilis*, named MtaN (Busiek et al., 2012). It is intriguing to speculate that swapping in the dimerization domain of MtaN (*y-gle1ΔCC+MtaN*) will not rescue the function of coiled-coil region of yGle1. Suggesting that the spatial orientation of the Gle1 C-terminal domains within the oligomer is critical for function *in vivo*. Future studies are needed to investigate this exciting possibility.

Molecular pathological dissection of Gle1 disease mechanisms

One striking characteristic of LCCS-1 and LAAHD pathology is that the patients survive relatively far into the pregnancy term (Nousiainen et al., 2008). This is surprising given the importance of bulk mRNA export for cellular homeostasis. There are two possible explanations for how dysregulation of Gle1 activity contributes to the pathology in these patients: (1) The Fin_{Major} mutation is a partial loss of function allele. Only subsets of cell types require a high amount of Gle1 activity. Dysfunction of this subset of cells contributes to the disease pathology observed. (2) The Fin_{Major} mutation is a severe loss-of-function allele. The embryo is able to proceed far into development because only specific cell types strictly require Gle1 activity. While other cell-types have the ability to by-pass the requirement for Gle1 activity. A prior study has documented that a null *GLE1* mutation in mice results in embryonic lethality (Tsai et al., 2011). Specifically, the authors find that *GLE1* null mice embryos are not observed at any stage during development. Further, the authors were unable to generate a *GLE1* null embryonic stem cell line (Tsai et al., 2011). This data indicates proper Gle1 activity is essential for proper embryonic development. Given the central importance of Gle1 activity for bulk mRNA transport this is not unexpected. Severe or complete loss-of-function human disease alleles are not common among essential genes (Goh et al, 2007). This is because severe mutations in essential genes are likely to result in severe impairment of development and physiology, thus leading to the eventual extinction from human population. Thus, most human disease mutations found in essential genes are likely to be partial loss-of-function (Goh et al., 2007). Taken together, these data suggest that the Fin_{Major} is a hypomorphic disease allele.

Dysregulation of RNA metabolism has emerged as a potential key contributor to human disease pathology (Cooper et al., 2009). Our work builds on this paradigm showing that loss-of-function of Gle1 activity in mRNA export contributes directly to LCCS-1 and LAAHD pathologies. Prior analysis of the disease pathology in zebrafish indicated that Gle1 deficiency in the developing animal negatively influenced multiple cell and tissue types (Jao et al., 2012). In this study, it was documented that highly proliferative cells were more susceptible to Gle1 deficiency. Further, the authors documented that the susceptibility of these highly proliferative cell types to Gle1 deficiency likely constitutes the cellular basis of the pathological phenotypes observed in LCCS-1 patients (Jao et al., 2012).

The molecular pathological mechanism of why highly proliferative cell types are more sensitive to Gle1 deficiency is unknown. One possibility is that highly proliferative cells demand higher levels of Gle1 activity to maintain a high level of metabolic activity that is required during proliferation. Alternatively, Gle1 deficiency in these cells may lead to the selective retention of specific mRNAs in the nucleus that are critical for proliferation. Our previous analysis indicated that the Fin_{Major} protein is defective in function for the export bulk poly(A)$^+$ RNA. From this analysis, it is unclear if all mRNA transcripts are retained in the nucleus in the Fin_{Major} cells. In theory, subsets of transcripts may be selectively retained or exported in Fin_{Major} cells. To test this idea, one could utilize our established *GLE1*-siRNA depletion and add back cell culture system. In brief, the cytoplasmic and nuclear RNA pools of Gle1depleted cells expressing *GFP* alone, *GFP-hGle1B*^{R}, or *GFP-Fin*$_{Major}$^{R} could be isolated via the NP-40 lysis procedure (Greenberg and Ziff, 1984). The nuclear and cytoplasmic pools of RNA molecules could

then be analyzed using next generation sequencing technology (NextGen). Bioinformatic analysis of the NextGen data might reveal the identity and relative number of RNA molecules in the nuclear and cytoplasmic fractions in each respective sample. This analysis will allow for comprehensive analysis the mRNA export defect observed in the Fin_{Major} cells on the level of individual transcripts.

The *Fin_{Major}* mutant is a homozygous recessive mutation. This indicates that in the heterozygous state that the wild-type Gle1 protein may complement in trans the structural perturbation of the Fin_{Major} protein. Strikingly, the identified compound heterozygous alleles (*h-gle2B*^{I684T}, *h-gle1B*^{V617M}, and *h-gle1B*^{R569H}) do not complement the *Fin_{Major}* allele. All of these mutations occur within the C-terminal region of Gle1 and are thought to possibly disrupt the folding of this domain. The C-terminal domain of yGle1 is essential for regulation of Dbp5's ATPase activity (Weirich et al., 2006). It is unclear why these *h-gle1* disease alleles do not functionally complement the defect found with the Fin_{Major} protein. It is possible that altered proteins fail to complement because: (1) The altered proteins cannot rescue the perturbed oligomerization found with the Fin_{Major} protein. (2) The altered proteins are incapable of regulating DDX19 ATPase activity. (3) These altered proteins may have compromised oligomerization and DDX19 activation activity. To distinguish between these possibilities molecular complementation assays should be performed using our established *GLE1*-siRNA depletion and add back cell culture system. The goal of this experiment is to define the minimal biochemical requirement for rescue of the functional perturbation found in Fin_{Major} cells. To identify this requirement, Gle1 depleted cells could be co-transfected with YFP-hgle1B-Fin_{Major} and either CFP, CFP-hGle1B, CFP-hGle1(1-362), or CFP-

hgle1B^{19Mt} (gle1 DDX19 binding mutant). Importantly, this molecular complementation analysis will help define the biochemical and functional constraints that needed to rescue Fin_{Major} functionality.

Concluding remarks

Nuclear export of mRNA represents an essential step during gene expression. Over the last several decades many of the important protein components and regulatory paradigms have been documented. The work presented would not have been possible without collaborative multidisplinary analysis. Together, these integrated approaches allowed us to gain mechanistic insight into the regulation of Gle1 during mRNA export. I am grateful my work contributes to this paradigm and look forward to future discoveries in our field.

Appendix A

Yeast two hybrid screen identifies novel Gle1 interaction partners.

Introduction and results

In Chapter 2 of this thesis we documented that the coiled-coil domain mediates Gle1 self-association *in vitro* and in living cells. Further, we showed that self-association is critical for the function of Gle1 in mRNA export but not in translation. In biology, coiled-coil domain motifs are often utilized to mediate protein interactions (Burkhard et al., 2001). We hypothesized that the coiled-coil domain might facilitate additional biochemical interactions with unknown binding partners (in addition to Gle1 self-association). Thus, to identify novel interactions partners for the coiled-coil domain a yeast two hybrid screen was conducted with a Human Fetal Brain cDNA library (Matchmaker).

Previous yeast two hybrid screens utilized full-length hGle1 as the bait protein (Kendirgi et al., 2005a; Rayala et al., 2004). To minimize rediscovery of previous hits and expedite identification of coiled-coil domain interaction partners, we engineered the coiled-coil domain (aa. 1-362) of hGle1 to be the bait protein. Clones (n = 1.2 × 106) were screened for interaction with the GBD-hGle1(1-362) bait protein. An efficient mating based assay was used to remove false positives and identify interactions that were

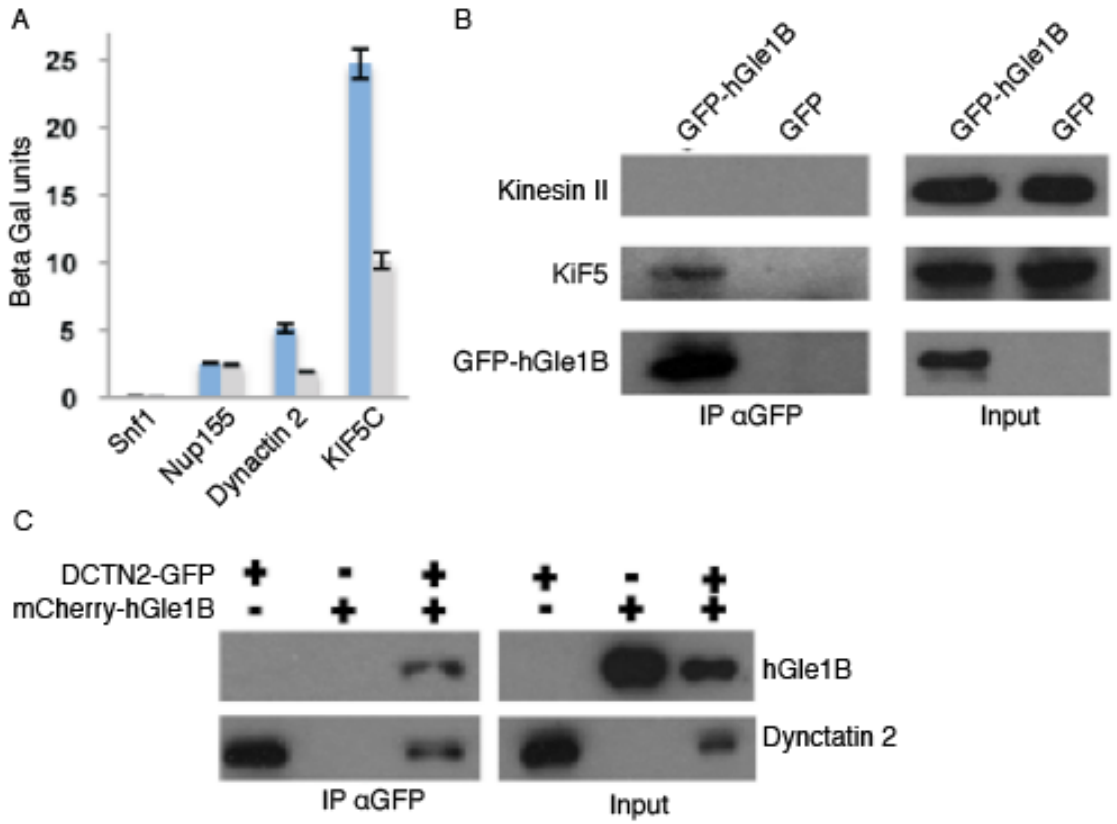

Figure A.1: hGle1 interacts with KIF5 and Dynactin 2: (A) Two-hybrid hGle1 interactions: Yeast transformed with *hGLE1* bait vectors (blue, wild-type; gray, Fin_{Major}) and noted prey plasmids were assayed for β-galactosidase levels. Error bars represent 1 SEM above and below the mean. (B-C) hGle1 biochemically interactions with KIF5 and Dynactin 2. (B) *GFP* or *GFP-hGle1B* plasmids were transfected into U2OS cells, and immunoprecipitations were performed with α-GFP antibodies. Samples were immunoblotted with either α-hGle1, α-Kinesin 5, or α-Kinesin II antibodies. (C) *Dynactin2-GFP* (abbreviated DCTN2-GFP) and *mCherry-hGle1B* plasmids were co-transfected into U2OS cells, and immunoprecipitations were performed with α-GFP antibodies. Samples were immunoblotted with α-GFP (bottom row) or α-hGle1 (top) antibodies.

perturbed with the Fin_{Major} protein. In brief, strains harboring the bait and library prey plasmids were selected by growth in media containing 5-FOA. The resulting prey strain was then mated against bait tester strains transformed with *SNF1*, *hGLE1B*, or *h-gle1B-Fin_{Major}* bait vectors. Using this system we were able to remove false positives and rapidly identify candidates that were perturbed with the Fin_{Major} protein.

This strategy identified two novel coiled-coil interaction partners (KIF5C and Dynactin 2 (DCTN2)) that were specifically perturbed by the Fin_{Major} PFQ insertion (Figure A1.A). Interestingly, both KIF5C and DCTN2 have documented function in the trafficking of cargo along microtubules (Goldstein and Yang, 2000). KIF5C is a plus-end directed microtubule motor, where DCTN2 is a subunit of dynactin, a macromolecular complex that regulates minus-end directed microtubule motor dynein (Schroer, 2004). Interestingly, both KIF5C and DCTN2 are important for cytoplasmic mRNA trafficking (Martin and Ephrussi, 2009). In neurons, where mRNPs are transported long distances, directional movement of RNA granules along microtubules is determined by the balance between the molecular motors: kinesins moving granules towards the plus ends, and dynein moving granules towards the minus ends (Kanai et al., 2004; Kiebler and Bassell, 2006).

To verify the hGle1-KIF5 and hGle1-DCTN2 interactions, we performed co-immunoprecipitation experiments in cultured cells. A mammalian expression construct coding for *GFP-hGle1B* cDNA was transfected into U2OS cells. Immunoprecipitation were conducted using anti-GFP antibodies and co-isolation of endogenous KIF5B was detected by immunoblotting with a commercially available anti-KIF5 antibody (Figure A.1B). Importantly, this experiment documented that GFP-hGle1B biochemically

interacts with endogenous KIF5B protein. hGle1B did not interact with the abundant Kinesin II (Figure A.1B). Using a similar experimental strategy, we tested if hGle1 biochemically interacted with DCTN2. GFP-tagged *DCTN2* and mCherry-tagged *hGLE1* genes were co-transfected into U2OS cells. Following immunoprecipitation using anti-GFP antibodies, the samples were separated by SDS PAGE and the hGle1 and DCTN2 was detected by immunoblotting with anti-hGle1 and anti-GFP antibodies (Figure A.1C). Strikingly, we observed that hGle1B co-isolated with DCTN2. Taken together, these data indicated that hGle1B biochemically interacts with both DCTN2 and KIF5C in cultured cells.

Discussion

Coiled-coils are one of the most common motifs found in proteins. In *S. cerevisiae* 1 of every 11 proteins is predicted to contain a coiled-coil domain. In a prior study, a yeast two-hybrid screen was done using the predicted coiled-coil domains found in *S. cerevisiae* as bait and prey (Newman et al., 2000). This study assayed 162 putative coiled-coil regions from 121 proteins in pairwise tests. Doing this 213 interactions (33 were homotypic, 175 were heterotypic) were found from 77 different proteins. Many of the analyzed coiled-coil domains interacted with multiple partners. The biological significance of these multiprotein interactions is not clear (Newman et al., 2000). This raises the possibility that some of these identified interaction may not be biologically significant and merely represent the affinity of coiled-coil domains for a similar tertiary protein fold.

Both KIF5C and DCTN2 contain multiple coiled-coil domains (Schroer, 2004; Verhey and Hammond, 2009). The two-hybrid interaction with hGle1's coiled-coil domain and KIF5C and DCNT2 suggests that the interaction may be direct. The fact that the Fin_{Major} PFQ insertion disrupts this interaction is additional evidence for the specificity of these interactions. Using co-immunoprecipation analysis we showed that hGle1 biochemically interacts with both KIF5C and DCNT2. Given the established roles of DCNT2/KIF5C in polarized mRNP transport, it is intriguing to speculate that Gle1 might also be involved in this process (Martin and Ephrussi, 2009). This hypothesis, however, needs to be tempered with the alternative conclusion that the interaction between hGle1 with KIF5C or DCNT2 might represent the non-specific affinity of coiled-coil motifs. Future studies are needed to distinguish between these possibilities.

Appendix B

miRNA depletion of Gle1 and DDX19 in cultured cells

Introduction

In Chapter 2 of this thesis, siRNA technology was used to deplete endogenous hGle1 protein levels in HeLa cells. Additionally, we found that depletion of hGle1 proteins levels contributed to a export defect of bulk poly(A)$^+$ RNA. In a parallel set of studies we used different technology (miRNA RNAi) to deplete hGle1 protein levels in cultured cells. The results of these experiments are summarized below.

Results

The BLOCK-iT Pol II miR RNAi expression system (Invitrogen) was used to reduce endogenous levels of hGle1 in cultured cells. A *pcDNA-GFP-miR* expression vector was generated to express two separate engineered miRNAs with 100% homology to a target *GLE1* sequence (CTAGATCAACCCTCATTTGTT and CCCAAGCTATCTTCTTATTCT). This *pcDNA-GFP-miR*^{hGle1} expression vector was used to knockdown endogenous hGle1 protein levels in U2OS cells. As a control, a *pcDNA-GFP-miR*^{CTRL} vector that expresses a scrambled miRNA was tested in parallel. We examined the ability of our *pcDNA-GFP-miR*^{hGle1} to deplete endogenous levels of hGle1 protein in cultured U2OS cells. In brief, U2OS cells were transfected with either *pcDNA-GFP-miR*^{hGle1} or *pcDNA-GFP-miR*^{CTRL} vectors. Seventy-two hours post transfection, the cells were harvested and the knockdown efficiency was examined by

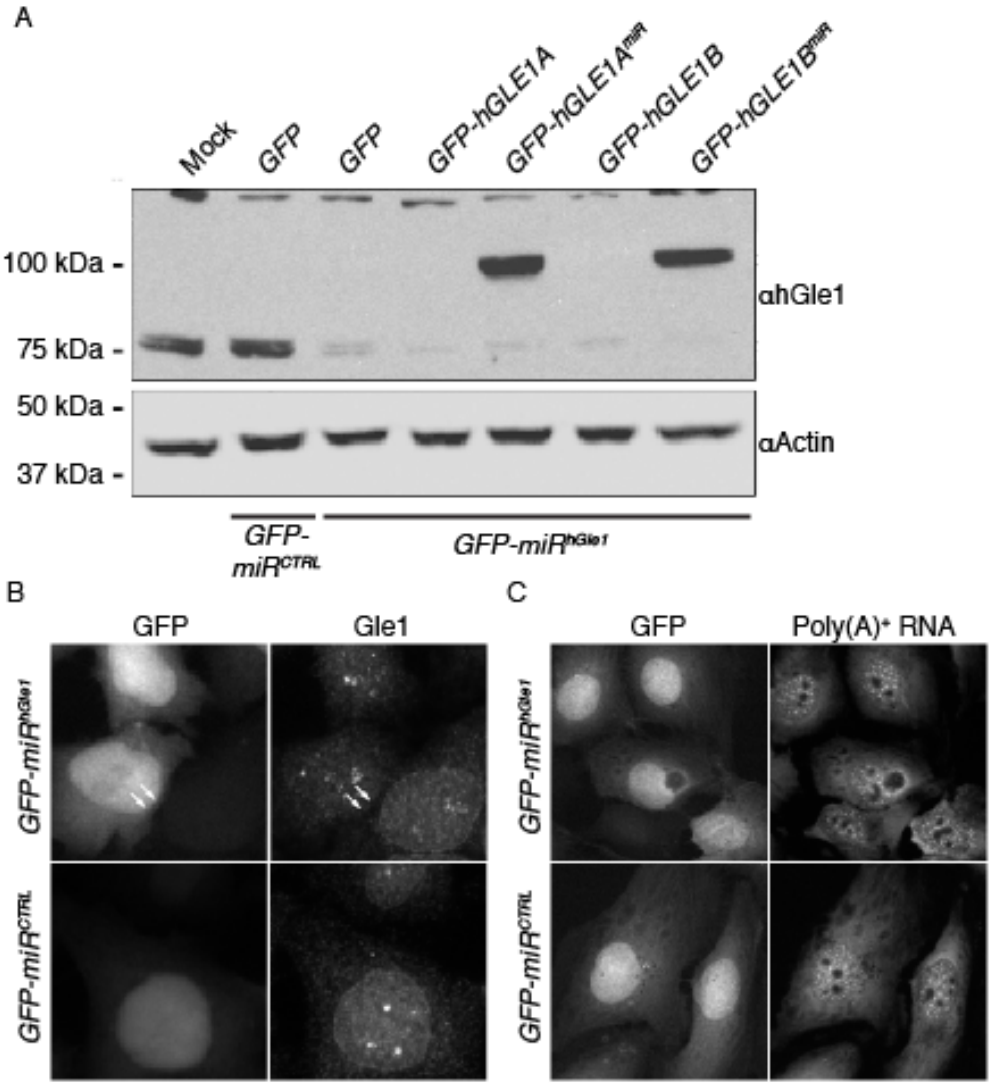

Figure B.1: miRNA technology effectively depletes Gle1 protein levels. (A).U2OS cells werer transfected with *pcDNA-GFP-miR*^{hGle1} or *pcDNA-GFP-miR*^{CTRL} (abbreviated *GFP-miR*^{hGle1}, and *GFP-miR*^{CTRL}) vectors. Immunoblot analysis of hGle1 levels in control *GFP-miR*^{hGle1} and *GFP-miR*^{CTRL} treated cells transfected with the indicated GFP-tagged proteins is shown. (C-D) U2OS cells were transfected with either *GFP-miR*^{hGle1} or *GFP-miR*^{CTRL} plasmids. Cells were processed for: (C) immunohistochemistry with α-hGle1 antibodies to detect Gle1 protein levels. Cells expressing the *pcDNA-miR*^{hGle1} had decreased levels of Gle1 protein as indicated by white arrows. (D) *in situ* hybridization with a CY3-conjugated oligo(dT) probe to detect total poly(A)$^+$ RNA. Cells expressing the *pcDNA-miR*^{hGle1} shows a similar distribution of poly(A)$^+$ RNA to the control *pcDNA-miR*^{CTRL} cells.

immunoblotting with anti-hGle1 antibody (Figure B.1A). We observed that cells transfected with *pcDNA-GFP-miR*^{hGle1} vector but not the *pcDNA-GFP-miR*^{CTRL} had depleted hGle1 protein levels. Further, we were able to rescue expression by co-transfection with GFP-tagged miRNA-resistant *hGLE1* vectors (Figure B.1A).

In a parallel set of analysis, we examined the depletion of hGle1 protein levels on a single cell basis using fluorescence microscopy. Co-cistronic expression of a GFP reporter in the *pcDNA-GFP-miR* vector enables visual tracking of cells expressing the engineered miRNAs by direct fluorescence microscopy. U2OS cells were transfected with either *pcDNA-GFP-miR*^{hGle1} or *pcDNA-GFP-miR*^{CTRL} vectors. hGle1 protein levels were examined by immunohistochemistry with anti-hGle1 antibody followed by detection by fluorescence microscopy. This analysis revealed that the cells transfected with *pcDNA-GFP-miR*^{hGle1} expression vector (marked by GFP expression) had depleted Gle1 protein levels, as indicated by reduced nuclear rim signal (Figure A2.1B). In contrast, the cells expressing *pcDNA-GFP-miR*^{CTRL} showed no effect on Gle1 level (Figure A2.1B). Taken together, these data suggested that expression of the *pcDNA-GFP-miR*^{hGle1} vector effectively depletes Gle1 protein levels in cultured U2OS cells. It should be noted that similar results were found also in HeLa cells (data not shown).

We next tested if depletion of hGle1 protein levels using the *pcDNA-GFP-miR*^{hGle1} results in disruption of export of poly(A)$^+$ RNA. U2OS cells were transfected with *pcDNA-GFP-miR*^{hGle1} or *pcDNA-GFP-miRNA*^{CTRL}. Seventy-two hours post transfection the cells were fixed and processed for *in situ* hybridization with Cy3-conjugated oligo (dT) probe. Using this approach, we were unable to detect accumulation of poly(A)$^+$ RNA upon expression of either *pcDNA-GFP-miR*^{hGle1} or *pcDNA-GFP-*

miRNA^{CTRL} vectors (Figure A2.1C). This suggested that these cells do not have a defect in mRNA export. In Chapter 2 we observed a robust accumulation of poly(A)$^+$ RNA in our *GLE1*-siRNA treated cells. Taken together, these data suggest that the expression of the *pcDNA-GFP-miR*^{hGle1} vector in cells is unable to deplete Gle1 to a level that would elicit a perturbation in bulk mRNA export.

In a parallel set of studies, we utilized the BLOCK-iT Pol II miR RNAi expression system (Invitrogen) to reduce endogenous levels of DDX19 in cultured cells. A *pcDNA-GFP-miR* expression vector was generated to express an artificially engineered miRNA with 100% homology to a target *DDX19* sequence (GAACTTAATTGCCCAATCTCA). U2OS cells were transfected with *pcDNA-GFP-miR*^{DDX19} or *pcDNA-GFP-miRNA*^{CTRL}. Seventy-two hours post transfection, the cells were fixed and processed for *in situ* hybridization with CY3-conjugated oligo(dT) probe. Doing this we detected robust accumulation of poly(A)$^+$ RNA in the nucleus upon expression of the *pcDNA-GFP-miR*^{DDX19} vector but not with the *pcDNA-GFP-miR*^{CTRL} vector (Figure B.2).

Discussion

In this study, we documented that expression of the *pcDNA-GFP-miR*^{DDX19} vector results in a robust mRNA export defect. Moving forward it is essential to analyze the knockdown efficiency of the *pcDNA-GFP- miR*^{DDX19} vector by immunoblotting with a commercially available DDX19 antibody. This analysis is critical for proper interpretation of the *pcDNA-GFP-miR*^{DDX19} data sets.

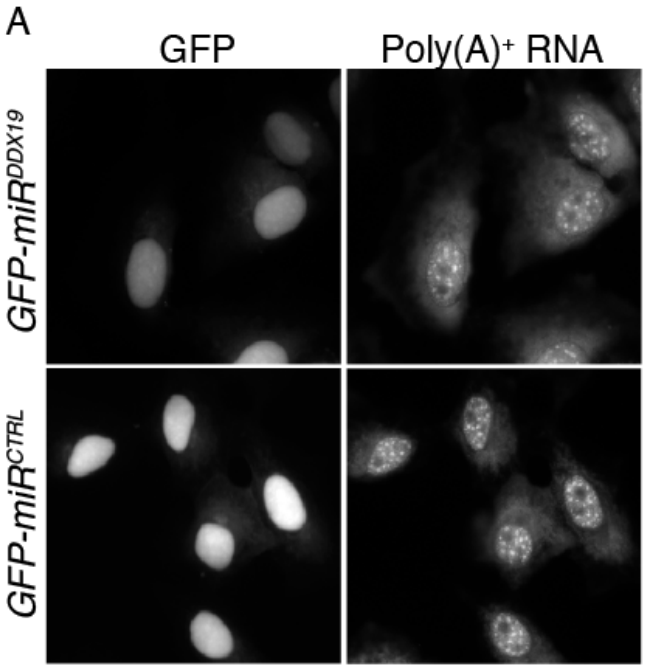

Figure B.2: Expression of *pcDNA-GFP-miR*^{DDX19} vector disrupts mRNA export. U2OS cells were transfected with *pcDNA-GFP-miR*^{DDX19} or *pcDNA-GFP-miR*^{CTRL} (abbreviated *GFP-miR*^{DDX19}, and *GFP-miR*^{CTRL}) vectors. Cells were processed for *in situ* hybridization with a Cy3-conjugated oligo (dT) probe to detect total poly(A)$^+$ RNA. Cells expressing the *GFP-miR*^{DDX19} vector show accumulation of nuclear poly(A)$^+$ RNA.

In Chapter 2 we show that depletion of hGle1 protein levels using siRNA technology results in the robust accumulation of poly(A)$^+$ RNA in the nucleus. Expression of the *pcDNA-GFP-miR*^{hGle1} vector also effectively depleted hGle1 protein levels (Figure B.1A-B). In contrast, we could not detect a robust mRNA export defect in *pcDNA-GFP-miR*^{hGle1} expressing cells (Figure B.1C). These results suggest that expression of the *pcDNA-GFP-miR*^{hGle1} vector is unable to deplete Gle1 protein to a level that would elicit a defect in mRNA export. This may suggest that there is a critical threshold of Gle1 activity at the NPC that is required for efficient mRNA export. The ability to identify Gle1 depleted cells via GFP expression with the *pcDNA-GFP-miR* technology is a very powerful experimental readout. In conclusion, the *pcDNA-GFP-miR*^{hGle1} vector is not a useful reagent for studying Gle1's role in mRNA export. However, this vector may be useful in examining Gle1 functionality in other experimental contexts. Future studies are needed to explore this exciting possibility.

Appendix C

Structural analysis of the Fin_{Major} and y-gle1-136$^{\wedge PFQ}$ proteins

Introduction

In Chapter 2 of this thesis we documented that Gle1 self-associates *in vitro* to form high molecular mass disk complexes. Further, our analysis documented that the MBP-h-gle1(1-365)-Fin_{Major} disk structures appeared malformed and disordered. The precise nature of how the Fin_{Major} PFQ insertion disrupts Gle1 self-association remains unclear. In this study we investigated the biochemical, and structural consequence of insertion of a PFQ peptide within the coiled-coil domain of Gle1. To analyze the potential perturbations of PFQ insertion on Gle1 self-association, a series of experiments with human and yeast Gle1 proteins were performed. A summary of these results is presented below.

Results

Structural characterization of the hgle1-Fin_{Major} protein

Our structural analysis using NegEM indicated that the Fin_{Major} protein perturbs Gle1 self-association. Given these structural perturbations, we hypothesized that the Fin_{Major} disk structures may be sensitive to treatment with mild denaturing challenges. Wild-type and Fin_{Major} samples were subjected to the following treatments: (1) flash freeze/thaw, (2) incubation at 40°C and 60°C, (3) incubation at 23°C or 4°C for 24 hours, or (4) addition of SDS to the sample. We hypothesized that challenging the

Fin_{Major} disks would cause the disk structures to fall apart or aggregate in solution. This, in turn, would lead to reduction in the total number of disk structures in the Fin_{Major} sample after treatment. In contrast, we predicted that the wild-type hGle1 samples would not be influenced by these treatments. For all treatments described below, purified recombinant MBP-hGle1(1-362) and MBP-hgle1(1-365)-Fin_{Major} proteins were used. The preparation of the disk samples for both wild-type and Fin_{Major} was done as previously described in Chapter 2.

For the rapid freeze/thaw treatment, protein samples were aliquoted into small 1.5mL eppendorf tubes. The samples were then flash frozen in liquid nitrogen and immediately thawed on ice. Analysis of the samples by NegEM revealed that both wild-type and Fin_{Major} samples still contained disk structures after treatment. However, both wild-type and Fin_{Major} samples had a significant reduction in the number of particles as compared to the untreated sample (Figure C.1B,F). The reduction in total number of disks indicated that both wild-type and Fin_{Major} disk structures are sensitive to rapid freeze/thaw treatment.

For the temperature treatment challenges, protein samples were aliquoted into small 1.5mL eppendorf tube. The samples were incubated 45°C or 60°C for 70 minutes. Analysis of the samples by NegEM revealed that both wild-type and Fin_{Major} samples still contained disk structures after each treatment. In the 45°C treatment there was no significant reduction of disk number with the either wild-type or Fin_{Major} samples (Figure C.1C,G). In contrast, we observed a significant reduction of the total number of disk structures for both wild-type and Fin_{Major} samples after treatment at 60°C (Figure C.1C,G). In a parallel set of analysis, wild-type and Fin_{Major} samples were incubated at

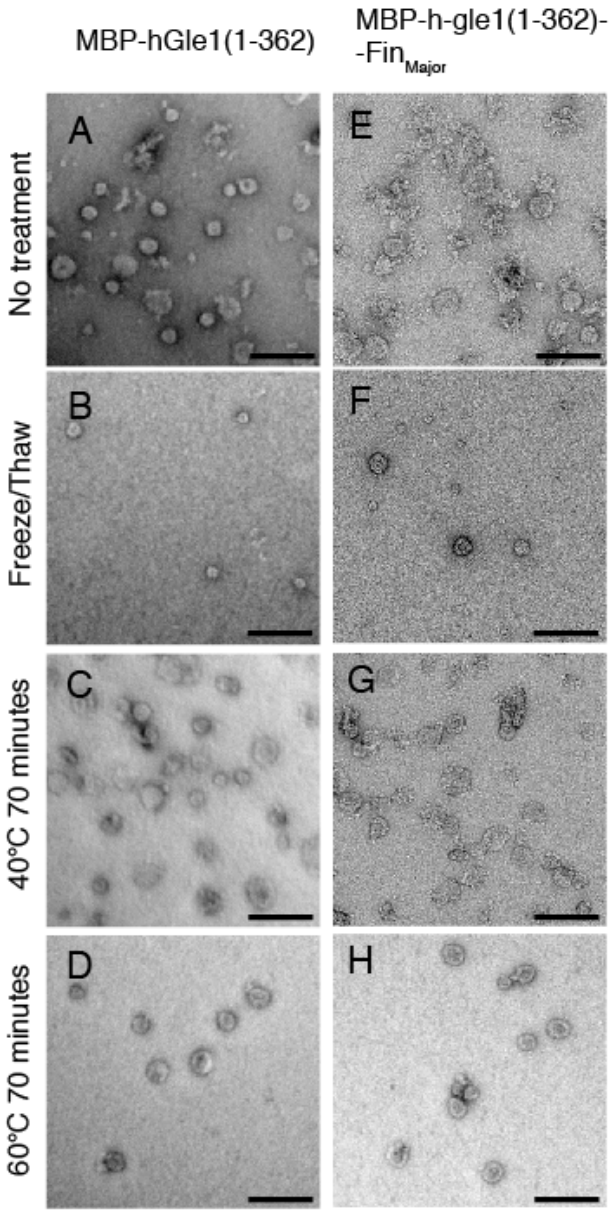

Figure C.1: Gle1 disk structures are sensitive to harsh variations in temperature. (A-D) Representative EM image for purified MBP-hGle1(1-362) is shown for indicated treatments. (E-H) Representative EM image for purified MBP-hGle1(1-362) is shown for indicated treatments. Bar, 100 nm.

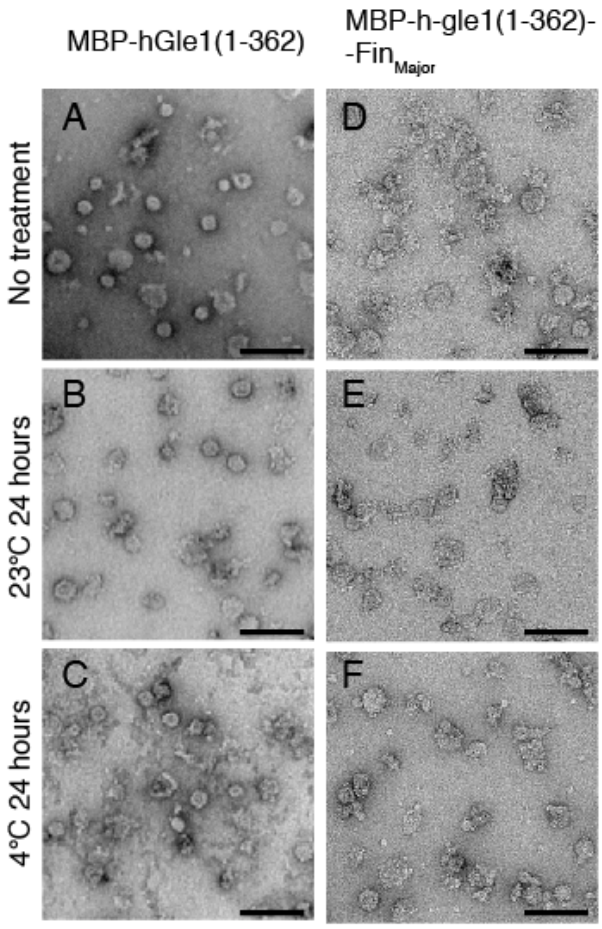

Figure C.2: hGle1 disk structures are sensitive to mild variations in temperature. (A-C) Representative EM image for purified MBP-hGle1(1-362) is shown for indicated treatments. (D-F) Representative EM image for purified MBP-h-gle1(1-362)-Fin$_{Major}$ is shown for indicated treatments. Bar, 100 nm.

23°C or 4°C for 24 hours. We observed increased aggregation for both wild-type and Fin_{Major} samples after treatment at 4°C for 24 hours. In contrast, we saw decreased numbers of aggregated disk structures for both wild-type and Fin_{Major} samples after treatment at 23°C for 24 hours (Figure C.2 B,E). Taken together, these results indicate that the hGle1 disk structures are sensitive to both mild and severe changes in temperature. Importantly, this data indicated that Fin_{Major} and wild-type disk structures have identical sensitivity to variations in temperature.

For the SDS treatment challenges, only the wild-type disk structures were tested. In brief, the MBP-hGle1(1-362) disk sample was aliquoted into small 1.5mL eppendorf tube. The samples then treated with either 0.1%, 0.05%, and 0.01% SDS on ice for 30 minutes. Analysis of the samples by NegEM revealed wild-type samples contain no disk structures after treatment with 0.1%, 0.05%, and 0.01% SDS (Figure C.3). This data indicated that SDS treatment caused the oligomeric complex to fall apart in solution. Of note, these results documented that hGle1 self-association is very sensitive to low levels of anionic detergents.

Structural characterization of the y-gle1-136$^{\wedge PFQ}$ protein

Our *in silco* analysis suggested that the y-gle1-136$^{\wedge PFQ}$ should behave biochemically similar to that of the human Fin_{Major} protein. A prediction that stems from this analysis would be that the y-gle1-136$^{\wedge PFQ}$ protein would also have malformed disk structures. To test this, we analyzed the disk structures of the y-gle1-136$^{\wedge PFQ}$ protein using NegEM. Recombinant untagged full-length yGle1 and y-gle1-136$^{\wedge PFQ}$ disk

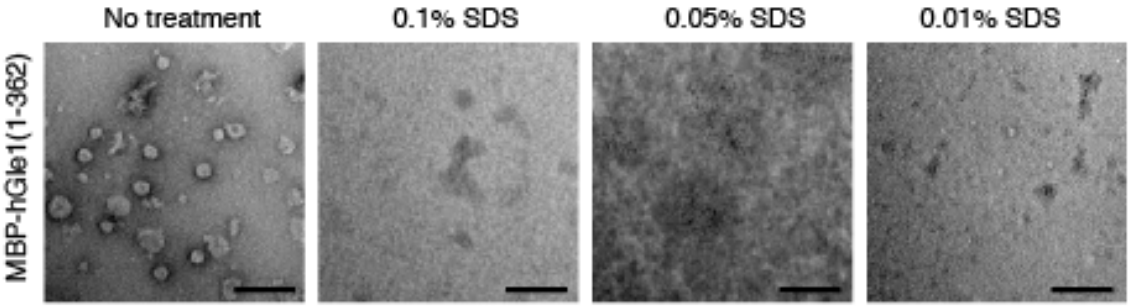

Figure C.3: hGle1 disk structures are highly sensitive to anionic detergent treatment. Representative EM image for purified MBP-hGle1(1-362) is shown for indicated treatments. Bar, 100 nm.

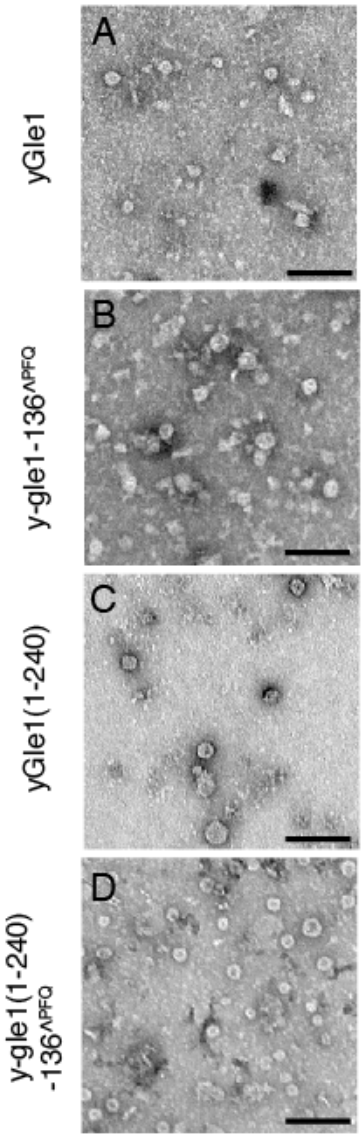

Figure C.4: Structural analysis of y-gle1-136$^{\wedge PFQ}$ protein. (A-D) Representative EM images for specified yGle1 protein variants is shown. Bar, 100 nm

complexes were purified. Analysis these samples by NegEM revealed that y-gle1-136$^{\wedge PFQ}$ formed disk structures that had identical structural characteristics to that of wild-type yGle1 disk structures (Figure C.4A-B). In contrast to the phenotype observed with the human Fin_{Major} PFQ insertion, this data indicated that insertion of the PFQ motif after residue 136 in yeast Gle1 did not grossly perturb the structure of the oligomeric disk of the full-length yGle1 protein.

For both wild-type and Fin_{Major} proteins the N-terminal domain (aa. 1-362) of hGle1 was analyzed *in vitro* for self-association and disk formation. However, in our initial analysis of the y-gle1-136$^{\wedge PFQ}$ the full-length protein was used. Thus we hypothesized that the use of the full-length yGle1 protein may have masked the possible perturbations found in the y-gle1-136$^{\wedge PFQ}$ disk structure. We next tested if the N-terminal domain of Gle1 (amino acids 1-240) is sufficient for gle1 self-association and disk formation *in vitro*. Recombinant untagged yGle1(1-240) was purified and fractionated by size exclusion chromatography. Analysis by NegEM revealed that yGle1(1-240) formed large disk structures (Figure C.4C). We then tested if the y-gle1(1-240)-136$^{\wedge PFQ}$ protein formed disk structures. Recombinant untagged y-gle1(1-240)-136$^{\wedge PFQ}$ was purified and fractionated by size exclusion chromatography. Analysis of this sample by NegEM revealed that y-gle1(1-240)-136$^{\wedge PFQ}$ formed large disk structures that appeared identical to disk structures found in the wild-type yGle1(1-240) sample (Figure C3.4C-D). Taken together, this data indicated that insertion of PFQ at residue 136 does not grossly perturb the structure of yGle1(1-240) oligomeric disk structure.

Discussion

In this study we analyzed the consequence of treatment of wild-type and Fin_{Major} oligomeric disk samples with mild denaturing treatments. We had anticipated due to the malformed nature of the Fin_{Major} disks that they would be more sensitive to these treatments. In contrast to this hypothesis, we found that both the wild-type and Fin_{Major} proteins behaved similarly in all treatments tested. This data suggests that the Fin_{Major} PFQ insertion does not influence the overall stability of the oligomeric complex. This is consistent with our previously biochemical analysis of the Fin_{Major} protein by SVAU (Figure 2.3).

Our *in silco* analysis indicated that the y-gle1-136$^{\wedge PFQ}$ protein should biochemically mimic the human Fin_{Major} protein. In support of this conclusion, similar to the Fin_{Major} protein we observed that the y-gle1-136$^{\wedge PFQ}$ protein is also defective in mRNA export (Figure 2.9). We hypothesized that the y-gle1-136$^{\wedge PFQ}$ protein would also form malformed disk structures *in vitro*. We were surprised to find that the structural characteristics of the y-gle1-136$^{\wedge PFQ}$ disk structures appeared to be identical to that of the wild-type yGle1 protein. This data indicates unlike the Fin_{Major} protein the y-gle1-136$^{\wedge PFQ}$ protein does not grossly influence the overall structure of the oligomeric complex. However, the NegEM approach has limited resolution to resolve structural perturbations when observing single molecules. Thus, future experiments are needed to define the structural perturbations that occur in the altered y-gle1-136$^{\wedge PFQ}$ protein.

Appendix D:

Plasmids used in this study

Plasmid	Description	Source
mCerulean3-C1	Mammalian expression vector	(Markwardt et al., 2011)
mVenus-C1	Mammalian expression vector	(Nagai et al., 2002)
mVenus-N1	Mammalian expression vector	(Nagai et al., 2002)
eGFP-C1	Mammalian expression vector	Clontech
pGex4T-3	*GST* expression vector	GE Healthcare
pMal-Cri	*MBP* expression vector	New England Biosciences
pRS315	*CEN/URA3*	(Sikorski and Hieter, 1989)
mCerulean-C1	Mammalian expression vector	(Rizzo et al, 2004)
PAGFP-C1	Mammalian expression vector	Clontech
CFP-C1	Mammalian expression vector	Clontech
YFP-C1	Mammalian expression vector	Clontech
mCherry-C1	Mammalian expression vector	Clontech
3XmCitrine-C1	Mammalian expression vector	(Cai et al., 2007)
pIRES2-DsRed2	Mammalian expression vector	Clontech
mCerulean-N1	Mammalian expression vector	(Rizzo et al., 2004)
pRS316	*CEN/LEU2*	(Sikorski and Hieter, 1989)
pGBD-C	Yeast two-hybrid expression vector	(James et al., 1996)
Pom121-mCherry	Mammalian expression of *Pom121-mCherry*	(Dultz et al., 2008)
pBRR118b	*yGLE1-GFP/CEN/TRP1*	This Study
pSW3779	*y-gle1-136$^{\wedge PFQ}$-GFP/CEN/TRP1*	This Study
pSW1482	Mammalian expression of *eGFP-hGLE1B*	(Kendirgi et al., 2003)
pSW3903	Mammalian expression of *eGFP-h-gle1B-Fin$_{Major}$*	This Study
pSW3894	Mammalian expression of *eGFP-h-gle1BDCC*	This Study
pSW3908	Mammalian expression of *eGFP-hGLE1B^{R}*	This Study
pSW3945	Mammalian expression of *eGFP-h-gle1B^{R}-Fin$_{Maior}$*	This Study
pSW3775	Mammalian expression of *mCerulean3-hGLE1B*	This Study
pSW3774	Mammalian expression of *mVenus-hGLE1B*	This Study
pSW3932	Mammalian expression of *mVenus-hGLE1(362-698)*	This Study
pSW3017	*G$_{BD}$-hGLE1B/2μ/URA3*	(Rayala et al., 2004)
pSW3904	*G$_{BD}$-h-gle1B-Fin$_{Major}$/2μ/URA3*	This Study
CP261	G$_{AD}$-eIF3F/2μ/LEU2	(Kendirgi et al., 2005)
pSW233	*G$_{AD}$-NUP155/2μ/LEU2*	(Rayala et al., 2004)
pSW3068	*G$_{AD}$-hCG1/2μ/LEU2*	(Kendirgi et al., 2005)
pSW3723	*in vitro* translation vector *hGLE1(1-360)*	This Study
pSW1423	Expression plasmid for *GST-hGLE1(1-362)*	This Study
pSW3851	Expression plasmid for *MBP-hGLE1(1-362)*	This Study
pSW3852	Expression plasmid for *MBP-h-gle1(1-365)-Fin$_{Major}$*	This Study
pSW3242	Expression plasmid for *MBP-6TEV-yGLE1*	(Alcázar-Román et al., 2006)
pSW3830	Expression plasmid for *MBP-6TEV-y-gle1-136$^{\wedge PFQ}$*	This Study
pSW3831	Expression plasmid for *MBP-6TEV-y-gle1-149$^{\wedge PFQ}$*	This Study
pSW3327	Expression plasmid for *MBP-6TEV-yGLE1(241-538)*	This Study
pSW410	*yGLE1/CEN/URA3*	(Murphy et al., 1996)
pSW399	*yGLE1/CEN/LEU2*	(Murphy et al., 1996)
pSW3743	*y-gle1-136$^{\wedge PFQ}$/CEN/LEU2*	This Study
pSW3742	*y-gle1-149$^{\wedge PFQ}$/CEN/LEU2*	This Study
pSW3760	*y-gle1-157$^{\wedge PFQ}$/CEN/LEU2*	This Study
pSW3829	*y-gle1ΔCC/CEN/LEU2*	(Watkins et al., 1998)
pSW3792	*y-gle1ΔCC+yCC/CEN/LEU2*	This Study
pSW3826	*y-gle1ΔCC+hCC/CEN/LEU2*	This Study
pSW3828	*y-gle1ΔCC+-/CEN/LEU2*	This Study
pSW3827	*y-gle1ΔCC+hFin$_{Major}$CC/CEN/LEU2*	This Study
pSW3827	*y-gle1ΔCC+hFin$_{Major}$CC/CEN/LEU2*	This Study
pSW3253	Mammalian expression of *eGFP-DDX19*	This Study
pSW3971	Mammalian expression of *eGFP-h-gle1B^{R569H}*	This Study
pSW3972	Mammalian expression of *eGFP-h-gle1B^{V617M}*	This Study
pSW3973	Mammalian expression of *eGFP-h-gle1B^{I684T}*	This Study

Plasmids used in this study

Plasmid	Description	Source
pSW4033	Mammalian expression of *IRES-hGLE1B-dsRED2*	This Study
pSW4034	Mammalian expression of *IRES-hGLE1B^{miR}-dsRED2*	This Study
pSW4035	Mammalian expression of *IRES-hGLE1A-dsRED2*	This Study
pSW4036	Mammalian expression of *IRES-hGLE1B-Fin$_{Major}$-dsRED2*	This Study
pSW4037	Mammalian expression of *IRES-hGLE1B^{miR}-Fin$_{Major}$-dsRED2*	This Study
pSW4038	Mammalian expression of *CFP-hGLE1B*	This Study
pSW4039	Mammalian expression of *CFP-hgle1B-Fin$_{Major}$*	This Study
pSW4040	Mammalian expression of *YFP-hGLE1B*	This Study
pSW4041	Mammalian expression of *YFP-hgle1B-Fin$_{Major}$*	This Study
pSW4044	Mammalian expression of *mCerulean3-hgle1B-Fin$_{Major}$*	This Study
pSW4042	Mammalian expression of *mVenus-hgle1B-Fin$_{Major}$*	This Study
pSW4045	Mammalian expression of *hGLE1B-mCerulean*	This Study
pSW4046	Mammalian expression of *hGLE1B-Fin$_{Major}$-mCerulean*	This Study
pSW4047	Mammalian expression of *mCherry-hGLE1B*	This Study
pSW4048	Mammalian expression of *mCherry-hgle1B-Fin$_{Major}$*	This Study
pSW4049	Mammalian expression of *eGFP-hgle1(1-100)*	This Study
pSW4050	Mammalian expression of *mCerulean3-hgle1(1-100)*	This Study
pSW4051	Mammalian expression of *mVenus-hgle1(1-100)*	This Study
pSW4052	Mammalian expression of *eGFP-hgle1B^{miR}*	This Study
pSW4053	Mammalian expression of *eGFP-hgle1A^{miR}*	This Study
pSW4054	Mammalian expression of *eGFP-hgle1B$^{miR,\ R569G}$*	This Study
pSW4055	Mammalian expression of *eGFP-hgle1B$^{miR,\ V617M}$*	This Study
pSW4056	Mammalian expression of *eGFP-hgle1B$^{miR,\ I684T}$*	This Study
pSW4057	*G$_{BD}$-hgle1(30-430)/2μ/URA3*	This Study
pSW4058	*G$_{BD}$-hGle1B-Fin$_{Major}$/2μ/URA3*	This Study
pSW4059	*in vitro* translation vector *hGLE1-Fin$_{Major}$(1-360)*	This Study
CP3888	*G$_{AD}$-DCNT21/2μ/LEU2)*	This Study
CP3889	*G$_{AD}$-KIF5C/2μ/LEU2*	This Study
pSW4069	*G$_{AD}$-hGle1(31-430)/2μ/URA3*	This Study
pSW4066	*G$_{AD}$-hGle1A-Fin$_{Major}$/2μ/URA3*	This Study
pSW4073	*G$_{AD}$-hGle1B^{R569H}/2μ/URA3*	This Study
pSW4074	*G$_{AD}$-hGle1B^{V617M}/2μ/URA3*	This Study
pSW4075	*G$_{AD}$-hGle1B^{I684T}/2μ/URA3*	This Study
pSW4064	*in vitro* translation vector *hgle1(1-360)-Fin$_{Major}$*	This Study
pSW4063	*in vitro* translation vector *hgle1B-Fin$_{Major}$*	This Study
pSW4062	Mammalian expression of *IRES-hGLE1A^{miR}-dsRED2*	This Study
pSW4061	Mammalian expression of *IRES-Δ30hGLE1AmiR-dsRED2*	This Study
pSW4067	Mammalian expression of *IRES-Δ30hGLE1B^{miR}-dsRED2*	This Study

Appendix E:

Yeast strains used in this study

Strain	Genotype	Source
W303	*MATα ade2-1 ura3-1 his3-11,15 leu2-3,112 trp1-1 can1-100*	(Thomas and Rothstein, 1989)
PJ69-4A	*MATa trp1-901 leu2-3,112 ura3-52 his3-200 gal4Δ gal80Δ LYS2::GAL1-HIS3 GAL2-ADE2 met::GAL7-lacZ*	(James et al., 1996)
PJ69-4A	*MATα trp1-901 leu2-3,112 ura3-52 his3-200 gal4Δ gal80Δ LYS2::GAL1-HIS3 GAL2-ADE2 met::GAL7-lacZ*	(This Study)
SWY1831	*MATα ade2-1 ura3-1 his3-11 leu2-3,112 trp1-1 gle1::HIS3* + pSW410 (*GLE1*)	(Murphy et al., 1996)
SWY1258	*MATa ade2-1 ura3-1 his3-11 leu2-3,112 trp1-1 gle1::HIS3* + pSW410 (*GLE1*)	This Study
SWY1259	*MATα ade2-1 ura3-1 his3-11 leu2-3,112 trp1-1 gle1::HIS3* + pSW410 (*GLE1*)	This Study
SWY1789	*MATa ade2-1 ura3-1 his3-11,15 leu2-3,112 trp1-1 can1-100 ipk1::KAN*	(Murphy et al., 1996)
SWY4209	*MATα ade2 ura3 his3 leu2 trp1 gle1-4*	(Alcázar-Román et al., 2006)
SWY4605	*MATα ade2 his3 leu2 trp1 gle1::HIS3 nup100::HIS3 + pSW410* (*GLE1*)	This Study
SWY1017	*MATα ade2 ura3 his3 leu2 trp1 nup100::HIS3*	(Murphy et al., 1996)
SWY3902	*MATa ade2-1 ura3-1 his3-11 leu2-3,112 trp1-1 gle1-2 nip1-1*	(Bolger et al., 2008)
B8302	*MATa ura3-52 lys5-10 cyc1-NLS cyc7-67 nip1-1*	(Gu et al., 1992)
SWY3828	*MATα ade2 ura3 his3 leu2 trp1 can1 gle1::HIS3* + pSW399 (*GLE1*)	(Alcázar-Román et al., 2006)
SWY4908	*MATα ade2-1 ura3-1 his3-11 leu2-3,112 trp1-1 gle1::HIS3* + pSW3743 (*gle1-136$^{\wedge PFQ}$*)	This Study
SWY4909	*MATα ade2-1 ura3-1 his3-11 leu2-3,112 trp1-1 gle1::HIS3* + pSW3742 (*gle1-149$^{\wedge PFQ}$*)	This Study
SWY4961	*MATα ade2-1 ura3-1 his3-11 leu2-3,112 trp1-1 gle1::HIS3* + pSW3760 (*gle1-157$^{\wedge PFQ}$*)	This Study
SWY4081	*MATa ade2 ura3 his3 leu2 trp1 nip1-1 gle1::HIS3* + pSW410 (*GLE1*)	This Study
SWY4952	*MATa ade2 ura3 his3 leu2 trp1 nip1-1 gle1::HIS3* + pSW399 (*GLE1*)	This Study
SWY4911	*MATa ade2 ura3 his3 leu2 trp1 nip1-1 gle1::HIS3* + pSW3743 (*gle1-136$^{\wedge PFQ}$*)	This Study
SWY4912	*MATa ade2 ura3 his3 leu2 trp1 nip1-1 gle1::HIS3* + pSW3742 (*gle1-149$^{\wedge PFQ}$*)	This Study
SWY4976	*MATa ade2 ura3 his3 leu2 trp1 nip1-1 gle1::HIS3* + pSW3760 (*gle1-157$^{\wedge PFQ}$*)	This Study
SWY4059	*MATα ade2-1 ura3-1 his3-11,15 leu2-3,112 trp1-1 can1-100 sup45-2*	This Study
SWY4079	*MATa ade2 ura3 his3 leu2 trp1 sup45-2 gle1::HIS3* + pSW410 (*GLE1*)	This Study
SWY4953	*MATa ade2 ura3 his3 leu2 trp1 sup45-2 gle1::HIS3* + pSW399 (*GLE1*)	This Study
SWY4913	*MATa ade2 ura3 his3 leu2 trp1 sup45-2 gle1::HIS3* + pSW3743 (*gle1-136$^{\wedge PFQ}$*)	This Study
SWY4914	*MATa ade2 ura3 his3 leu2 trp1 sup45-2 gle1::HIS3* + pSW3742 (*gle1-149$^{\wedge PFQ}$*)	This Study
SWY5002	*MATa ade2 ura3 his3 leu2 trp1 sup45-2 gle1::HIS3* + pSW3760 (*gle1-157$^{\wedge PFQ}$*)	This Study
CSY802	*hisD300 leu2D1 ura3-52 rat8-2 gle1::HIS* + p*GLE1/CEN/URA3*	C. Cole
SWY4936	*hisD300 leu2D1 ura3-52 rat8-2 gle1::HIS* + pSW399 (*GLE1*)	This Study
SWY4937	*hisD300 leu2D1 ura3-52 rat8-2 gle1::HIS* + pSW3743 (*gle1-136$^{\wedge PFQ}$*)	This Study
SWY4938	*hisD300 leu2D1 ura3-52 rat8-2 gle1::HIS* + pSW3742 (*gle1-149$^{\wedge PFQ}$*)	This Study
SWY4979	*hisD300 leu2D1 ura3-52 rat8-2 gle1::HIS* + pSW3760 (*gle1-157$^{\wedge PFQ}$*)	This Study
SWY4600	*MATα ura3-1 his3-11,15 trp1-1 leu2-3,112 ipk1::KAN gle1::HIS3* + pSW410 (*GLE1*)	This Study
SWY5635	*MATα ura3-1 his3-11,15 trp1-1 leu2-3,112 ipk1::KAN* + pSW399 (*GLE1)*	This Study
SWY5636	*MATα ura3-1 his3-11,15 trp1-1 leu2-3,112 ipk1::KAN gle1::HIS3* + pSW3743 (*gle1-136$^{\wedge PFQ}$*)	This Study
SWY5637	*MATα ura3-1 his3-11,15 trp1-1 leu2-3,112 ipk1::KAN gle1::HIS3* + pSW3742 (*gle1-149$^{\wedge PFQ}$*)	This Study
SWY5638	*MATα ura3-1 his3-11,15 trp1-1 leu2-3,112 ipk1::KAN gle1::HIS3* + pSW3760 (*gle1-157$^{\wedge PFQ}$*)	This Study
SWY4053	*MATa ura3 his3 leu2 rat7-1 gle1::HIS3* + pSW410 (*GLE1*)	This Study
LGY101	*MATα ura3-52 his3Δ200 leu2Δ1 rat7-1*	(Gorsch et al., 1995)
SWY3813	*MATα ade2 ura3 leu2 his3 nup42::HIS3 ipk1::KAN gle1::HIS3* + pSW410 (*GLE1*)+ pSW929 (*IPK1*)	This Study

REFERENCES

Al-Qattan, M.M., Shamseldin, H.E., and Alkuraya, F.S. (2012). Familial dorsalization of the skin of the proximal palm and the instep of the sole of the foot. Gene *500*, 216-219.

Alcazar-Roman, A.R., Bolger, T.A., and Wente, S.R. (2010). Control of mRNA export and translation termination by inositol hexakisphosphate requires specific interaction with Gle1. J Biol. Chem. *285*, 16683-16692.

Alcazar-Roman, A.R., Tran, E.J., Guo, S., and Wente, S.R. (2006). Inositol hexakisphosphate and Gle1 activate the DEAD-box protein Dbp5 for nuclear mRNA export. Nat. Cell Biol. *8*, 711-716.

Ashkenazy, H., Erez, E., Martz, E., Pupko, T., and Ben-Tal, N. (2010). ConSurf 2010: calculating evolutionary conservation in sequence and structure of proteins and nucleic acids. Nucleic Acids Res. *38*, W529-533.

Ballut, L., Marchadier, B., Baguet, A., Tomasetto, C., Seraphin, B., and Le Hir, H. (2005). The exon junction core complex is locked onto RNA by inhibition of eIF4AIII ATPase activity. Nat. Struc. & Mol. Biol. *12*, 861-869.

Bentley, D.L. (2005). Rules of engagement: co-transcriptional recruitment of pre-mRNA processing factors. Curr. Opin. Cell Biol. *17*, 251-256.

Bolger, T.A., Folkmann, A.W., Tran, E.J., and Wente, S.R. (2008). The mRNA export factor Gle1 and inositol hexakisphosphate regulate distinct stages of translation. Cell *134*, 624-633.

Bolger, T.A., and Wente, S.R. (2011). Gle1 is a multifunctional DEAD-box protein regulator that modulates Ded1 in translation initiation. J Biol. Chem. *286*, 39750-39759.

Bowers, H.A., Maroney, P.A., Fairman, M.E., Kastner, B., Luhrmann, R., Nilsen, T.W., and Jankowsky, E. (2006). Discriminatory RNP remodeling by the DEAD-box protein DED1. RNA *12*, 903-912.

Braud, C., Zheng, W., and Xiao, W. (2012). LONO1 encoding a nucleoporin is required for embryogenesis and seed viability in Arabidopsis. Plant Physiol. *160*, 823-836.

Burkhard, P., Stetefeld, J., and Strelkov, S.V. (2001). Coiled coils: a highly versatile protein folding motif. Trends Cell Biol. *11*, 82-88.

Burtey, A., Schmid, E.M., Ford, M.G., Rappoport, J.Z., Scott, M.G., Marullo, S., Simon, S.M., McMahon, H.T., and Benmerah, A. (2007). The conserved isoleucine-valine-phenylalanine motif couples activation state and endocytic functions of beta-arrestins. Traffic *8*, 914-931.

Busiek, K.K., Eraso, J.M., Wang, Y., and Margolin, W. (2012). The early divisome protein FtsA interacts directly through its 1c subdomain with the cytoplasmic domain of the late divisome protein FtsN. J Bacteriol. *194*, 1989-2000.

Chen, Y., Potratz, J.P., Tijerina, P., Del Campo, M., Lambowitz, A.M., and Russell, R. (2008). DEAD-box proteins can completely separate an RNA duplex using a single ATP. Proc. Natl. Acad. Sci. U S A *105*, 20203-20208.

Cheng, H., Dufu, K., Lee, C.S., Hsu, J.L., Dias, A., and Reed, R. (2006). Human mRNA export machinery recruited to the 5' end of mRNA. Cell *127*, 1389-1400.

Collins, R., Karlberg, T., Lehtio, L., Schutz, P., van den Berg, S., Dahlgren, L.G., Hammarstrom, M., Weigelt, J., and Schuler, H. (2009). The DEXD/H-box RNA helicase DDX19 is regulated by an {alpha}-helical switch. J Biol. Chem. *284*, 10296-10300.

Cooper, T.A., Wan, L., and Dreyfuss, G. (2009). RNA and disease. Cell *136*, 777-793.
Cordin, O., Banroques, J., Tanner, N.K., and Linder, P. (2006). The DEAD-box protein family of RNA helicases. Gene *367*, 17-37.

Dever, T.E., and Green, R. (2012). The elongation, termination, and recycling phases of translation in eukaryotes. Cold Spring Harbor perspectives in biology *4*, a013706.
Dreyfuss, G., Kim, V.N., and Kataoka, N. (2002). Messenger-RNA-binding proteins and the messages they carry. Nat. Rev. Mol. Cell Biol. *3*, 195-205.

Fairman, M.E., Maroney, P.A., Wang, W., Bowers, H.A., Gollnick, P., Nilsen, T.W., and Jankowsky, E. (2004). Protein displacement by DExH/D "RNA helicases" without duplex unwinding. Science *304*, 730-734.

Fan, J.S., Cheng, Z., Zhang, J., Noble, C., Zhou, Z., Song, H., and Yang, D. (2009). Solution and crystal structures of mRNA exporter Dbp5p and its interaction with nucleotides. J Mol. Biol. *388*, 1-10.

Folkmann, A., Collier, S., Zhan, X., Aditi, Ohi, M., and Wente, S. (2013). Gle1 functions during mRNA export in an oligomeric complex that is altered in human disease. Cell *155*, 582-593

Folkmann, A.W., Noble, K.N., Cole, C.N., and Wente, S.R. (2011). Dbp5, Gle1-IP6 and Nup159: a working model for mRNP export. Nucleus *2*, 540-548.

Frenkiel-Krispin, D., Maco, B., Aebi, U., and Medalia, O. (2010). Structural analysis of a metazoan nuclear pore complex reveals a fused concentric ring architecture. J Mol. Biol. *395*, 578-586.

Fried, H., and Kutay, U. (2003). Nucleocytoplasmic transport: taking an inventory. Cell. Mol. Life Sci. *60*, 1659-1688.

Ghaemmaghami, S., Huh, W.K., Bower, K., Howson, R.W., Belle, A., Dephoure, N., O'Shea, E.K., and Weissman, J.S. (2003). Global analysis of protein expression in yeast. Nature *425*, 737-741.

Gilbert, W., and Guthrie, C. (2004). The Glc7p nuclear phosphatase promotes mRNA export by facilitating association of Mex67p with mRNA. Mol. Cell *13*, 201-212.

Gilbert, W., Siebel, C.W., and Guthrie, C. (2001). Phosphorylation by Sky1p promotes Npl3p shuttling and mRNA dissociation. RNA *7*, 302-313.

Glaser, F., Pupko, T., Paz, I., Bell, R.E., Bechor-Shental, D., Martz, E., and Ben-Tal, N. (2003). ConSurf: identification of functional regions in proteins by surface-mapping of phylogenetic information. Bioinformatics *19*, 163-164.

Goh, K.I., Cusick, M.E., Valle, D., Childs, B., Vidal, M., and Barabasi, A.L. (2007). The human disease network. Proc. Natl. Acad. Sci. U S A *104*, 8685-8690.

Goldstein, L.S., and Yang, Z. (2000). Microtubule-based transport systems in neurons: the roles of kinesins and dyneins. Annu. Rev. Neurosci. *23*, 39-71.

Goss, D.J., and Kleiman, F.E. (2013). Poly(A) binding proteins: are they all created equal? Wiley interdisciplinary reviews RNA *4*, 167-179.

Grifo, J.A., Abramson, R.D., Satler, C.A., and Merrick, W.C. (1984). RNA-stimulated ATPase activity of eukaryotic initiation factors. J Biol. Chem. *259*, 8648-8654.

Gross, T., Siepmann, A., Sturm, D., Windgassen, M., Scarcelli, J.J., Seedorf, M., Cole, C.N., and Krebber, H. (2007). The DEAD-box RNA helicase Dbp5 functions in translation termination. Science *315*, 646-649.

Grunwald, D., and Singer, R.H. (2010). In vivo imaging of labelled endogenous beta-actin mRNA during nucleocytoplasmic transport. Nature *467*, 604-607.

Gruter, P., Tabernero, C., von Kobbe, C., Schmitt, C., Saavedra, C., Bachi, A., Wilm, M., Felber, B.K., and Izaurralde, E. (1998). TAP, the human homolog of Mex67p, mediates CTE-dependent RNA export from the nucleus. Mol. Cell *1*, 649-659.

Hall, J.G. (1985). Genetic aspects of arthrogryposis. Clin Orthop Relat Res, 44-53.
Henn, A., Cao, W., Hackney, D.D., and De La Cruz, E.M. (2008). The ATPase cycle mechanism of the DEAD-box rRNA helicase, DbpA. J Mol. Biol. *377*, 193-205.

Herva, R., Leisti, J., Kirkinen, P., and Seppanen, U. (1985). A lethal autosomal recessive syndrome of multiple congenital contractures. Am J Med Genet *20*, 431-439.
Hinnebusch, A.G. (2014). The Scanning Mechanism of Eukaryotic Translation Initiation. Annu. Rev. Biochem.

Hodge, C.A., Tran, E.J., Noble, K.N., Alcazar-Roman, A.R., Ben-Yishay, R., Scarcelli, J.J., Folkmann, A.W., Shav-Tal, Y., Wente, S.R., and Cole, C.N. (2011a). The Dbp5 cycle at the nuclear pore complex during mRNA export I: dbp5 mutants with defects in RNA binding and ATP hydrolysis define key steps for Nup159 and Gle1. Genes Dev. *25*, 1052-1064.

Hodge, C.A., Tran, E.J., Noble, K.N., Alcazar-Roman, A.R., Ben-Yishay, R., Scarcelli, J.J., Folkmann, A.W., Shav-Tal, Y., Wente, S.R., and Cole, C.N. (2011b). The Dbp5 cycle at the nuclear pore complex during mRNA export I: dbp5 mutants with defects in RNA binding and ATP hydrolysis define key steps for Nup159 and Gle1. Genes Dev. *25*, 1052-1064.

Hoelz, A., Debler, E.W., and Blobel, G. (2011). The structure of the nuclear pore complex. Annu. Rev. Biochem. *80*, 613-643.

Holm, L., and Park, J. (2000). DaliLite workbench for protein structure comparison. Bioinformatics *16*, 566-567.

Houseley, J., LaCava, J., and Tollervey, D. (2006). RNA-quality control by the exosome. Nature reviews Mol. Cell Biol. *7*, 529-539.

Huang, Y., Gattoni, R., Stevenin, J., and Steitz, J.A. (2003). SR splicing factors serve as adapter proteins for TAP-dependent mRNA export. Mol. Cell *11*, 837-843.

Huang, Y., Yario, T.A., and Steitz, J.A. (2004). A molecular link between SR protein dephosphorylation and mRNA export. Proc. Natl. Acad. Sci. USA *101*, 9666-9670.

Hurt, J.A., and Silver, P.A. (2008). mRNA nuclear export and human disease. Dis. Model Mech. *1*, 103-108.

Jankowsky, E. (2011a). RNA helicases at work: binding and rearranging. Trends Biochem. Sci. *36*, 19-29.

Jankowsky, E. (2011b). RNA helicases at work: binding and rearranging. Trends Biochem. Sci. *36*, 19-29.

Jankowsky, E., and Bowers, H. (2006). Remodeling of ribonucleoprotein complexes with DExH/D RNA helicases. Nucleic Acids Res. *34*, 4181-4188.

Jankowsky, E., and Fairman, M.E. (2007). RNA helicases--one fold for many functions. Curr. Opin. Struct. Biol. *17*, 316-324.

Jankowsky, E., Gross, C.H., Shuman, S., and Pyle, A.M. (2001). Active disruption of an RNA-protein interaction by a DExH/D RNA helicase. Science *291*, 121-125.

Jao, L.E., Appel, B., and Wente, S.R. (2012). A zebrafish model of lethal congenital contracture syndrome 1 reveals Gle1 function in spinal neural precursor survival and motor axon arborization. Development *139*, 1316-1326.

Kanai, Y., Dohmae, N., and Hirokawa, N. (2004). Kinesin transports RNA: isolation and characterization of an RNA-transporting granule. Neuron *43*, 513-525.

Kapp, L.D., and Lorsch, J.R. (2004). The molecular mechanics of eukaryotic translation. Annu. Rev. Biochem. *73*, 657-704.

Kelley, L.A., and Sternberg, M.J. (2009). Protein structure prediction on the Web: a case study using the Phyre server. Nat. Prot. *4*, 363-371.

Kendirgi, F., Barry, D.M., Griffis, E.R., Powers, M.A., and Wente, S.R. (2003). An essential role for hGle1 nucleocytoplasmic shuttling in mRNA export. J Cell. Biol. *160*, 1029-1040.

Kendirgi, F., Rexer, D.J., Alcazar-Roman, A.R., Onishko, H.M., and Wente, S.R. (2005). Interaction between the shuttling mRNA export factor Gle1 and the nucleoporin hCG1: a conserved mechanism in the export of Hsp70 mRNA. Mol. Biol. Cell *16*, 4304-4315.

Kiebler, M.A., and Bassell, G.J. (2006). Neuronal RNA granules: movers and makers. Neuron *51*, 685-690.

Kiseleva, E., Allen, T.D., Rutherford, S., Bucci, M., Wente, S.R., and Goldberg, M.W. (2004). Yeast nuclear pore complexes have a cytoplasmic ring and internal filaments. J Struct. Biol. *145*, 272-288.

Kiseleva, E., Visa, N., Wurtz, T., and Daneholt, B. (1997). Immunocytochemical evidence for a stepwise assembly of Balbiani ring premessenger ribonucleoprotein particles. Eur. J Cell. Biol. *74*, 407-416.

Klostermeier, D. (2011). Single-molecule FRET reveals nucleotide-driven conformational changes in molecular machines and their link to RNA unwinding and DNA supercoiling. Biochem. Soc. Trans. *39*, 611-616.

Kohler, A., and Hurt, E. (2007). Exporting RNA from the nucleus to the cytoplasm. Nature reviews Mol. Cell Biol. *8*, 761-773.

Korneeva, N.L., First, E.A., Benoit, C.A., and Rhoads, R.E. (2005). Interaction between the NH2-terminal domain of eIF4A and the central domain of eIF4G modulates RNA-stimulated ATPase activity. J Biol. Chem. *280*, 1872-1881.

Landau, M., Mayrose, I., Rosenberg, Y., Glaser, F., Martz, E., Pupko, T., and Ben-Tal, N. (2005). ConSurf 2005: the projection of evolutionary conservation scores of residues on protein structures. Nucleic Acids Res. *33*, W299-302.

Lee, K.M., and Tarn, W.Y. (2013). Coupling pre-mRNA processing to transcription on the RNA factory assembly line. RNA biology *10*, 380-390.

Lewis, J.D., and Izaurralde, E. (1997). The role of the cap structure in RNA processing and nuclear export. Eur. J Biochem. *247*, 461-469.

Licatalosi, D.D., and Darnell, R.B. (2010). RNA processing and its regulation: global insights into biological networks. Nat. Rev. Genet. *11*, 75-87.

Linder, P. (2006). Dead-box proteins: a family affair--active and passive players in RNP-remodeling. Nucleic Acids Res. *34*, 4168-4180.

Liu, F., Putnam, A., and Jankowsky, E. (2008). ATP hydrolysis is required for DEAD-box protein recycling but not for duplex unwinding. Proc. Natl. Acad. Sci. U S A *105*, 20209-20214.

Lorson, C.L., Strasswimmer, J., Yao, J.M., Baleja, J.D., Hahnen, E., Wirth, B., Le, T., Burghes, A.H., and Androphy, E.J. (1998). SMN oligomerization defect correlates with spinal muscular atrophy severity. Nat. Genet. *19*, 63-66.

Lund, M.K., and Guthrie, C. (2005). The DEAD-box protein Dbp5p is required to dissociate Mex67p from exported mRNPs at the nuclear rim. Mol. Cell *20*, 645-651.

Maimon, T., Elad, N., Dahan, I., and Medalia, O. (2012). The human nuclear pore complex as revealed by cryo-electron tomography. Structure *20*, 998-1006.

Marcotrigiano, J., Lomakin, I.B., Sonenberg, N., Pestova, T.V., Hellen, C.U., and Burley, S.K. (2001). A conserved HEAT domain within eIF4G directs assembly of the translation initiation machinery. Mol. Cell *7*, 193-203.

Martin, K.C., and Ephrussi, A. (2009). mRNA localization: gene expression in the spatial dimension. Cell *136*, 719-730.

McKee, A.E., and Silver, P.A. (2007). Systems perspectives on mRNA processing. Cell. Res. *17*, 581-590.

Mehlin, H., Daneholt, B., and Skoglund, U. (1992). Translocation of a specific premessenger ribonucleoprotein particle through the nuclear pore studied with electron microscope tomography. Cell *69*, 605-613.

Mehlin, H., Daneholt, B., and Skoglund, U. (1995). Structural interaction between the nuclear pore complex and a specific translocating RNP particle. J Cell Biol. *129*, 1205-1216.

Miller, A.L., Suntharalingam, M., Johnson, S.L., Audhya, A., Emr, S.D., and Wente, S.R. (2004). Cytoplasmic inositol hexakisphosphate production is sufficient for mediating the Gle1-mRNA export pathway. J Biol. Chem. *279*, 51022-51032.

Montpetit, B., Thomsen, N.D., Helmke, K.J., Seeliger, M.A., Berger, J.M., and Weis, K. (2011). A conserved mechanism of DEAD-box ATPase activation by nucleoporins and InsP6 in mRNA export. Nature *472*, 238-242.

Moon, D., Bae, J., Cho, H., and Yoon, J. (1998). The fission yeast homologue of Glel is essential for growth and involved in mRNA expor. The Journal of Microbilogy *46*, 422-428.

Mor, A., Suliman, S., Ben-Yishay, R., Yunger, S., Brody, Y., and Shav-Tal, Y. (2010). Dynamics of single mRNP nucleocytoplasmic transport and export through the nuclear pore in living cells. Nat Cell Biol. *12*, 543-552.

Muller-McNicoll, M., and Neugebauer, K.M. (2013). How cells get the message: dynamic assembly and function of mRNA-protein complexes. Nat. Rev. Genet. *14*, 275-287

Murphy, R., and Wente, S.R. (1996). An RNA-export mediator with an essential nuclear export signal. Nature *383*, 357-360.

Nakamura, Y., and Ito, K. (2003). Making sense of mimic in translation termination. Trends Biochem. Sci. *28*, 99-105.

Nenninger, A., Mastroianni, G., and Mullineaux, C.W. (2010). Size dependence of protein diffusion in the cytoplasm of Escherichia coli. J Bacteriol *192*, 4535-4540.
Newman, J.R., Wolf, E., and Kim, P.S. (2000). A computationally directed screen identifying interacting coiled coils from Saccharomyces cerevisiae. Proc. Natl. Acad. Sci. U S A *97*, 13203-13208.

Nielsen, K.H., Chamieh, H., Andersen, C.B., Fredslund, F., Hamborg, K., Le Hir, H., and Andersen, G.R. (2009). Mechanism of ATP turnover inhibition in the EJC. RNA *15*, 67-75.

Noble, K.N., Tran, E.J., Alcazar-Roman, A.R., Hodge, C.A., Cole, C.N., and Wente, S.R. (2011). The Dbp5 cycle at the nuclear pore complex during mRNA export II: nucleotide cycling and mRNP remodeling by Dbp5 are controlled by Nup159 and Gle1. Genes Dev. *25*, 1065-1077.

Nousiainen, H.O., Kestila, M., Pakkasjarvi, N., Honkala, H., Kuure, S., Tallila, J., Vuopala, K., Ignatius, J., Herva, R., and Peltonen, L. (2008). Mutations in mRNA export mediator GLE1 result in a fetal motoneuron disease. Nat. Genet. *40*, 155-157.

O'Shea, E.K., Klemm, J.D., Kim, P.S., and Alber, T. (1991). X-ray structure of the GCN4 leucine zipper, a two-stranded, parallel coiled coil. Science *254*, 539-544.

Ohi, M., Li, Y., Cheng, Y., and Walz, T. (2004). Negative Staining and Image Classification - Powerful Tools in Modern Electron Microscopy. Biol. Proced. Online *6*, 23-34.

Pante, N., and Kann, M. (2002). Nuclear pore complex is able to transport macromolecules with diameters of about 39 nm. Mol. Biol. Cell *13*, 425-434.

Papadopoulos, S., Jurgens, K.D., and Gros, G. (2000). Protein diffusion in living skeletal muscle fibers: dependence on protein size, fiber type, and contraction. Biophys. J *79*, 2084-2094.

Pellizzoni, L., Charroux, B., and Dreyfuss, G. (1999). SMN mutants of spinal muscular atrophy patients are defective in binding to snRNP proteins. Proc. Natl. Acad. Sci. U S A *96*, 11167-11172.

Pemberton, L.F., and Paschal, B.M. (2005). Mechanisms of receptor-mediated nuclear import and nuclear export. Traffic *6*, 187-198.

Polach, K.J., and Uhlenbeck, O.C. (2002). Cooperative binding of ATP and RNA substrates to the DEAD/H protein DbpA. Biochemistry (Mosc) *41*, 3693-3702.
Proudfoot, N.J. (2011). Ending the message: poly(A) signals then and now. Genes Dev. *25*, 1770-1782.

Raboy, V. (2001). Seeds for a better future: 'low phytate' grains help to overcome malnutrition and reduce pollution. Trends in Plant Science *6*, 458-462.

Rayala, H.J., Kendirgi, F., Barry, D.M., Majerus, P.W., and Wente, S.R. (2004). The mRNA export factor human Gle1 interacts with the nuclear pore complex protein Nup155. Mol. Cell. Proteomics *3*, 145-155.

Renoux, A.J., and Todd, P.K. (2012). Neurodegeneration the RNA way. Prog. Neurobiol. *97*, 173-189.

Roberts-Galbraith, R.H., Ohi, M.D., Ballif, B.A., Chen, J.S., McLeod, I., McDonald, W.H., Gygi, S.P., Yates, J.R., 3rd, and Gould, K.L. (2010). Dephosphorylation of F-BAR protein Cdc15 modulates its conformation and stimulates its scaffolding activity at the cell division site. Mol. Cell *39*, 86-99.

Rocak, S., and Linder, P. (2004). DEAD-box proteins: the driving forces behind RNA metabolism. Nature reviews Mol. Cell Biol. *5*, 232-241.

Rogers, G.W., Jr., Richter, N.J., Lima, W.F., and Merrick, W.C. (2001a). Modulation of the helicase activity of eIF4A by eIF4B, eIF4H, and eIF4F. J Biol. Chem. *276*, 30914-30922.

Rogers, G.W., Jr., Richter, N.J., Lima, W.F., and Merrick, W.C. (2001b). Modulation of the helicase activity of eIF4A by eIF4B, eIF4H, and eIF4F. J Biol. Chem. *276*, 30914-30922.

Rout, M.P., Aitchison, J.D., Suprapto, A., Hjertaas, K., Zhao, Y., and Chait, B.T. (2000). The yeast nuclear pore complex: composition, architecture, and transport mechanism. J Cell Biol. *148*, 635-651.

Roy, R., Hohng, S., and Ha, T. (2008). A practical guide to single-molecule FRET. Nat. Met. *5*, 507-516.

Schmitt, C., von Kobbe, C., Bachi, A., Pante, N., Rodrigues, J.P., Boscheron, C., Rigaut, G., Wilm, M., Seraphin, B., Carmo-Fonseca, M.*, et al.* (1999). Dbp5, a DEAD-box protein required for mRNA export, is recruited to the cytoplasmic fibrils of nuclear pore complex via a conserved interaction with CAN/Nup159p. EMBO J *18*, 4332-4347.

Schoenberg, D.R., and Maquat, L.E. (2012). Regulation of cytoplasmic mRNA decay. Nat. Rev. Genet. *13*, 246-259.

Schroer, T.A. (2004). Dynactin. Annu. Rev. Cell. Dev. Biol. *20*, 759-779.

Schuck, P., and Rossmanith, P. (2000). Determination of the sedimentation coefficient distribution by least-squares boundary modeling. Biopolymers *54*, 328-341.

Schutz, P., Bumann, M., Oberholzer, A.E., Bieniossek, C., Trachsel, H., Altmann, M., and Baumann, U. (2008). Crystal structure of the yeast eIF4A-eIF4G complex: an RNA-helicase controlled by protein-protein interactions. Proc. Natl. Acad. Sci. U S A *105*, 9564-9569.

Schutz, P., Karlberg, T., van den Berg, S., Collins, R., Lehtio, L., Hogbom, M., Holmberg-Schiavone, L., Tempel, W., Park, H.W., Hammarstrom, M.*, et al.* (2010). Comparative structural analysis of human DEAD-box RNA helicases. PloS One *5*.

Segref, A., Sharma, K., Doye, V., Hellwig, A., Huber, J., Luhrmann, R., and Hurt, E. (1997). Mex67p, a novel factor for nuclear mRNA export, binds to both poly(A)+ RNA and nuclear pores. EMBO J *16*, 3256-3271.

Shatkin, A.J. (1976). Capping of eucaryotic mRNAs. Cell *9*, 645-653.

Shpargel, K.B., and Matera, A.G. (2005). Gemin proteins are required for efficient assembly of Sm-class ribonucleoproteins. Proc. Natl. Acad. Sci. U S A *102*, 17372-17377.

Snay-Hodge, C.A., Colot, H.V., Goldstein, A.L., and Cole, C.N. (1998). Dbp5p/Rat8p is a yeast nuclear pore-associated DEAD-box protein essential for RNA export. EMBO J *17*, 2663-2676.

Stahl, G., Bidou, L., Rousset, J.P., and Cassan, M. (1995). Versatile vectors to study recoding: conservation of rules between yeast and mammalian cells. Nucleic Acids Res. *23*, 1557-1560.

Stewart, M. (2007). Ratcheting mRNA out of the nucleus. Mol. Cell *25*, 327-330.

Strahm, Y., Fahrenkrog, B., Zenklusen, D., Rychner, E., Kantor, J., Rosbach, M., and Stutz, F. (1999). The RNA export factor Gle1p is located on the cytoplasmic fibrils of the NPC and physically interacts with the FG-nucleoporin Rip1p, the DEAD-box protein Rat8p/Dbp5p and a new protein Ymr 255p. EMBO J *18*, 5761-5777.

Strasser, K., and Hurt, E. (2000). Yra1p, a conserved nuclear RNA-binding protein, interacts directly with Mex67p and is required for mRNA export. EMBO J *19*, 410-420.

Strasser, K., Masuda, S., Mason, P., Pfannstiel, J., Oppizzi, M., Rodriguez-Navarro, S., Rondon, A.G., Aguilera, A., Struhl, K., Reed, R.*, et al.* (2002). TREX is a conserved complex coupling transcription with messenger RNA export. Nature *417*, 304-308.

Stutz, F., Bachi, A., Doerks, T., Braun, I.C., Seraphin, B., Wilm, M., Bork, P., and Izaurralde, E. (2000). REF, an evolutionary conserved family of hnRNP-like proteins, interacts with TAP/Mex67p and participates in mRNA nuclear export. RNA *6*, 638-650.

Stutz, F., Kantor, J., Zhang, D., McCarthy, T., Neville, M., and Rosbash, M. (1997). The yeast nucleoporin rip1p contributes to multiple export pathways with no essential role for its FG-repeat region. Genes Dev. *11*, 2857-2868.

Terry, L.J., Shows, E.B., and Wente, S.R. (2007). Crossing the nuclear envelope: hierarchical regulation of nucleocytoplasmic transport. Science *318*, 1412-1416.

Terry, L.J., and Wente, S.R. (2009). Flexible gates: dynamic topologies and functions for FG nucleoporins in nucleocytoplasmic transport. Eukaryotic Cell *8*, 1814-1827.

Theissen, B., Karow, A.R., Kohler, J., Gubaev, A., and Klostermeier, D. (2008). Cooperative binding of ATP and RNA induces a closed conformation in a DEAD box RNA helicase. Proc. Natl. Acad. Sci. U S A *105*, 548-553.

Tran, E.J., Zhou, Y., Corbett, A.H., and Wente, S.R. (2007). The DEAD-box protein Dbp5 controls mRNA export by triggering specific RNA:protein remodeling events. Mol. Cell *28*, 850-859.

Tsai, Joseph. (2011). Establishing vertebrate model systems for the study of Gle1 mediated motor neuron disease. UC San Diego: b7093676. Retrieved from: http://escholarship.org/uc/item/6v8887xt

Tseng, S.S., Weaver, P.L., Liu, Y., Hitomi, M., Tartakoff, A.M., and Chang, T.H. (1998). Dbp5p, a cytosolic RNA helicase, is required for poly(A)+ RNA export. EMBO J *17*, 2651-2662.

Tzschach, A., Grasshoff, U., Schaferhoff, K., Bonin, M., Dufke, A., Wolff, M., Haas-Lude, K., Bevot, A., and Riess, O. (2012). Interstitial 9q34.11-q34.13 deletion in a patient with severe intellectual disability, hydrocephalus, and cleft lip/palate. American Journal of Medical Genetics Part A *158A*, 1709-1712.

Valkov, E., Dean, J.C., Jani, D., Kuhlmann, S.I., and Stewart, M. (2012). Structural basis for the assembly and disassembly of mRNA nuclear export complexes. Biochim. Biophys. Acta. *1819*, 578-592.

Verhey, K.J., and Hammond, J.W. (2009). Traffic control: regulation of kinesin motors. Nature reviews Mol. Cell. Biol. *10*, 765-777.

Vuopala, K., Ignatius, J., and Herva, R. (1995). Lethal arthrogryposis with anterior horn cell disease. Hum. Pathol. *26*, 12-19.

Wan, L., Battle, D.J., Yong, J., Gubitz, A.K., Kolb, S.J., Wang, J., and Dreyfuss, G. (2005). The survival of motor neurons protein determines the capacity for snRNP assembly: biochemical deficiency in spinal muscular atrophy. Mol. Cell. Biol. *25*, 5543-5551.

Watkins, J.L., Murphy, R., Emtage, J.L., and Wente, S.R. (1998). The human homologue of Saccharomyces cerevisiae Gle1p is required for poly(A)+ RNA export. Proc. Natl. Acad. Sci.U S A *95*, 6779-6784.

Weirich, C.S., Erzberger, J.P., Berger, J.M., and Weis, K. (2004). The N-terminal domain of Nup159 forms a beta-propeller that functions in mRNA export by tethering the helicase Dbp5 to the nuclear pore. Mol. Cell *16*, 749-760.

Weirich, C.S., Erzberger, J.P., Flick, J.S., Berger, J.M., Thorner, J., and Weis, K. (2006). Activation of the DExD/H-box protein Dbp5 by the nuclear-pore protein Gle1 and its coactivator InsP6 is required for mRNA export. Nat. Cell Biol. *8*, 668-676.

Weis, K. (2003). Regulating access to the genome: nucleocytoplasmic transport throughout the cell cycle. Cell *112*, 441-451.

Wente, S.R., and Blobel, G. (1993). A temperature-sensitive NUP116 null mutant forms a nuclear envelope seal over the yeast nuclear pore complex thereby blocking nucleocytoplasmic traffic. J Cell Biol. *123*, 275-284.

Winey, M., Yarar, D., Giddings, T.H., Jr., and Mastronarde, D.N. (1997). Nuclear pore complex number and distribution throughout the Saccharomyces cerevisiae cell cycle by three-dimensional reconstruction from electron micrographs of nuclear envelopes. Mol. Biol. Cell *8*, 2119-2132.

Wolf, A., Krause-Gruszczynska, M., Birkenmeier, O., Ostareck-Lederer, A., Huttelmaier, S., and Hatzfeld, M. (2010a). Plakophilin 1 stimulates translation by promoting eIF4A1 activity. J Cell Biol. *188*, 463-471.

Wolf, A., Krause-Gruszczynska, M., Birkenmeier, O., Ostareck-Lederer, A., Huttelmaier, S., and Hatzfeld, M. (2010b). Plakophilin 1 stimulates translation by promoting eIF4A1 activity. J Cell Biol. *188*, 463-471.

Xia, Z., and Liu, Y. (2001). Reliable and global measurement of fluorescence resonance energy transfer using fluorescence microscopes. Biophys. J *81*, 2395-2402.

Yang, H.S., Jansen, A.P., Komar, A.A., Zheng, X., Merrick, W.C., Costes, S., Lockett, S.J., Sonenberg, N., and Colburn, N.H. (2003). The transformation suppressor Pdcd4 is a novel eukaryotic translation initiation factor 4A binding protein that inhibits translation. Mol. Cell Biol, *23*, 26-37.

Yang, Q., Rout, M.P., and Akey, C.W. (1998). Three-dimensional architecture of the isolated yeast nuclear pore complex: functional and evolutionary implications. Mol. Cell *1*, 223-234.

York, J.D., Odom, A.R., Murphy, R., Ives, E.B., and Wente, S.R. (1999). A phospholipase C-dependent inositol polyphosphate kinase pathway required for efficient messenger RNA export. Science *285*, 96-100.

Zhao, J., Jin, S.B., Bjorkroth, B., Wieslander, L., and Daneholt, B. (2002). The mRNA export factor Dbp5 is associated with Balbiani ring mRNP from gene to cytoplasm. EMBO J *21*, 1177-1187.